



Universiteit  
Leiden  
The Netherlands

## Activity-based protein profiling in drug-discovery

Esbroeck, A.C.M. van

### Citation

Esbroeck, A. C. M. van. (2019, May 28). *Activity-based protein profiling in drug-discovery*. Retrieved from <https://hdl.handle.net/1887/74006>

Version: Not Applicable (or Unknown)

License: [Leiden University Non-exclusive license](#)

Downloaded from: <https://hdl.handle.net/1887/74006>

**Note:** To cite this publication please use the final published version (if applicable).

Cover Page



Universiteit Leiden



The following handle holds various files of this Leiden University dissertation:

<http://hdl.handle.net/1887/74006>

**Author:** Esbroeck, A.C.M. van

**Title:** Activity-based protein profiling in drug-discovery

**Issue Date:** 2019-05-28

# Activity-based protein profiling in drug discovery

PROEFSCHRIFT

ter verkrijging van  
de graad van Doctor aan de Universiteit Leiden,  
op gezag van Rector Magnificus prof.mr. C.J.J.M. Stolker,  
volgens besluit van het College voor Promoties  
te verdedigen op dinsdag 28 mei 2019  
klokke 13:45 uur

door

**Annelot Clementine Mathilda van Esbroeck**

geboren te Zoetermeer in 1990

## Promotiecommissie

Promotoren	Prof. dr. M. van der Stelt, Leiden University Prof. dr. J. Brouwer, Leiden University
Overige leden	Prof. dr. H.S. Overkleeft, Leiden University Prof. dr. H. Spaink, Leiden University Prof. dr. T. Hankemeier, Leiden University Prof. dr. S. Kushner, Erasmus Medical Centre Rotterdam Mw. dr. J. Meijerink, University of Wageningen

ISBN: 978-94-028-1497-2

Printed by: Proefschriften.net

Cover design: Van Esbroeck  Weevers

Quote page 3: Isaac Newton's letter to Robert Hooke, 5 February 1675  
Available via the Historical Society of Pennsylvania

All rights reserved. No part of this thesis may be reproduced in any matter or by any means without permission from the author.

*If I have seen further it is by  
standing on the shoulders of giants.*

Isaac Newton - 1675





# Table of contents

<b>Chapter 1</b>	<b>7</b>
<i>General introduction: Activity-based protein profiling in drug discovery</i>	
<b>Chapter 2</b>	<b>19</b>
<i>Activity-based protein profiling of the human ischemic heart</i>	
<b>Chapter 3</b>	<b>37</b>
<i>Applications of activity-based protein profiling in developing zebrafish</i>	
<b>Chapter 4</b>	<b>59</b>
<i>Activity-based protein profiling reveals off-target proteins of FAAH inhibitor BIA 10-2474</i>	
<b>Chapter 5</b>	<b>83</b>
<i>Identification of ABHD6 as a diacylglycerol lipase</i>	
<b>Chapter 6</b>	<b>103</b>
<i>Summary &amp; future prospects</i>	
<b>Nederlandse samenvatting</b>	<b>119</b>
<b>List of publications</b>	<b>124</b>
<b>Curriculum vitae</b>	<b>126</b>







# General introduction: Activity-based protein profiling in drug discovery

## Drug discovery & development

The quest for treatments against disease and for symptom relief goes back at least several millennia. Around 1700 BC, the Mesopotamians described the use of drugs for medicinal purposes in a series of 40 tablets collectively known as “Treatise of medical diagnosis and prognosis”<sup>1</sup>. It was not until the beginning of the twentieth century that Paul Ehrlich (1854-1915) hypothesized that chemicals can exert specific biological effects due to the existence of ‘chemoreceptors’ on cells. With his notion that differential ‘chemoreceptors’, e.g. in infectious organisms or cancer cells, could be exploited for therapeutic benefit and that the chemical structure of a compound is linked to its specific pharmacological activity, he unknowingly provided the foundation for modern drug discovery<sup>2</sup>.

The drug discovery and development process covers all steps from the discovery of a therapeutically relevant biological target (Paul Ehrlich’s ‘chemoreceptors’) to the approval and launch of a drug (Figure 1). The drug discovery process generally starts with target discovery, which aims to identify biological targets in the pathology of interest that can be modified by chemical intervention. Once a target is validated (e.g. using genetically modified animal models), small molecule modulators (hits) are generally identified by

high-throughput screens of chemical libraries. After evaluation and limited optimization, hits can be identified as lead compounds, which show proof-of-principle in an animal model. Analogs with improved potency, reduced off-target activity and optimal physicochemical and metabolic properties are synthesized during lead optimization. The most promising compounds are assessed on pharmacodynamic, pharmacokinetic and toxicological properties. The main goal of the preclinical phase is to successfully demonstrate *in vivo* efficacy in a suitable animal model and to determine the safe dose for first-in-human studies. The investigational new drug then proceeds to the drug development stage, consisting of several clinical testing phases. During clinical phase I the dosage and safety is assessed in a small group of healthy volunteers. Phase II focuses on preliminary efficacy and side effects in a small patient group, whereas during phase III efficacy and adverse reactions are monitored in a large patient group. Roughly 10 percent of the investigational new drugs passes all clinical tests and can be launched as novel drug application after their approval by regulatory bodies<sup>3-5</sup>.

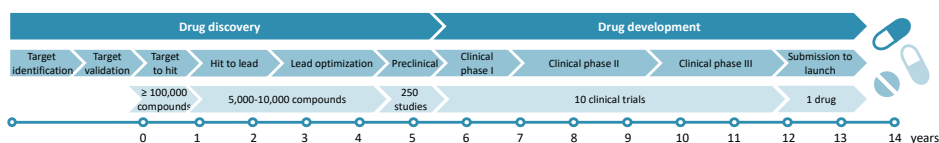


**Figure 1 | The drug discovery and drug development process.** Schematic representation of the stages in drug discovery and drug development, with their estimated duration and number of compounds/studies required for the development of a single approved drug (modified from literature<sup>3-5</sup>).

Drug discovery and development is a time- and resource-demanding process. On average, it takes more than 13 years to progress from hit to launch and the estimated costs currently exceed \$ 2.5 billion<sup>5-7</sup> for each new drug that enters the market. Despite technological advances, the introduction rate of new drugs is at a low, while development costs are rising substantially (mainly due to late-stage clinical failures caused by limited efficacy or unexpected toxicology)<sup>4,8,9</sup>. Although the target-based drug discovery process described above is effective in early stages of drug development, it often fails to predict pharmacological properties and clinical efficacy. The alternative phenotypic drug discovery approach is postulated to have more predictive power on pharmacological success in later stages<sup>10,11</sup>. In phenotypic screens compounds are directly screened in a relevant cellular or animal model for desirable phenotypic effects and responsible target(s) are identified in later stages of the drug discovery process<sup>12</sup>. In either drug discovery approach target identification is a crucial step, because the clinical success of a drug-candidate is highly dependent on understanding the relevance of its biological target(s) in the intended disease. The target identification process is challenging, but advancements are made due to continuous development of novel tools, methods and strategies, e.g. patient-derived induced pluripotent stem cells (iPSCs)<sup>13</sup> and zebrafish<sup>14</sup> as alternative models in phenotypic screening, single-cell analysis techniques<sup>15</sup> like RNA-seq<sup>16</sup>, and computational approaches<sup>17</sup>. In the last decades, activity-based protein profiling (ABPP) has emerged as a powerful chemical biology technique in drug discovery as well.

## Activity-based protein profiling

ABPP is a chemical proteomic method that uses active-site directed probes to assess the functional state of an entire enzyme class in complex biological samples<sup>18–20</sup>. These probes covalently interact with their target enzyme and report on the abundance of active protein, hence the term activity-based probe (ABP). An ABP typically consists of three main parts (Figure 2A): a reactive group or ‘warhead’ that covalently interacts with the enzyme’s active site, a chemical linker or spacer element, and a reporter tag that enables detection of the probe targets<sup>19</sup>. The reporter tag can be incorporated in the ABP itself (direct probes, Figure 2B) or can be introduced at a later stage by bio-orthogonal chemistry (two-step probe, Figure 2C). Copper(I)-catalyzed azide-alkyne cycloaddition (“click” chemistry) is one of the most common bio-orthogonal reactions to introduce a reporter group<sup>21</sup>. Although the workflow of direct probes is more efficient, a large reporter tag may alter the probe’s affinity and selectivity and may affect cell permeability<sup>22</sup>.

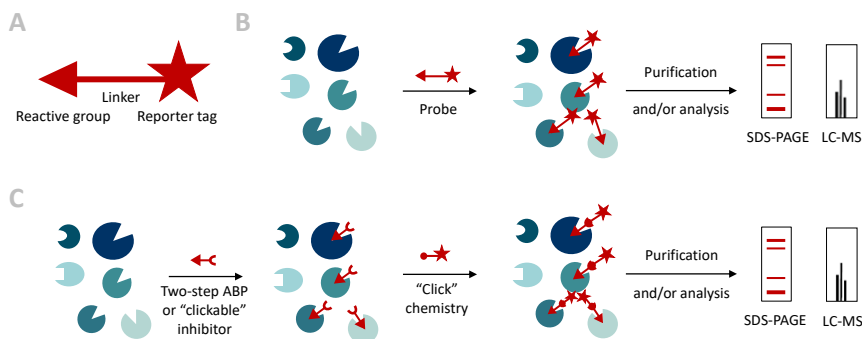


**Figure 2 | Activity-based protein profiling.** (A) An activity-based probe consists of a reactive group coupled to a reporter tag (a fluorophore for gel-based analysis by SDS-PAGE or an affinity tag for purification and analysis by LC-MS) by a chemical linker element. (B, C) Schematic representation of (B) direct ABPP in which a complex proteome is incubated with a probe containing a reporter tag and (C) two-step ABPP which requires bio-orthogonal chemistry (“click” chemistry) to introduce a reporter tag to a two-step probe.

Complex protein samples can be labeled with ABPs in different experimental settings, including in cell or tissue lysates (*in vitro*), live cells (*in situ*), and living organisms (*in vivo*)<sup>23</sup>. The readout of the experiment is generally dependent on the type of reporter tag that is used. Fluorescent reporter tags enable rapid analysis in a gel-based assay. The labeled proteome is separated by sodium dodecyl sulfate polyacrylamide gel electrophoresis (SDS-PAGE). In-gel fluorescence scanning provides a rapid readout, but sensitivity is limited and target identification heavily relies on specific inhibitors. Affinity tags, like biotin, enable target enrichment e.g. by avidin chromatography (pull-down). After tryptic digestion of the enriched targets, the resulting peptides can be identified by liquid chromatography-mass spectrometry (LC-MS) (Figure 2B, C)<sup>19,24</sup>. This MS-based ABPP method (also called chemical proteomics) is much lower throughput, but the high sensitivity and high information content make the technique very attractive nonetheless.

## Comparative and competitive ABPP

Two types of experimental setups are commonly used in ABPP: comparative and competitive ABPP (Figure 3). The comparative ABPP approach enables comparison of the activity landscapes of two or more biologically distinct samples<sup>19,25</sup>, e.g. healthy versus diseased<sup>26,27</sup> (Figure 3A). Altered enzyme activities can provide insight in (the regulation of) biological pathways and can serve as a starting point in target discovery. An important advantage of ABPP over gene expression studies, is that ABPP provides a direct readout of the enzymatic state of the protein and thus also accounts for the effects post-translational modifications.

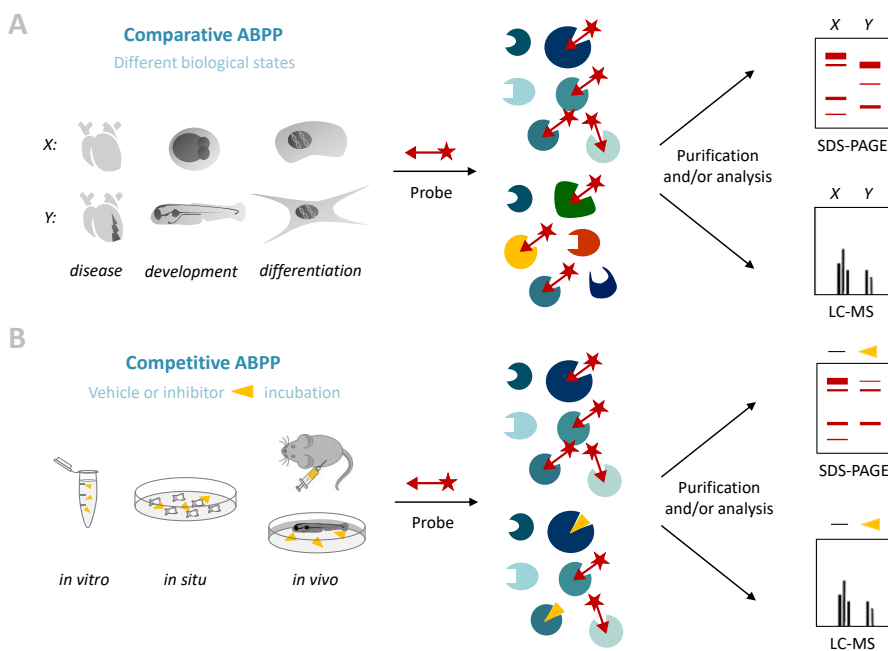


**Figure 3 | Competitive and comparative ABPP.** (A) In comparative ABPP two proteomes from different biological states, e.g. healthy versus diseased or different cell types, are compared by gel- or MS-based analysis of probe treated samples. (B) Competitive ABPP enables target-engagement assessment and off-target profiling. Inhibitor treatment can be done *in vitro* (cell or tissue lysate), *in situ* (live cells), or *in vivo* (living organisms), followed by *in vitro* probe incubation and gel- or MS-based analysis.

Competitive ABPP, the second major application, is particularly suitable for inhibitor profiling (Figure 3B)<sup>19,23,24</sup>. It enables simultaneous assessment of inhibitor potency and selectivity and is a powerful tool for target engagement studies. In the drug discovery process, competitive ABPP can guide the lead identification, optimization, and the pre-clinical testing phase. Prior to labeling with an ABP, the proteome is incubated *in vitro*, *in situ*, or *in vivo* with inhibitor. Targets are identified as those with reduced probe labeling after inhibitor pre-incubation. Target identification is restricted to the enzymes identified by the probe, therefore broad-spectrum ABPs are especially suitable for competitive ABPP. Alternatively, introduction of a ligation handle in the inhibitor enables identification of all covalent interaction partners with two-step ABPP

(Figure 2C). Since the ligation handle can affect potency and selectivity, it is important to cross-check with the original inhibitor<sup>28</sup>.

Finally, ABPP can serve as a tool for the characterization of unannotated proteins. Interaction between an ABP and an uncharacterized protein can facilitate the assignment of the protein to a specific enzymatic class or family<sup>19</sup>.

### Activity-based probes

A variety of enzyme classes can be targeted with ABPs<sup>19,24</sup>, including the serine hydrolases<sup>18,29</sup>, cysteine and threonine proteases<sup>30,31</sup>, kinases<sup>32</sup>, phosphatases, cytochrome P450s<sup>33</sup>, and glycosidases<sup>34,35</sup>. Photoaffinity probes provide an alternative labeling method for enzymes (e.g. metallohydrolases) or other druggable targets (e.g. receptors) that otherwise cannot interact covalently with a probe. The photoreactive group in these probes can form a covalent bond with the associated protein after UV- irradiation<sup>36</sup>.

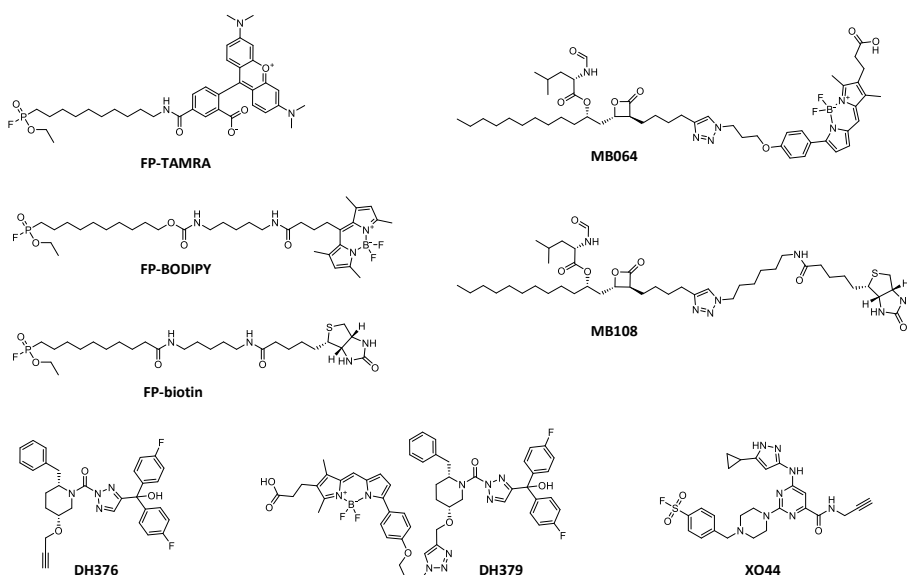


**Figure 4 | Activity-based probes.** Broad-spectrum serine-hydrolase probes fluorophosphonate (FP)-TAMRA, FP-BODIPY and FP-biotin. Tailored lipase probes MB064 and MB108, targeting e.g. DAGLα/β. Two-step DAGL-probe DH376, containing an alkyne ligation handle, and its derived direct probe DH379. Reactive-lysine targeting kinase probe XO44.

The work in this thesis focuses on activity-profiling of the serine hydrolases, which represent ~ 1 % of all proteins in mammals. The serine hydrolases are characterized by a well conserved GX SXG amino acid motif and are involved in a broad spectrum of physiological and pathological processes<sup>37,38</sup>. The active-site serine can interact covalently with fluorophosphonate (FP)-based probes, such as FP-rhodamine (FP-TAMRA)<sup>18</sup> and FP-BODIPY<sup>22</sup>, which are especially suitable for broad-spectrum profiling. Tailored probes like the β-lactone-based MB064<sup>39</sup> and MB108<sup>40</sup> or selective

probes like DH376 and DH379<sup>41</sup> enable assessment of specific hydrolases such as the diacylglycerol lipases (Figure 4) (see *The endocannabinoid system*).

In addition, the kinase-targeting probe XO44 is used (Figure 4)<sup>32</sup>. The kinases, a large protein family comprising over 500 members, are known for their pivotal roles in cell signaling processes, differentiation, proliferation, and disease<sup>42,43</sup>. A conserved lysine in the kinase active-site offers a reactive group for XO44<sup>32</sup>. Of note, in contrast to the serine hydrolase probes, XO44 labels available kinase active-sites dependent on their affinity, but not necessarily on their active state.

## The endocannabinoid system

The endocannabinoid system (ECS, Figure 5) plays a central role in the work described in this thesis. The ECS mediates the physiological effects of  $\Delta^9$ -tetrahydrocannabinol (THC), the psychoactive compound in *Cannabis sativa*, to which the ECS owes its name<sup>44,45</sup>. The ECS is comprised of the cannabinoid receptors type 1 and 2 (CB1R, CB2R), their endogenous ligands, also known as the endocannabinoids, and the enzymes for ligand biosynthesis and degradation. CB1R and CB2R are G protein-coupled receptors and are activated by the endocannabinoids, as well as by plant-derived cannabinoids (phytocannabinoids) like THC<sup>46</sup>. The CB1R is most abundant in the central nervous system<sup>47</sup>, while CB2R is mainly expressed in cells of the immune system<sup>48</sup>. The ECS mediates numerous physiological processes, including appetite and metabolism, learning and memory, pain sensation and anxiety, and inflammation<sup>45,49–51</sup>.

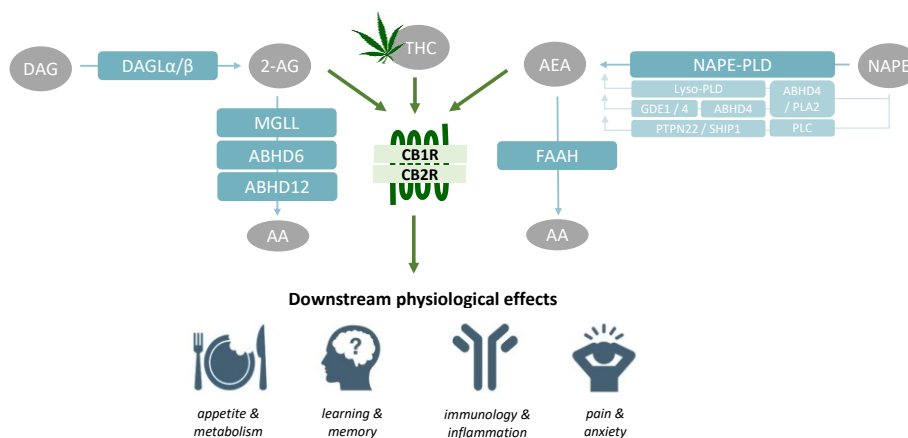


**Figure 5 | The endocannabinoid system.** The endocannabinoid system is involved in multiple physiological processes and is comprised of the cannabinoid receptors 1 and 2 (CB1R, CB2R), their endogenous ligands (endocannabinoids) and their metabolic enzymes. Ligands & metabolites (grey): DAG: diacylglycerol, 2-AG: 2-arachidonoylglycerol, AA: arachidonic acid, THC:  $\Delta^9$ -tetrahydrocannabinol, AEA: anandamide, NAPE: N-acylphosphatidylethanolamine. Endocannabinoid metabolic enzymes (blue): DAGLα/β: diacylglycerol lipase α and β. MGLL: monoacylglycerol lipase. ABHD4/6/12: α,β-hydrolase domain containing proteins 4, 6 and 12. FAAH: fatty acid amide hydrolase. NAPE-PLD: N-acylphosphatidylethanolamine phospholipase D, PLA2: phospholipase A<sub>2</sub>, GDE1/4: glycerophosphodiesterase 1 and 4, Lyso-PLD: unidentified lysophospholipase D, PLC: unidentified phospholipase C, PTPN22: tyrosine-protein phosphatase non-receptor type 22, SHIP1: phosphatidylinositol 3,4,5-trisphosphate 5-phosphatase 1.

In the early 90s *N*-arachidonylethanolamide (anandamide, AEA) was identified as the first endocannabinoid<sup>52</sup>. In the following years, 2-arachidonoylglycerol (2-AG)<sup>53,54</sup> as well as several other endocannabinoids were identified. However, AEA and 2-AG are considered to be the two main endocannabinoids<sup>45</sup>. In the brain the endocannabinoids are synthesized on-demand at the membrane, in contrast to classical neurotransmitters which are stored in presynaptic vesicles. The endocannabinoids activate the presynaptic CB1R in a retrograde fashion and signaling is terminated by their hydrolysis. This mechanism implies that endocannabinoid levels at the synapse must be tightly controlled by their metabolic enzymes<sup>46</sup>.

Several metabolic pathways control the endocannabinoid levels (Figure 5). Diacylglycerol lipase  $\alpha$  and  $\beta$  (DAGL $\alpha$ , DAGL $\beta$ ) are the two main enzymes producing 2-AG, by catalyzing the hydrolysis of diacylglycerol (DAG) to 2-AG<sup>55</sup>. The majority of 2-AG is hydrolyzed to arachidonic acid (AA) by monoacylglycerol lipase (MGLL)<sup>56,57</sup>, but  $\alpha$ , $\beta$ -hydrolase domain containing proteins 6 and 12 (ABHD6, ABHD12) can also catalyze this reaction<sup>57–59</sup>. The biosynthesis of AEA is less straightforward, due to the existence of multiple *N*-acylethanolamine (NAE) biosynthetic pathways. Direct hydrolysis of *N*-acylphosphatidylethanolamines (NAPEs) to NAEs (including AEA) by NAPE phospholipase D (NAPE-PLD) is considered to be the canonical pathway<sup>60</sup>. The NAEs are hydrolyzed to ethanolamine and free fatty acid by fatty acid amide hydrolase (FAAH)<sup>61,62</sup>. Of note, three alternative multistep pathways exist for the biosynthesis of AEA from NAPEs: (I) phospholipase A<sub>2</sub> (PLA2) and ABHD4 mediated conversion of NAPE to lyso-NAPE, followed by conversion to AEA by an unknown lysophospholipase D (Lyso-PLD); (II) conversion of lyso-NAPE to glycerophospho-AEA by ABHD4 and subsequent hydrolysis to AEA by glycerophosphodisesterase 1 or 4 (GDE1, GDE4); or (III) conversion of NAPE to phospho-AEA by an unidentified phospholipase C and cleavage to AEA by tyrosine-protein phosphatase non-receptor type 22 (PTPN22) or phosphatidylinositol 3,4,5-trisphosphate 5-phosphatase 1 (SHIP1)<sup>60</sup>.

### The ECS as a therapeutic target

The role of the ECS in various pathological conditions, including neurological<sup>63</sup> and cardiovascular<sup>64</sup> disorders, makes it a promising target for therapeutic intervention<sup>51,65,66</sup>. At the same time, its involvement in multiple physiological processes makes drug discovery challenging and requires accurate balancing of activation and inhibition to achieve only the desired effects. Several synthetic CB1R and CB2R ligands have been developed, but thus far their clinical success was limited. Rimonabant, a CB1R antagonist, was an efficacious anorectic drug for the treatment of obesity, but two years after its launch in 2006 it was withdrawn from the market due to severe psychiatric side effects<sup>67,68</sup>. Several CB2R agonists were effective in the treatment of (inflammatory) pain in preclinical animal models, but their development has been discontinued due to a lack of analgesic effects in clinical trials<sup>69</sup>.

Regulating endogenous ligand levels may provide a more controlled modulation of cannabinoid receptor signaling than direct modulation by synthetic ligands. Therefore, targeting the endocannabinoid metabolic enzymes is a promising avenue for the development of ECS-directed therapeutics. Recently, positive results have been obtained in a phase Ib clinical trial using selective MGLL inhibitor ABX-1431 for the treatment of Tourette syndrome<sup>70–72</sup>. ABPP played a central part in the development of ABX-1431. This technique had previously been used for selectivity profiling of PF04457845, a FAAH inhibitor<sup>73</sup>. Although PF04457845 was effective in increasing plasma levels of NAEs in a first-in-human study<sup>74</sup>, the drug exerted no analgesic effects in clinical trials<sup>75</sup>. Several clinical trials for other indications are, however, still on-going<sup>76</sup>. BIA 10-2474, another FAAH inhibitor, produced mild-to-severe neurological symptoms and resulted in the death of a healthy volunteer in a recent phase I clinical trial<sup>77,78</sup>. Given the clinical safety profile of PF04457845, off-target activities of BIA 10-2474 are likely to have contributed to its clinical neurotoxicity. Competitive ABPP may provide insight in the BIA 10-2474 interaction profile.

A better understanding of the ECS in (patho)physiological processes will provide insight in how to regulate cannabinoid receptor signaling and will guide its therapeutic exploitation. Most endocannabinoid metabolic enzymes (including DAGL $\alpha$ , DAGL $\beta$ , MGLL, FAAH, ABHD4, ABHD6, ABHD12) belong to the serine hydrolases family and can thus be studied by ABPP using the probes described in Figure 4. ABPP is anticipated to provide new insights in the regulation of the ECS by mapping the endocannabinoid metabolic enzymes in biological processes and facilitate ECS-related drug discovery.

## Aim and outline

*The aim of the research described in this thesis is to explore activity-based protein profiling (ABPP) as a versatile tool in drug discovery and cell biology.*

**Chapter 2** describes comparative ABPP as a tool for mapping the serine hydrolase activity profile in clinical samples from patients with terminal-stage heart failure (due to previous ischemic pathology). In **Chapter 3**, the comparative ABPP is method optimized for broad-spectrum profiling of serine hydrolases and kinases in zebrafish larvae during early zebrafish development. In addition, this chapter reports the use of zebrafish larvae as a pre-clinical animal model for *in vivo* target engagement and selectivity screening using FAAH inhibitor PF04457845 in a competitive ABPP setup. In **Chapter 4**, competitive ABPP is employed to investigate the *in vitro* and *in situ* interaction landscape of BIA 10-2474, the FAAH inhibitor that caused severe neurological adverse effects in a recent clinical trial<sup>77,78</sup>. In **Chapter 5**, the enzymes involved in 2-AG biosynthesis during neuronal differentiation are identified using retinoic acid (RA)-induced differentiation of Neuro-2a cells as a model system. A combined strategy of ABPP, CRISPR/Cas9 gene editing, biochemistry and lipidomics identifies ABHD6 as a 2-AG biosynthetic diacylglycerol lipase. **Chapter 6** summarizes the work described in this thesis and discusses the future perspective for ABPP in drug discovery and cellular biology.



## References

1. Borchardt, J. K. The Beginnings of Drug Therapy: Ancient Mesopotamian Medicine. *Drug News Perspect.* **15**, 187–192 (2002).
2. Klaeger, S. *et al.* The target landscape of clinical kinase drugs. *Science* **358**, eaan4368 (2017).
3. Scannell, J. W., Blanckley, A., Boldon, H. & Warrington, B. Diagnosing the decline in pharmaceutical R&D efficiency. *Nature Reviews Drug Discovery* **11**, 191–200 (2012).
4. Paul, S. M. *et al.* How to improve RD productivity: The pharmaceutical industry's grand challenge. *Nature Reviews Drug Discovery* **9**, 203–214 (2010).
5. Blass, B. E. *Basic principles of drug discovery and development.*
6. DiMasi, J. A., Hansen, R. W. & Grabowski, H. G. The price of innovation: New estimates of drug development costs. *J. Health Econ.* **22**, 151–185 (2003).
7. DiMasi, J. A., Grabowski, H. G. & Hansen, R. W. Innovation in the pharmaceutical industry: New estimates of R&D costs. *J. Health Econ.* **47**, 20–33 (2016).
8. David, E., Tramontin, T. & Zimmel, R. Pharmaceutical R&D: The road to positive returns. *Nat. Rev. Drug Discov.* **8**, 609–610 (2009).
9. Khanna, I. Drug discovery in pharmaceutical industry: Productivity challenges and trends. *Drug Discovery Today* **17**, 1088–1102 (2012).
10. Nicolaou, K. C. The chemistry-biology-medicine continuum and the drug discovery and development process in academia. *Chemistry and Biology* **21**, 1039–1045 (2014).
11. Eder, J., Sedrani, R. & Wiesmann, C. The discovery of first-in-class drugs: Origins and evolution. *Nat. Rev. Drug Discov.* **13**, 577–587 (2014).
12. Zheng, W., Thorne, N. & McKew, J. C. Phenotypic screens as a renewed approach for drug discovery. *Drug Discovery Today* **18**, 1067–1073 (2013).
13. Avior, Y., Sagi, I. & Benvenisty, N. Pluripotent stem cells in disease modelling and drug discovery. *Nature Reviews Molecular Cell Biology* **17**, 170–182 (2016).
14. MacRae, C. A. & Peterson, R. T. Zebrafish as tools for drug discovery. *Nat. Rev. Drug Discov.* **14**, 721–731 (2015).
15. Heath, J. R., Ribas, A. & Mischel, P. S. Single-cell analysis tools for drug discovery and development. *Nat. Publ. Gr.* **15**, (2015).
16. Tang, F. *et al.* mRNA-Seq whole-transcriptome analysis of a single cell. *Nat. Methods* **6**, 377–382 (2009).
17. Katsila, T., Spyroulias, G. A., Patrinos, G. P. & Matsoukas, M. T. Computational approaches in target identification and drug discovery. *Comput. Struct. Biotechnol. J.* **14**, 177–184 (2016).
18. Liu, Y., Patricelli, M. P. & Cravatt, B. F. Activity-based protein profiling: The serine hydrolases. *Proc. Natl. Acad. Sci.* **96**, 14694–14699 (1999).
19. Cravatt, B. F., Wright, A. T. & Kozarich, J. W. Activity-Based Protein Profiling: From Enzyme Chemistry to Proteomic Chemistry. *Annu. Rev. Biochem.* **77**, 383–414 (2008).
20. Moellering, R. E. & Cravatt, B. F. How chemoproteomics can enable drug discovery and development. *Chemistry and Biology* **19**, 11–22 (2012).
21. Rostovtsev, V. V., Green, L. G., Fokin, V. V. & Sharpless, K. B. A stepwise Huisgen cycloaddition process: Copper(I)-catalyzed regioselective 'ligation' of azides and terminal alkynes. *Angew. Chemie - Int. Ed.* **41**, 2596–2599 (2002).
22. Janssen, A. P. A. *et al.* Development of a Multiplexed Activity-Based Protein Profiling Assay to Evaluate Activity of Endocannabinoid Hydrolase Inhibitors. *ACS Chem. Biol.* **13**, 2406–2413 (2018).
23. Niphakis, M. J. & Cravatt, B. F. Enzyme Inhibitor Discovery by Activity-Based Protein Profiling. *Annu. Rev. Biochem.* **83**, 341–377 (2014).
24. van Rooden, E. J., Bakker, A. T., Overkleeft, H. S. & van der Stelt, M. Activity-Based Protein Profiling. *eLS* 1–9 (2018).

25. Baggelaar, M. P. *et al.* Chemical Proteomics Maps Brain Region Specific Activity of Endocannabinoid Hydrolases. *ACS Chem. Biol.* **12**, 852–861 (2017).
26. Nomura, D. K., Dix, M. M. & Cravatt, B. F. Activity-based protein profiling for biochemical pathway discovery in cancer. *Nature Reviews Cancer* **10**, 630–638 (2010).
27. van Rooden, E. J. *et al.* Chemical proteomic analysis of serine hydrolase activity in Niemann-Pick Type C mouse brain. *Front. Neurosci.* **12**, 440 (2018).
28. Van Esbroeck, A. C. M. *et al.* Activity-based protein profiling reveals off-target proteins of the FAAH inhibitor BIA 10-2474. *Science* **356**, 1084–1087 (2017).
29. Simon, G. M. & Cravatt, B. F. Activity-based proteomics of enzyme superfamilies: Serine hydrolases as a case study. *Journal of Biological Chemistry* **285**, 11051–11055 (2010).
30. Kato, D. *et al.* Activity-Based Probes that Target Diverse Cysteine Protease Families. *Nature Chemical Biology* **1**, 33–38 (2005).
31. Li, N. *et al.* Relative quantification of proteasome activity by activity-based protein profiling and LC-MS/MS. *Nat. Protoc.* **8**, 1155–1168 (2013).
32. Zhao, Q. *et al.* Broad-spectrum kinase profiling in live cells with lysine-targeted sulfonyl fluoride probes. *J. Am. Chem. Soc.* **139**, 680–685 (2017).
33. Wright, A. T. & Cravatt, B. F. Chemical Proteomic Probes for Profiling Cytochrome P450 Activities and Drug Interactions In Vivo. *Chem. Biol.* **14**, 1043–1051 (2007).
34. Vocadlo, D. J. & Bertozzi, C. R. A strategy for functional proteomic analysis of glycosidase activity from cell lysates. *Angew. Chemie - Int. Ed.* **43**, 5338–5342 (2004).
35. Kallemijn, W. W. *et al.* Novel activity-based probes for broad-spectrum profiling of retaining  $\beta$ -exoglucosidases in situ and in vivo. *Angew. Chemie - Int. Ed.* **51**, 12529–12533 (2012).
36. Geurink, P. P., Prely, L. M., Van Der Marel, G. A., Bischoff, R. & Overkleeft, H. S. Photoaffinity labeling in activity-based protein profiling. *Topics in Current Chemistry* **324**, 85–113 (2012).
37. Long, J. Z. & Cravatt, B. F. The metabolic serine hydrolases and their functions in mammalian physiology and disease. *Chem. Rev.* **111**, 6022–6063 (2011).
38. Bachovchin, D. A. & Cravatt, B. F. The pharmacological landscape and therapeutic potential of serine hydrolases. *Nat. Rev. Drug Discov.* **11**, 52–68 (2012).
39. Baggelaar, M. P. *et al.* Development of an activity-based probe and in silico design reveal highly selective inhibitors for diacylglycerol lipase- $\alpha$  in brain. *Angew. Chemie - Int. Ed.* **52**, 12081–12085 (2013).
40. Baggelaar, M. P. *et al.* Highly Selective, Reversible Inhibitor Identified by Comparative Chemoproteomics Modulates Diacylglycerol Lipase Activity in Neurons. *J. Am. Chem. Soc.* **137**, 8851–8857 (2015).
41. Ogasawara, D. *et al.* Rapid and profound rewiring of brain lipid signaling networks by acute diacylglycerol lipase inhibition. *Proc. Natl. Acad. Sci.* **113**, 26–33 (2016).
42. Tarkiainen, T. H. *et al.* Stability over time of short-term heart rate variability. *Clin. Auton. Res.* **15**, 394–399 (2005).
43. Manning, G., Whyte, D. B., Martinez, R., Hunter, T. & Sudarsanam, S. The protein kinase complement of the human genome. *Science* **298**, 1912–34 (2002).
44. Gaoni, Y. & Mechoulam, R. Isolation, Structure, and Partial Synthesis of an Active Constituent of Hashish. *J. Am. Chem. Soc.* **86**, 1646–1647 (1964).
45. Mechoulam, R. & Parker, L. A. The Endocannabinoid System and the Brain. *Annu. Rev. Psychol.* **64**, 21–47 (2012).
46. Di Marzo, V. Endocannabinoid signaling in the brain: biosynthetic mechanisms in the limelight. *Nat. Neurosci.* **14**, 9–15 (2011).
47. Herkenham, M. *et al.* Cannabinoid receptor localization in brain. *Proc. Natl. Acad. Sci.* **87**, 1932–1936 (1990).
48. Cabral, G. A. & Griffin-Thomas, L. Emerging role of the cannabinoid receptor CB 2 in immune regulation: Therapeutic prospects for neuroinflammation. *Expert Reviews in Molecular Medicine* **11**, e3 (2009).

49. Calignano, A., Rana, G. La, Giuffrida, A. & Piomelli, D. Control of pain initiation by endogenous cannabinoids. *Nature* **394**, 277–281 (1998).
50. Di Marzo, V. & Matias, I. Endocannabinoid control of food intake and energy balance. *Nat. Neurosci.* **8**, 585–589 (2005).
51. Pacher, P., Bátkai, S. & Kunos, G. The Endocannabinoid System as an Emerging Target of Pharmacotherapy. *Pharmacol. Rev.* **58**, 389–462 (2006).
52. Devane, W. A. *et al.* Isolation and structure of a brain constituent that binds to the cannabinoid receptor. *Science* **258**, 1946–1949 (1992).
53. Mechoulam, R. *et al.* Identification of an endogenous 2-monoglyceride, present in canine gut, that binds to cannabinoid receptors. *Biochem. Pharmacol.* **50**, 83–90 (1995).
54. Sugiura, T. *et al.* 2-arachidonoylglycerol: A possible endogenous cannabinoid receptor ligand in brain. *Biochemical and Biophysical Research Communications* **215**, 89–97 (1995).
55. Bisogno, T. *et al.* Cloning of the first sn1-DAG lipases points to the spatial and temporal regulation of endocannabinoid signaling in the brain. *J. Cell Biol.* **163**, 463–468 (2003).
56. Dinh, T. P., Freund, T. F. & Piomelli, D. A role for monoglyceride lipase in 2-arachidonoylglycerol inactivation. in *Chemistry and Physics of Lipids* **121**, 149–158 (2002).
57. Savinainen, J. R., Saario, S. M. & Laitinen, J. T. The serine hydrolases MAGL, ABHD6 and ABHD12 as guardians of 2-arachidonoylglycerol signalling through cannabinoid receptors. *Acta Physiologica* **204**, 267–276 (2012).
58. Marrs, W. R. *et al.* The serine hydrolase ABHD6 controls the accumulation and efficacy of 2-AG at cannabinoid receptors. *Nat. Neurosci.* **13**, 951–7 (2010).
59. Blankman, J. L., Simon, G. M. & Cravatt, B. F. A comprehensive profile of brain enzymes that hydrolyze the endocannabinoid 2-arachidonoylglycerol. *Chem. Biol.* **14**, 1347–1356 (2007).
60. Ueda, N., Tsuboi, K. & Uyama, T. Metabolism of endocannabinoids and related N-acyl ethanolamines: Canonical and alternative pathways. *FEBS J.* **280**, 1874–1894 (2013).
61. Cravatt, B. F. *et al.* Molecular characterization of an enzyme that degrades neuromodulatory fatty-acid amides. *Nature* **384**, 83–87 (1996).
62. McKinney, M. K. & Cravatt, B. F. Structure and function of Fatty Acid Amide Hydrolase. *Annu. Rev. Biochem.* **74**, 411–432 (2005).
63. Di Marzo, V., Stella, N. & Zimmer, A. Endocannabinoid signalling and the deteriorating brain. *Nat. Rev. Neurosci.* **16**, 30–42 (2015).
64. Montecucco, F. & Di Marzo, V. At the heart of the matter: The endocannabinoid system in cardiovascular function and dysfunction. *Trends in Pharmacological Sciences* **33**, 331–340 (2012).
65. Di Marzo, V., Bifulco, M. & De Petrocellis, L. The endocannabinoid system and its therapeutic exploitation. *Nature Reviews Drug Discovery* **3**, 771–784 (2004).
66. Di Marzo, V. Targeting the endocannabinoid system: To enhance or reduce? *Nature Reviews Drug Discovery* **7**, 438–455 (2008).
67. Christensen, R., Kristensen, P. K., Bartels, E. M., Bliddal, H. & Astrup, A. Efficacy and safety of the weight-loss drug rimonabant: a meta-analysis of randomised trials. *Lancet* **370**, 1706–1713 (2007).
68. Moreira, F. A. & Crippa, J. A. S. The psychiatric side-effects of rimonabant. *Rev. Bras. Psiquiatr.* **31**, 145–153 (2009).
69. Dhopeswarkar, A. & Mackie, K. CB2 Cannabinoid Receptors as a Therapeutic Target--What Does the Future Hold? *Mol. Pharmacol.* **86**, 430–437 (2014).
70. Abide Therapeutics. Abide Therapeutics Presents Positive Data from a Phase 1b Study of ABX-1431 in Tourette Syndrome at the American Academy of Neurology 70th Annual Meeting. Available at: <http://abidetx.com/news/abide-therapeutics-presents-positive-data-from-a-phase-1b-study-of-abx-1431-in-tourette-syndrome-at-the-american-academy-of-neurology-70th-annual-meeting/>. (Accessed: 28th January 2019)

71. Therapeutics, A. Abide Therapeutics Announces Initiation of Phase 2 Clinical Trial of ABX-1431 in Tourette Syndrome. Available at: <http://abidetx.com/news/abide-therapeutics-announces-initiation-of-phase-2-clinical-trial-of-abx-1431-in-tourette-syndrome/>. (Accessed: 28th January 2019)
72. Cisar, J. S. *et al.* Identification of ABX-1431, a Selective Inhibitor of Monoacylglycerol Lipase and Clinical Candidate for Treatment of Neurological Disorders. *J. Med. Chem.* **61**, 9062–9084 (2018).
73. Johnson, D. S. *et al.* Discovery of PF-04457845: A highly potent, orally bioavailable, and selective urea FAAH inhibitor. *ACS Med. Chem. Lett.* **2**, 91–96 (2011).
74. Li, G. L. *et al.* Assessment of the pharmacology and tolerability of PF-04457845, an irreversible inhibitor of fatty acid amide hydrolase-1, in healthy subjects. *Br. J. Clin. Pharmacol.* **73**, 706–716 (2012).
75. Huggins, J. P., Smart, T. S., Langman, S., Taylor, L. & Young, T. An efficient randomised, placebo-controlled clinical trial with the irreversible fatty acid amide hydrolase-1 inhibitor PF-04457845, which modulates endocannabinoids but fails to induce effective analgesia in patients with pain due to osteoarthritis of the. *Pain* **153**, 1837–1846 (2012).
76. National Institute of Health. Home - ClinicalTrials.gov. *U.S. National Library of Medicine* (2017). Available at: <https://www.clinicaltrials.gov/>. (Accessed: 28th January 2019)
77. Bégaud, B. *et al.* BIA 10-2474: Minutes of the Temporary Specialist Scientific Committee (TSSC) meeting on 'FAAH (Fatty Acid Amide Hydrolase) Inhibitors'. *Meet. Minutes* 1–14 (2016).
78. Kerbrat, A. *et al.* Acute Neurologic Disorder from an Inhibitor of Fatty Acid Amide Hydrolase. *N. Engl. J. Med.* **375**, 1717–1725 (2016).

# 2

## Activity-based protein profiling of the human ischemic heart

A.C.M. van Esbroeck  
Z.V. Varga  
X. Di  
E.J. van Rooden  
V.E. Toth  
Z. Onodi  
P. Leszek  
M. Kuśmierczyk  
P. Ferdinandy  
T. Hankemeier  
M. van der Stelt  
P. Pacher

**ABSTRACT** | Acute myocardial infarction and subsequent post-infarction heart failure are among the leading causes of mortality worldwide. Recently, the endocannabinoid system (ECS) has emerged as a critical modulator of cardiovascular disease, but the role of endocannabinoid metabolic enzymes had not been investigated thus far. Here, targeted lipidomics and activity-based protein profiling (ABPP) enabled investigation of the endocannabinoids and their metabolic enzymes in ischemic end-stage failing human hearts and non-failing controls. Based on lipidomics analysis, two subgroups were identified within the ischemic group; the first similar to control hearts and the second with decreased levels of the endocannabinoid 2-arachidonoyl-glycerol (2-AG) and drastically increased levels of the endocannabinoid anandamide (AEA), other *N*-acylethanolamines (NAEs) and free fatty acids. The altered lipid profile was accompanied by strong reductions in the activity of 13 hydrolases, including the 2-AG hydrolytic enzyme monoacylglycerol lipase (MGLL). These data suggest the presence of different biological states within the ischemic group, despite the lack of a clinical characteristic clearly distinguishing the patients. In addition, this study demonstrates ABPP as a tool to rapidly analyze enzyme activity in clinical samples, which may be valuable for drug-target and biomarker discovery.

## Introduction

Ischemic heart disease, involving acute myocardial infarction and subsequent heart failure development, was responsible for 12.7% of the total global mortality (2008), thereby making it the leading cause of mortality worldwide<sup>1</sup>. Recently, the endocannabinoid system (ECS) has emerged as a modulator of the cardiovascular system, especially under diseased conditions<sup>2–4</sup>. The ECS is comprised of the cannabinoid receptor type 1 and 2 (CB1R, CB2R), their endogenous ligands, the endocannabinoids 2-arachidonoylglycerol (2-AG) and anandamide (AEA), and their metabolic enzymes (Figure 1)<sup>5</sup>. Diacylglycerol lipase  $\alpha$  and  $\beta$  (DAGL $\alpha$ , DAGL $\beta$ ) are the two main 2-AG biosynthetic enzymes<sup>6</sup>. The majority of 2-AG is hydrolyzed to arachidonic acid (AA) by monoacylglycerol lipase (MGLL)<sup>7,8</sup>, but  $\alpha,\beta$ -hydrolase domain containing proteins 6 and 12 (ABHD6, ABHD12) hydrolyze 2-AG as well<sup>8–10</sup>. The existence of multiple *N*-acylethanolamine (NAE) metabolic pathways makes AEA biosynthesis more complex. Direct hydrolysis of *N*-acylphosphatidylethanolamines (NAPEs) to NAEs by NAPE phospholipase D (NAPE-PLD), is considered the canonical pathway<sup>11</sup>, but alternative multi-step pathways exist as well<sup>11</sup>. The NAEs are hydrolyzed to ethanolamines and free fatty acids by fatty acid amide hydrolase (FAAH)<sup>12,13</sup>. Of note, several other NAE species have been reported as bioactive lipids, suggesting an important modulatory role for this lipid class. For example, oleoylethanolamide (OEA) and stearoylethanolamide (SEA) have anorexic effects in the periphery<sup>14,15</sup> and palmitoylethanolamide (PEA) was reported to enhance antinociception<sup>16,17</sup>.

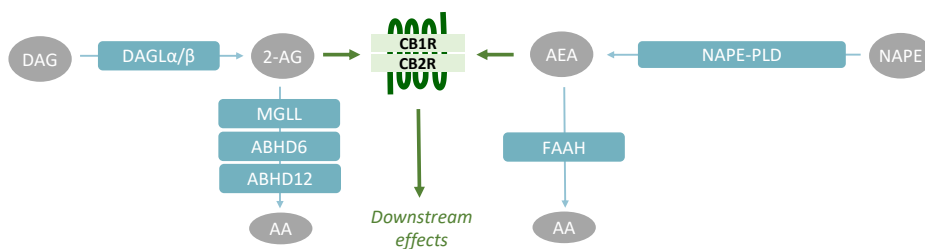


**Figure 1 | The endocannabinoid system.** The endocannabinoid system comprises of cannabinoid receptors type 1 and 2 (CB1R, CB2R), their endogenous ligands 2-arachidonoylglycerol (2-AG) and anandamide (AEA) and their metabolic enzymes: diacylglycerol lipase  $\alpha$  and  $\beta$  (DAGL $\alpha$ , DAGL $\beta$ ), monoacylglycerol lipase (MGLL),  $\alpha,\beta$ -hydrolase domain containing proteins 6 and 12 (ABHD6, ABHD12), *N*-acylphosphatidylethanolamine phospholipase D (NAPE-PLD), and fatty acid amide hydrolase (FAAH). Alternative multi-step pathways for AEA biosynthesis are not shown.

The ECS regulates a broad spectrum of physiological and pathological processes, including energy balance, obesity, pain, inflammation, neurological and immunological disorders<sup>18–20</sup>. In the cardiovascular system, the endocannabinoids are implicated in various contexts in receptor dependent and independent cardiac and vascular effects, including vasodilation and vasoconstriction, cardiac protection against atherogenic inflammation, depression of cardiac function, and cell death of cardiomyocytes and endothelial cells<sup>3,21–23</sup>. *In vivo* cardiovascular effects of the endocannabinoids may be exerted through the central and peripheral nervous system as well as through direct

effects on the myocardium and vasculature<sup>24,25</sup>. The two cannabinoid receptors have been shown to have opposing effects, e.g. CB1R facilitates the development of cardiometabolic disease and cardiac dysfunction<sup>3,26</sup>, whereas CB2R mainly exerts anti-inflammatory effects<sup>3,27,28</sup>.

CB1R-mediated endocannabinoid signaling has been implicated in the pathogenesis of shock, atherosclerosis, and numerous forms of cardiomyopathies (ischemic, diabetic, doxorubicin-induced)<sup>3,20</sup>. The beneficial *in vivo* effects of CB2R agonists in rodent models of myocardial infarction have primarily been attributed to limiting inflammatory cell infiltration<sup>27</sup>. FAAH knockout mice, having a threefold increase in myocardial AEA, displayed increased mortality, myocardial injury and neutrophil infiltration in experimental models of cardiomyopathy in a CB1R-dependent manner<sup>29</sup> and FAAH deficiency also enhanced intra-plaque neutrophil recruitment in atherosclerotic mice<sup>30</sup>. In obese humans, increased plasma levels of AEA and 2-AG strongly correlated with impaired coronary endothelial function and adverse cardiovascular events<sup>31,32</sup>. In epicardial fat from ischemic human hearts, CB1R was upregulated, accompanied by down-regulation of CB2R and FAAH<sup>33</sup>. Similar upregulation of CB1R was observed in atherosclerotic coronary artery sections from patients with unstable angina and in obese human subjects<sup>34</sup>. In the Chinese Han population, a G1359A polymorphism in the CB1R gene was also linked to coronary artery disease<sup>35</sup>. These findings strongly suggest that the primary cardiovascular effects of endocannabinoids are deleterious and CB1R-mediated. Nonetheless, endocannabinoids have also been shown to exert protective effects in the heart via CB1R/CB2R-independent mechanisms, mostly based on *ex vivo* and indirect studies<sup>27</sup>.

Despite extensive investigation on the endocannabinoids and their receptors in cardiac (dys)function, only little is known about the endocannabinoid metabolic enzymes. Most endocannabinoid metabolic enzymes, with the exception of NAPE-PLD, belong to the serine hydrolase family. This protein class can be targeted by activity-based probes covalently interacting with their catalytic serine residue. Activity-based probes are used in chemical proteomics to assess the functional state of an entire enzyme classes in complex biological samples<sup>36–38</sup>. In this study, the endocannabinoid metabolic enzymes were evaluated in ischemic end-stage failing human hearts and non-failing controls by chemical proteomics.

## Results & Discussion

To investigate the involvement of the ECS in cardiac ischemia, tissue from the left ventricle was obtained from patients with terminal-stage heart failure (due to previous ischemic pathology) indicated for heart transplantation, as well as from non-failing control hearts (n=6, Table 1). The expression levels of ECS-related proteins in control and ischemic failing hearts were determined by quantitative real-time polymerase chain reaction (qRT-PCR) (Figure 2). CB1R (*CNR1*) expression strongly increased in half of the ischemic samples, however the overall increase was not significant (p=0.08). Reduced expression of the 2-AG biosynthetic enzyme DAGL $\beta$  and the 2-AG hydrolytic enzymes MGLL and ABHD6 was observed in the ischemic tissue. The AEA metabolic enzymes were not significantly altered, nor was CB2R (*CNR2*) expression.

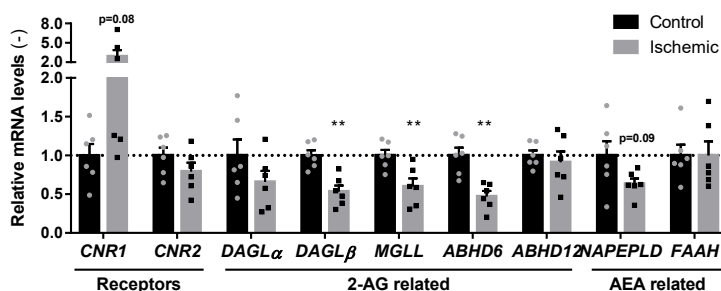


**Figure 2 | Quantitative PCR on ECS-related genes in cardiac ischemia.** mRNA levels of endocannabinoid related genes were normalized to house-keeping gene hypoxanthine-guanine phosphoribosyltransferase (*HPRT*) expression and expressed relative to control (mean  $\pm$  SEM, two-tailed *t*-test: \*\* *p* < 0.01).

In light of the altered mRNA expression of ECS-related enzymes, the endocannabinoid levels in control and ischemic failing cardiac tissues were compared. Lipids were extracted from a second set of cardiac tissues (n=9, Table 1) and were analyzed by liquid chromatography coupled to mass spectrometry (LC-MS) (Figure 3, Supplementary Figure S1A). NAEs, free fatty acids (FFA) and cortisol (COR) were included in the assay. The NAEs and their related FFA levels had strongly increased in the ischemic failing tissues (Figure 3, Supplementary Figure S1B). However, based on their lipid profile, the ischemic samples could be categorized into two separate subgroups. The first (Ischemic 1: I1-I3, I8-I9) had a lipid profile similar to control for most lipids including the endocannabinoids. Only several lipids were increased, including *N*-docosahexaenoyl ethanolamide (DHEA), eicosapentaenoyl ethanolamide (EPEA),  $\alpha$ - and  $\gamma$ -linoleic acid ( $\alpha$ -LA and  $\gamma$ -LA) (maximum fold-change: 2.8). In contrast, all NAE and FFA levels were increased with a fold change ranging from 4 to 120 in the second subgroup (Ischemic 2: I4-I7) as compared to controls. In addition, the endocannabinoid AEA was increased by a  $31 \pm 13$ -fold, while 2-AG was significantly reduced by a 5-fold in this subgroup.



**Table 1 | Clinical characteristics of study populations.** Values are given as mean  $\pm$  SEM. Set A: Figure 2. Set B: Figures 3-5. NYHA: New York Heart Association (3.5 is included in class IV), LVED: left ventricular end-diastolic diameter, LVSD: left ventricular end-systolic diameter, PW: posterior wall-thickness, IVS: interventricular septum thickness; SVR: systemic vascular resistance, CO: cardiac output, BMI: body mass index, n.a.: not applicable. Subgroups Ischemic 1 and 2 (set B) were compared by two-tailed *t*-test: \*  $p < 0.05$  \*\*\*  $p < 0.001$ .

	Control Set A	Ischemic Set A	Control Set B H1-9	Ischemic Set B I1-9	Ischemic 1 Set B I1-3, 8-9	Ischemic 2 Set B I4-7
<b>Samples (n)</b>	6	6	9	9	5	4
<b>Gender (female/male)</b>	1 / 5	1 / 5	2 / 7	9	5	4
<b>Age (year)</b>	34.7 $\pm$ 4.5	56.2 $\pm$ 4.1	37.8 $\pm$ 3.8	58.0 $\pm$ 2.7	60.4 $\pm$ 2.5	55.0 $\pm$ 5.5
<b>BMI (kg/m<sup>2</sup>)</b>	26.0 $\pm$ 5.0	26.1 $\pm$ 2.3	25.2 $\pm$ 1.3	26.6 $\pm$ 1.1	28.7 $\pm$ 1.2	24.0 $\pm$ 1.0 *
<b>NYHA functional class I/II/III/IV (n)</b>	n.a.	0/1/2/3	n.a.	0/1/5/3	0/1/2/2	0/0/3/1
<b>CO (L/min)</b>	n.a.	3.9 $\pm$ 0.6	n.a.	4.0 $\pm$ 0.21	4.5 $\pm$ 0.1	3.4 $\pm$ 0.2 ***
<b>LVED (mm)</b>	n.a.	69.2 $\pm$ 2.5	n.a.	75.0 $\pm$ 3.2	70.2 $\pm$ 3.6	81.0 $\pm$ 4.4
<b>LVSD (mm)</b>	n.a.	63.0 $\pm$ 3.2	n.a.	67.8 $\pm$ 4.5	62.3 $\pm$ 6.7	73.3 $\pm$ 5.5
<b>PW (mm)</b>	n.a.	9.1 $\pm$ 0.7	n.a.	8.4 $\pm$ 0.8	9.8 $\pm$ 1.0	6.7 $\pm$ 0.5 *
<b>IVS (mm)</b>	n.a.	8.4 $\pm$ 1.1	n.a.	9.5 $\pm$ 0.7	10.2 $\pm$ 1.2	8.7 $\pm$ 0.6
<b>SVR (mmHg·min/L)</b>	n.a.	18.3 $\pm$ 1.8	n.a.	19.0 $\pm$ 2.2	15.1 $\pm$ 2.5	23.8 $\pm$ 2.2 *

Increased AEA levels have been reported in the past e.g. due to various forms of ischemia/reperfusion (I/R) (e.g. hepatic, brain). In the liver, I/R increased 2-AG and AEA levels positively correlated with tissue damage markers such as tumor necrosis factor  $\alpha$  (TNF- $\alpha$ ), but inflammatory stimuli *per se* only increased AEA levels<sup>39</sup>. NAE levels have also been shown to drastically increase post-mortem<sup>40</sup> and in infarcted myocardium<sup>41-44</sup>, thus suggesting the observed effects may be related to the extent of tissue injury. Of note, there were no obvious differences in clinical characteristics (gender, age, comorbidity, recent ischemic events, etc.) between the two ischemic subgroups. Nonetheless, cardiac function in the second subgroup was more severely affected based on significantly decreased cardiac output (CO) and increased systemic vascular resistance (SVR) (Table 2). In addition, the body mass index (BMI) of the second subgroup was significantly lower than that of the first subgroup; however, it was not significantly different from controls.

Next, the activity of the ECS metabolic enzymes was investigated by activity-based protein profiling (ABPP). The tissue was lysed by dounce homogenization and clear lysates were labeled with fluorescent activity-based probes (Figure 4), which enabled visualization of probe targets by sodium dodecyl sulfate polyacrylamide gel electrophoresis (SDS-PAGE) and in-gel fluorescence scanning. FP-TAMRA, a broad spectrum serine hydrolase probe fluorophosphonate-rhodamine (FP-TAMRA), labels ABHD6, MGLL, and FAAH amongst many other hydrolases<sup>36,38</sup>. The tailored lipase probe MB064 preferentially reacts with the DAGL $\alpha$ , DAGL $\beta$ , ABHD6, and ABHD12<sup>37,45</sup>. Probes DH379<sup>46</sup> and DH463 enabled more selective the labeling of DAGL/ABHD6 and MGLL respectively.

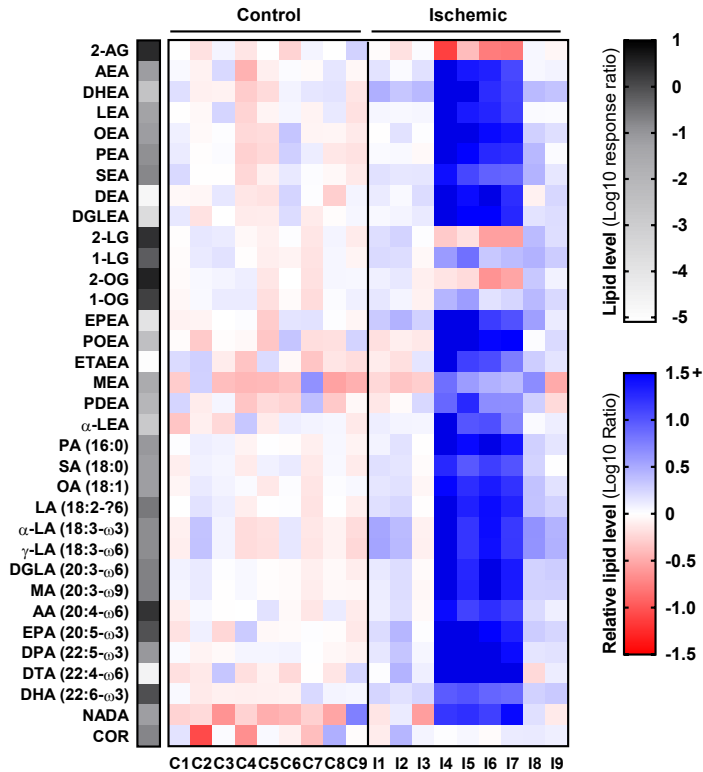


**Figure 3 | Ischemic heart tissues can be categorized into subgroups based on divergent lipid profiles.** Heatmap summary of lipid analysis of healthy (control) and ischemic cardiac tissue. Lipid levels were normalized to tissue weight and are expressed as mean response ratio of controls (grayscale, log10) or relative to mean control (red-blue scale, log10 ratio). Detailed lipid characteristics in Table 3.

In total, more than 20 hydrolases were labeled, including MGLL (33 and 35 kDa) (Figure 4). The overall hydrolase activity in ischemic samples I4-I7 (\*, subgroup 2 based on lipid profile) was reduced as compared to the remaining ischemic samples and controls for which only limited deviations in labeling were observed. In addition, MGLL activity and expression were nearly abolished in I4-7 (Figure 4B, D, F). However, there were no obvious differences in the overall protein staining (Figure 4E) and general post-mortem degradation by autolysis thus appears unlikely. Interestingly, an additional band was observed in the activity profile of samples I4-I7 (Figure 4B, indicated with #). Of note, the other ECS metabolic hydrolases, including DAGL $\alpha$  (~120 kDa), DAGL $\beta$  (~70 kDa), ABHD6 (~35 kDa), and FAAH (~60 kDa) were not detected (Figure 4A, C), even though ABHD6 activity was detected in murine myocardium in the past<sup>47</sup>.

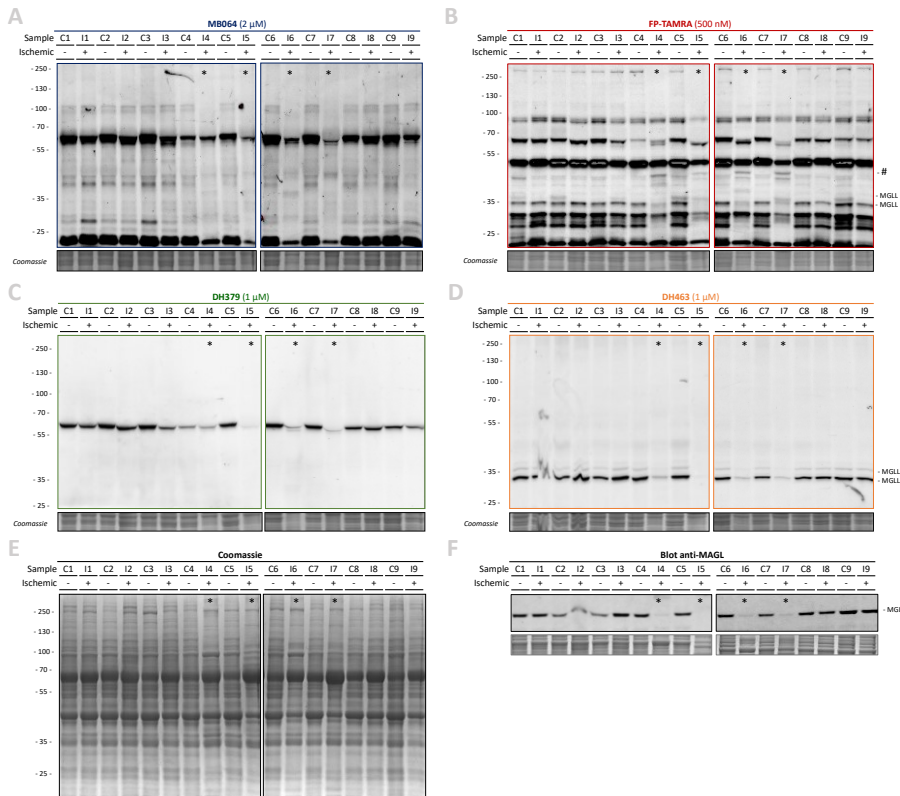


**Figure 4 | Activity-based protein profiling of healthy and ischemic human hearts.** (A-D) Gel-based ABPP analysis of healthy (control) and ischemic cardiac tissue. Whole lysates were labeled with activity-based probes (20 min, rt), resolved by SDS-PAGE and in-gel fluorescence was detected. Coomassie served as a protein loading control. (A)  $\beta$ -lactone probe MB064 (2  $\mu$ M). (B) Broad-spectrum hydrolase probe FP-TAMRA (500 nM). (C) DAGL-probe DH379 (1  $\mu$ M). (D) MAGL-probe DH459 (1  $\mu$ M). (E) Coomassie staining. (F) Western-blot using anti-MGLL (1:200, O/N, 4  $^{\circ}$ C) verified MGLL expression. \* Denotes samples with overall reduced serine hydrolase labeling.

The biotinylated counterparts of FP-TAMRA and MB064, FP-biotin and MB108 respectively, were then used for target identification by mass spectrometry-based chemical proteomics (Figure 5). In total, 31 hydrolases were identified, including MGLL as the only ECS-related hydrolase (Figure 5A, Supplementary Table S1). A slight, but non-significant, upregulation of CES1, NCEH1, and DPP4 was observed in the ischemic group, as well as downregulation of several hydrolases, including MGLL (Figure 5B). Strikingly, separation of the ischemic samples into two subgroups (based on lipid profile, Figure 3) revealed that 13 hydrolase activities, including MGLL, were drastically and significantly reduced in the subgroup with an altered lipid profile (Ischemic 2, Figure 5C). Hydrolase activities from the first subgroup, however, were not significantly altered. Notably, not all hydrolase activities were affected in the second subgroup and the extent of activity reduction is different between the altered hydrolases. This reinforces the hypothesis that the observed alterations in these samples are indeed not artefacts resulting from a general process such as post-mortem autolysis.

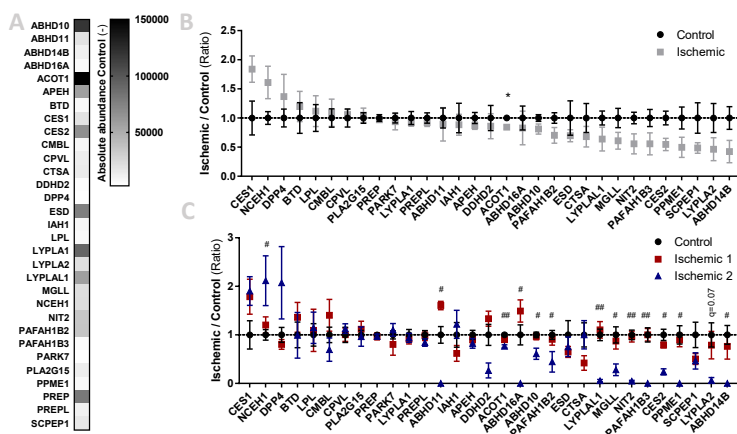


**Figure 5 | Activity-based proteomics on healthy and ischemic heart tissues.** (A-C) Lysates from healthy (control) and ischemic cardiac tissues were labeled with MB108 and FP-biotin (10  $\mu$ M each, 30 min, 37  $^{\circ}$ C) and analyzed by mass-spectrometry. A pre-boiled sample (10% SDS, 100  $^{\circ}$ C, 5 min) served as negative control. (A) Heatmap summary of mean abundance of hydrolases from control tissues. (B) Hydrolase activity relative to mean control. Data is expressed as mean  $\pm$  SEM (n=9), *t*-test with Benjamini-Hochberg correction: \* *q* < 0.05. (C) Hydrolase activity relative to mean control, ischemic samples categorized in subgroups. Data is expressed as mean  $\pm$  SEM (control n=9, ischemic 1 n=5, ischemic 2 n=4), *t*-test with Benjamini-Hochberg correction. Control versus ischemic 1: not significant; control versus ischemic 2: # *q* < 0.05, ## *q* < 0.01.

Taken together, lipidomics and ABPP enabled the identification of a subgroup within the ischemic sample set, which showed drastic increases in NAE and FFA levels, whereas many hydrolase activities had decreased. Aside from MGLL, no endocannabinoid metabolic enzymes were detected, possibly due to instability or inactivity as a result of tissue preparation. Despite accurate sample handling, differences in the sample collection procedure cannot be excluded as a potential cause for the observed subgroups. In addition, therapeutic interventions or unknown clinical factors may separate the ischemic tissues from one another. Nonetheless these data demonstrated that ABPP can be used for the rapid analysis of serine hydrolases in clinical samples. In the future, this technique may aid in the discovery of drug targets or biomarkers.

## Conclusion

In summary, an MS-based approach was used to investigate the endocannabinoids and their metabolic enzymes in cardiac ischemia using ischemic end-stage failing hearts and non-failing controls. Targeted lipidomics analysis revealed the existence of two subgroups within the ischemic samples; the first largely similar to controls and the second with decreased 2-AG and increased AEA, NAE and FFA levels. The altered lipid profile was accompanied by a strong reduction in the activity of multiple hydrolases, including the 2-AG hydrolytic enzyme MGLL. These data suggested the presence of different biological states within the ischemic group, possibly the extent of tissue injury, despite the lack of a clinical characteristic separating the patients other than cardiac damage. In addition, this study demonstrated ABPP as a tool to rapidly assess clinical samples which may be valuable in drug-target and biomarker discovery.

## Experimental procedures

### Materials and probes

Activity-based fluorophosphonate-based probes FP-TAMRA and FP-biotin were purchased from ThermoFisher and Santa Cruz biotechnology respectively. MB064 and MB108 were synthesized in-house as previously described<sup>45</sup>. All synthesized compounds were at least 95% pure and were analyzed by LC-MS, NMR and HRMS. Other chemicals, reagents, and primers were purchased from Sigma Aldrich unless indicated otherwise.

### Ethical statement

All experimental procedures were done in accordance with the ethical standards of the responsible institutional and national committee on human experimentation, adhering to the Helsinki Declaration (1975). Written informed consent was obtained from all patients involved in the study according to the protocol approved by the Local Ethics Committees of the Institute of Cardiology, Warszawa, Poland (IK-NP-0021-24/1426/14).

### Sample collection and preparation

Healthy (control) human hearts were obtained from organ donor patients (n=6/9) whose hearts were not used for transplantation due to technical reasons (e.g. donor/recipient incompatibility). The donors did not have any relevant previous cardiological history or any abnormalities in ECG and echocardiography (left ventricle dimensions/contractility within normal ranges). Explanted failing hearts were obtained from patients suffering from end-stage advanced heart failure of ischemic etiology (n=6/9).

Sample collection was performed as previously described<sup>48</sup>. In brief, human tissue samples were taken at the time of heart explantation (avoiding scarred, fibrotic, or adipose tissue, endocardium, epicardium, or coronary vessels). The samples were rinsed immediately in saline, blotted dry, frozen in liquid nitrogen, powdered with a pestle and mortar in liquid nitrogen and stored in cryovials at -80 °C until further analysis.

### Quantitative real-time PCR

#### *RNA isolation*

Total RNA was isolated from left ventricular samples (n = 6) with a chloroform/isopropanol precipitation method. In brief, Qiazol® (Qiagen) was added to each sample and homogenized with TissueLyser (Qiagen). Homogenates were centrifuged and DNA and protein were precipitated from the clean upper phase with chloroform. Total RNA was precipitated with isopropanol and pellets were washed twice with ethanol (VWR). Finally, total RNA was resuspended in nuclease-free water, and RNA concentration was determined by spectrophotometry (NanoDrop, Thermo Fischer Scientific).

#### *cDNA synthesis*

cDNA was synthesized from 1 µg total RNA by Sensifast cDNA synthesis kit (Bioline) according to the manufacturers protocol. cDNA was diluted 20 times with RNase-free water. qRT-PCR reactions were performed on a LightCycler® 480 II instrument (Roche) by using SensiFAST SYBR Green master mix (Bioline). Polymerase was heat-activated for 2 min at 95 °C and targets were amplified and quantified in 40 cycles (denaturation: 5 s at 93 °C; annealing: 10 s at 60 °C; synthesis: 20 s at 72 °C). Forward and reverse primers for the fatty acid amide hydrolase (*FAAH*), cannabinoid receptor 1 (*CNR1*), cannabinoid receptor 2 (*CNR2*), diacylglycerol lipase  $\alpha$  (*DAGL $\alpha$* ), diacylglycerol lipase  $\beta$  (*DAGL $\beta$* ), monoacylglycerol lipase (*MGLL*), *N*-acylphosphatidylethanolamine

phospholipase D (*NAPEPLD*),  $\alpha/\beta$ -hydrolase domain-containing 6 (*ABHD6*),  $\alpha/\beta$ -hydrolase domain-containing 12 (*ABHD12*) were used for analysis. Hypoxanthine-guanine phosphoribosyltransferase (*HPRT*) was used as a housekeeping gene. Results were calculated with  $2^{-\Delta\Delta C_p}$  evaluation method. Primer sequences are shown in Table 2.

Table 2 | qPCR primers.

Gene	Accession number	Product (bp)	Primer	Primer Sequence
<i>CNR1</i>	NM_016083.5	363	Forward	CCTTTTGCTGCCTAAATCCAC
			Reverse	CCACTGCTCAAACATCTGAC
<i>CNR2</i>	NM_001841.3	71	Forward	CCTTTTGCTGCCTAAATCCAC
			Reverse	AACAACCTGGGACTCCTCAGC
<i>DAGLA</i>	NM_006133.3	130	Forward	TGCTCTTCGGCCTGGTCTAT
			Reverse	CGCATGCTCAGCCAGATGAT
<i>DAGLB</i>	NM_139179.4	161	Forward	GAGTGCTGTGGTGGATTGGC
			Reverse	TCTCATGCTGACACACATGA
<i>MGLL</i>	NM_007283.6	162	Forward	CAAGGCCTCATCTTTGTGT
			Reverse	ACGTGGAAGTCAGACACTAC
<i>ABHD6</i>	NM_001320126.1	86	Forward	AGACATGTTGGCCAAGTCAA
			Reverse	TCCTGGGTCTTTCCATCACT
<i>ABHD12</i>	NM_001042472.2	232	Forward	TATTGGAGTCTGGCACAC
			Reverse	TGTTCTACTGAGTCACC
<i>NAPEPLD</i>	NM_001122838.1	178	Forward	GAAGCTGGCTTAAGAGTCAC
			Reverse	CCGCATCTATTGGAGGGAGT
<i>FAAH</i>	NM_000194.3	66	Forward	GCCTCAAGGAATGCTTCAGC
			Reverse	TGCCCTCATTCAGGCTCAAG
<i>HRPT</i>	NM_001441.2	192	Forward	TGCTCGAGATGTGATGAAGG
			Reverse	TCCCTGTTGACTGGTCATT

## Targeted lipidomics

### Lipid extraction

Lipid extraction was performed as previously described<sup>49</sup>, with minor adaptations. In brief, ~50 mg tissue was weighed into a pre-cooled 1.5 mL Eppendorf tube and reconstituted in ice-cold ammonium acetate buffer (0.1 M, pH 4) (4  $\mu$ L/mg tissue). The tissue was finely cut using surgical scissors and subsequently homogenized by probe sonication (3 cycles, 10 s, 30% amplitude) while kept on ice. Samples were spiked with 10  $\mu$ L of deuterated internal standard mix (Table 1). After extraction with 1000  $\mu$ L methyl *tert*-butyl ether (MTBE), the tubes were thoroughly mixed for 5 min using a bullet blender (Next Advance) at medium speed, followed by a centrifugation step (16,000 *g*, 5 min, 4 °C). Next, 850  $\mu$ L of the upper MTBE layer was transferred to clean 1.5 mL Eppendorf tube. Samples were dried in a speedvac (Eppendorf) followed by reconstitution in acetonitrile:water (50  $\mu$ L, 90:10, v/v). The reconstituted samples were centrifuged (16,000 *g*, 5 min, 4 °C) before transferring into LC-MS vials. 5  $\mu$ L of each sample was injected into the LC-MS/MS system.

### LC-MS/MS analysis

LC-MS/MS analysis was performed as previously described<sup>49</sup>, with minor adaptations. A targeted analysis of 31 compounds, including endocannabinoids and related *N*-acylethanolamines (NAEs) along with the fatty acids (Table 2), was measured using an Acquity UPLC I class Binary solvent manager pump (Waters) in conjugation with AB SCIEX 6500 quadrupole-ion trap (AB Sciex). The separation was performed with an Acquity HSS T3 column (1.2  $\times$  100 mm, 1.8  $\mu$ m) maintained at 45 °C. The aqueous mobile phase A consisted of 2 mM ammonium formate and 10 mM formic acid, and the organic mobile phase B was acetonitrile. The flow rate was set

to 0.55 mL/min; initial gradient conditions were 55% B held for 2 min and linearly ramped to 100% B over 6 min and held for 2 min; after 10 s the system returned to initial conditions and held 2 min next injection. Electrospray ionization-MS and a selective Multiple Reaction Mode (MRM) was used for endocannabinoid quantification. Individually optimized MRM transitions using their synthetic standards for target compounds and internal standards are described in Table 3.

Table 3 | LC-MS Standards and internal standards for lipidomics analysis.

Standards				
Abbreviation	Metabolite	Q1	Q3	Polarity
1&2-AG	2&1-Arachidonoylglycerol (20:4)	379	287	+
AEA	Anandamide (20:4)	348	62	+
DHEA	N-docosahexaenoylethanolamide (22:6)	372	62	+
LEA	N-linoleylethanolamide (18:2)	324	62	+
NADA	N-arachidonoyl dopamine (28:4)	440	137	+
OEA	N-oleoylethanolamide (18:1)	326	62	+
PEA	N-palmitoylethanolamide (16:0)	300	62	+
SEA	N-stearoylethanolamide (18:0)	328	62	+
2-AGE	2-arachidonyl glycerol ether (20:4)	365	273	+
DEA	N-docosatetraenoylethanolamide (22:4)	376	62	+
DGLEA	Dihomo-γ-linolenylethanolamide (18:3)	350	62	+
O-AEA	O-arachidonoyleethanolamine (20:4)	348	62	+
2-LG	2-Linoleoyl glycerol (18:2)	355	263	+
1-LG	1-Linoleoyl glycerol (18:2)	355	263	+
2-OG	2-Oleoyl glycerol (18:1)	357	265	+
EPEA	Eicosapentaenoyl ethanolamide (20:5)	346	62	+
POEA	N-palmitoleoylethanolamide (16:1)	298	62	+
ETAEA	Eicosatrienoic acid ethanolamide (20:3)	350	62	+
PDEA	N-pentadecanoylethanolamide (15:0)	286	62	+
α-LEA	N-α-linolenylethanolamide (18:2)	322	62	+
OA	Oleic acid (18:1)	281	263	-
LA	Linoleic acid (18:2-ω6)	279	261	-
α-LA	α-linolenic acid (18:3-ω3)	277	233	-
γ-LA	γ-linolenic acid (18:3-ω6)	277	233	-
DGLA	Dihomo-γ-linolenic acid (20:3-ω6)	305	261	-
MA	Mead acid (20:3-ω9)	305	261	-
AA	Arachidonic acid (20:4-ω6)	303	259	-
EPA	Eicosapentaenoic acid (20:5-ω3)	301	257	-
DTA	Docosatetraenoic acid (22:4-ω6)	332	288	-
DHA	Docosahexaenoic acid (22:6-ω3)	327	283	-
Internal Standards				
Abbreviation	Metabolite	Q1	Q3	Polarity
2-AG (20:4)-d8	2-Arachidonoylglycerol-d8	387	294	+
PEA (16:0)-d4	Palmitoyl ethanolamide-d4	304	62	+
SEA (18:0)-d3	Stearoyl ethanolamide-d3	331	62	+
OEA (18:1)-d4	Oleoyl ethanolamide-d4	330	66	+
LEA (18:2)-d4	Linoleoyl ethanolamide-d4	328	66	+
AEA (20:4)-d8	Arachidonoyl ethanolamide-d8	356	62	+
DHEA (22:6)-d4	Docosahexaenoyl ethanolamide-d4	376	66	+
NADA (28:4)-d8	N-Arachidonoyl dopamine-d8	448	137	+

## Activity-based protein profiling

### *Sample preparation*

Cardiac tissue was dounce homogenized in ice-cold lysis buffer (250 mM sucrose, 20 mM HEPES pH 7.2, 2 mM DTT, 1 mM MgCl<sub>2</sub>, 2 U/mL benzonase) and incubated on ice (15 min). Clear lysate was obtained as the supernatant fraction after two low-speed centrifugation steps (2500 *g*, 5 min, 4 °C). After dilution to 2 mg/mL in storage buffer (20 mM HEPES pH 7.2, 2 mM DTT), samples were used or flash frozen in liquid nitrogen and stored at -80 °C until further use.

### *Gel-based ABPP*

Clear lysates (2 mg/mL) were incubated with activity-based probes MB064 (2 μM), FP-TAMRA (500 nM), DH379 (1 μM) or DH463 (1 μM) (20 min, rt). The reaction was quenched with Laemmli buffer (30 min, rt) and 20 μg protein was resolved by SDS-PAGE (10% acrylamide gel, ~80 min, 180 V) along with protein marker (PageRuler™ Plus, Thermo Fisher). In-gel fluorescence was measured in the Cy2, Cy3 and Cy5 channels (ChemiDoc™ MP, Bio-Rad) and gels were stained with Coomassie after scanning. Fluorescence was quantified and normalized to Coomassie staining using ImageLab™ software (Bio-Rad).

### *Chemical proteomics with label-free quantification*

The chemical proteomics workflow was modified from a previously published protocol<sup>150</sup>. In short, for general profiling of the serine hydrolases the clear lysates (250 μg protein, 1 mg/mL) were incubated with serine hydrolase probe cocktail (10 μM MB108, 10 μM FP-Biotin, 30 min, 37 °C, 300 rpm). A denatured protein sample (1% SDS, 5 min, 100 °C) was taken along as a negative control. Precipitation, alkylation, avidin enrichment, on-bead digestion and sample preparation was performed according to protocol. Dried peptides were stored at -20 °C until LC-MS analysis. Prior to measurement, samples were reconstituted in 50 μL LC-MS solution and transferred to LC-MS vials. LC-MS data was analyzed by ProteinLynx Global SERVER™ (PLGS, Waters) and IsoQuant software<sup>51</sup> ([www.proteomeumb.org/MZw.html](http://www.proteomeumb.org/MZw.html)) (minimal peptide score 6, false discovery rate 1%). Excel was used for further analysis, with the following cut-offs: false discovery rate 1%, unique peptides ≥ 1, identified peptides ≥ 2, ratio positive over negative control ≥ 2, part of putative hydrolase target list. Graphs were created using GraphPad Prism 7 (GraphPad).

## Western blot

Clear lysates (2 mg/mL) were denatured with Laemmli buffer (5 min, 100 °C) and 45 μg lysate was resolved by SDS-PAGE (10% acrylamide gel, 65 min, 200V) along with PageRuler™ Plus Protein Marker (Thermo Scientific). Proteins were transferred to 0.2 μm polyvinylidene difluoride membranes by Trans-Blot Turbo™ Transfer system (Bio-Rad). Membranes were washed with TBS (50 mM Tris, 150 mM NaCl) and blocked with 5% milk in TBS-T (50 mM Tris, 150 mM NaCl, 0.05% Tween 20) (1 h, rt). Membranes were then incubated with primary antibody rabbit-anti-MAGL (ab24701, Abcam, 1:200 in 5% milk in TBS-T, O/N, 4 °C) washed with TBS-T, incubated with secondary donkey-anti-rabbit Alexa647 (A-31573, Thermo Fisher; 1:10000 in 5% milk TBS-T, 1 h, rt), and washed with TBS-T and TBS. Fluorescence was detected on the ChemiDoc™ MP (Bio-Rad) in the Alexa647 channel, and Cy3/Cy5 channels for the protein marker.

## Statistical methods

Statistical significance was determined by a Student's *t*-test (two-tailed, unpaired)(*p*-values) with Benjamini-Hochberg false discovery rate (FDR 10%, *q*-values) for lipidomics and proteomics data using GraphPad Prism 7 (GraphPad) software. Samples were compared to (mean) healthy controls and significance is indicated as \* < 0.05, \*\* < 0.01, \*\*\* < 0.001.



## Supplementary data

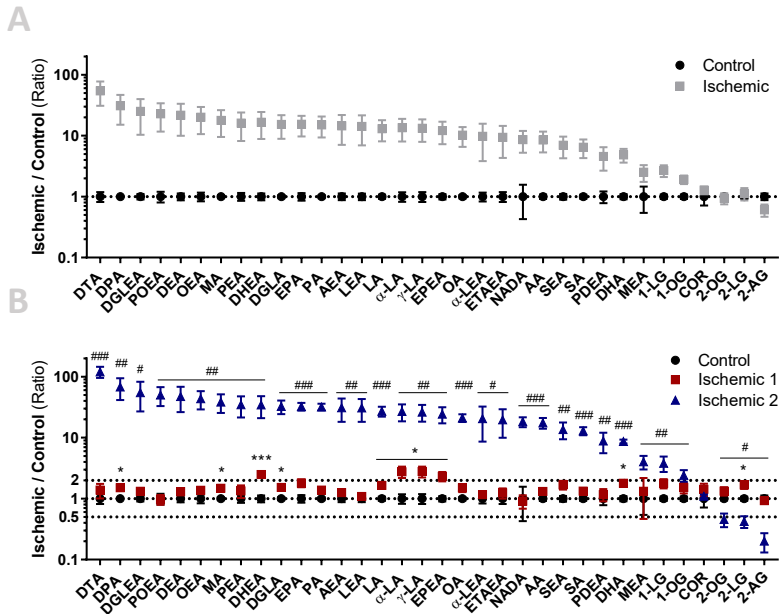


**Figure S1 | Targeted lipidomics of healthy and ischemic heart tissues reveals subgroups in ischemic samples.** Lipids were extracted from control and ischemic cardiac tissue, followed by targeted lipidomics analysis. Lipid levels were normalized to tissue weight and are expressed relative to mean control. **(A)** Lipid levels relative to mean control. Data is expressed as mean  $\pm$  SEM (n=9), *t*-test with Benjamini-Hochberg correction for multicomparison: not significant. **(B)** Lipid levels relative to mean control, ischemic samples categorized in subgroups. Data is expressed as mean  $\pm$  SEM (control: n=9, ischemic 1: n=5, ischemic 2: n=4), *t*-test with Benjamini-Hochberg correction for multicomparison. \*  $q < 0.05$ , \*\*\*  $q < 0.001$  (control vs. ischemic 1), #  $q < 0.05$ , ##  $q < 0.01$ , ###  $q < 0.001$  (control vs. ischemic 2).

**Table S1 | Identified hydrolase targets in human cardiac tissue.** Abbreviations and descriptions as annotated on uniprot.org.

Protein	Description
ABHD10	Mycophenolic acid acyl-glucuronide esterase, mitochondrial ( $\alpha,\beta$ -hydrolase domain containing protein 10)
ABHD11	Protein ABHD11 ( $\alpha,\beta$ -hydrolase domain containing protein 11)
ABHD14b	Protein ABHD14b ( $\alpha,\beta$ -hydrolase domain containing protein 14b)
ABHD16a	Protein ABHD16a ( $\alpha,\beta$ -hydrolase domain containing protein 16a)
ACOT1	Acyl-coenzyme A thioesterase 1
APEH	Acylamino-acid-releasing enzyme (acyl-peptide hydrolase)
BTD	Biotinidase
CES1	Liver carboxylesterase 1 (carboxylesterase 1)
CES2	Cocaine esterase (carboxylesterase 2)
CMBL	Carboxymethylenebutenolidase homolog
CPVL	Probable serine carboxypeptidase CPVL (Carboxypeptidase, vitellogenic-like)
CTSA	Lysosomal protective protein (cathepsin A)
DDHD2	Phospholipase DDHD2 (DDHD domain-containing protein 2)
DPP4	Dipeptidyl peptidase 4
ESD	S-formylglutathione hydrolase
IAH1	Isoamyl acetate-hydrolyzing esterase 1 homolog
LPL	Lipoprotein lipase
LYPLA1	Acyl-protein thioesterase 1 (Lysophospholipase 1)
LYPLA2	Acyl-protein thioesterase 2 (Lysophospholipase 2)
LYPLAL1	Lysophospholipase-like protein 1
MGLL	Monoglyceride lipase (monoacylglycerol lipase)
NCEH1	Neutral cholesterol ester hydrolase 1
NIT2	Omega-amidase NIT2
PAFAH1b2	Platelet-activating factor acetylhydrolase IB subunit beta
PAFAH1b3	Platelet-activating factor acetylhydrolase IB subunit gamma
PARK7	Protein DJ-1 (Protein/nucleic acid deglycase DJ-1, parkinson disease protein 7)
PLA2G15	Group XV phospholipase A2
PPME1	Protein phosphatase methylesterase 1
PREP	Prolyl endopeptidase
PREPL	Propyl endopeptidase-like
SCPEP1	Retinoid-inducible serine carboxypeptidase (Serine carboxypeptidase 1)

## References

1. Finegold, J. A., Asaria, P. & Francis, D. P. Mortality from ischaemic heart disease by country, region, and age: Statistics from World Health Organisation and United Nations. *Int. J. Cardiol.* **168**, 934–945 (2013).
2. O'Sullivan, S. E. in *Endocannabinoids* 393–422 (Springer, Cham, 2015).
3. Pacher, P., Steffens, S., Haskó, G., Schindler, T. H. & Kunos, G. *Cardiovascular effects of marijuana and synthetic cannabinoids: The good, the bad, and the ugly.* *Nature Reviews Cardiology* **15**, 151–166 (Nature Publishing Group, 2018).
4. Pacher, P. *et al.* Modulation of the endocannabinoid system in cardiovascular disease: therapeutic potential and limitations. *Hypertens.* **52**, 601–7 (2008).
5. Di Marzo, V. Endocannabinoid signaling in the brain: biosynthetic mechanisms in the limelight. *Nat. Neurosci.* **14**, 9–15 (2011).
6. Bisogno, T. *et al.* Cloning of the first sn1-DAG lipases points to the spatial and temporal regulation of endocannabinoid signaling in the brain. *J. Cell Biol.* **163**, 463–468 (2003).
7. Dinh, T. P., Freund, T. F. & Piomelli, D. A role for monoglyceride lipase in 2-arachidonoylglycerol inactivation. in *Chemistry and Physics of Lipids* **121**, 149–158 (2002).
8. Savinainen, J. R., Saario, S. M. & Laitinen, J. T. The serine hydrolases MAGL, ABHD6 and ABHD12 as guardians of 2-arachidonoylglycerol signalling through cannabinoid receptors. *Acta Physiologica* **204**, 267–276 (2012).
9. Marrs, W. R. *et al.* The serine hydrolase ABHD6 controls the accumulation and efficacy of 2-AG at cannabinoid receptors. *Nat. Neurosci.* **13**, 951–7 (2010).
10. Blankman, J. L., Simon, G. M. & Cravatt, B. F. A comprehensive profile of brain enzymes that hydrolyze the endocannabinoid 2-arachidonoylglycerol. *Chem. Biol.* **14**, 1347–1356 (2007).
11. Ueda, N., Tsuboi, K. & Uyama, T. Metabolism of endocannabinoids and related N-acyl ethanolamines: Canonical and alternative pathways. *FEBS J.* **280**, 1874–1894 (2013).
12. Cravatt, B. F. *et al.* Molecular characterization of an enzyme that degrades neuromodulatory fatty-acid amides. *Nature* **384**, 83–87 (1996).
13. McKinney, M. K. & Cravatt, B. F. Structure and function of Fatty Acid Amide Hydrolase. *Annu. Rev. Biochem.* **74**, 411–432 (2005).
14. Rodríguez De Fonseca, F. *et al.* An anorexic lipid mediator regulated by feeding. *Nature* **414**, 209–212 (2001).
15. Terrazzino, S. *et al.* Stearoyl ethanolamide exerts anorexic effects in mice via downregulation of liver stearoyl-coenzyme A desaturase-1 mRNA expression. *FASEB J.* **18**, 1580–1582 (2004).
16. Calignano, A., Rana, G. La, Giuffrida, A. & Piomelli, D. Control of pain initiation by endogenous cannabinoids. *Nature* **394**, 277–281 (1998).
17. Jaggar, S. I., Hasnie, F. S., Sellaturay, S. & Rice, A. S. . The anti-hyperalgesic actions of the cannabinoid anandamide and the putative CB2 receptor agonist palmitoylethanolamide in visceral and somatic inflammatory pain. *Pain* **76**, 189–199 (1998).
18. Mechoulam, R. & Parker, L. A. The Endocannabinoid System and the Brain. *Annu. Rev. Psychol.* **64**, 21–47 (2012).
19. Di Marzo, V., Bifulco, M. & De Petrocellis, L. The endocannabinoid system and its therapeutic exploitation. *Nature Reviews Drug Discovery* **3**, 771–784 (2004).
20. Pacher, P., Bátkai, S. & Kunos, G. The Endocannabinoid System as an Emerging Target of Pharmacotherapy. *Pharmacol. Rev.* **58**, 389–462 (2006).
21. Hiley, C. R. Endocannabinoids and the heart. *Journal of Cardiovascular Pharmacology* **53**, 267–276 (2009).
22. Montecucco, F. & Di Marzo, V. At the heart of the matter: The endocannabinoid system in cardiovascular function and dysfunction. *Trends in Pharmacological Sciences* **33**, 331–340 (2012).

23. Pacher, P. & Kunos, G. Modulating the endocannabinoid system in human health and disease - successes and failures. *FEBS J.* **280**, 1918–1943 (2013).
24. Bátkai, S. & Pacher, P. Endocannabinoids and cardiac contractile function: Pathophysiological implications. *Pharmacological Research* **60**, 99–106 (2009).
25. Pacher, P., Bátkai, S. & Kunos, G. Cardiovascular pharmacology of cannabinoids. *Handb. Exp. Pharmacol.* 599–625 (2005).
26. Valenta, I. *et al.* Feasibility Evaluation of Myocardial Cannabinoid Type 1 Receptor Imaging in Obesity: A Translational Approach. *JACC Cardiovasc. Imaging* **11**, 320–332 (2018).
27. Steffens, S. & Pacher, P. Targeting cannabinoid receptor CB2 in cardiovascular disorders: promises and controversies. *Br. J. Pharmacol.* **167**, 313–323 (2012).
28. Pacher, P. & Mechoulam, R. Is lipid signaling through cannabinoid 2 receptors part of a protective system? *Progress in Lipid Research* **50**, 193–211 (NIH Public Access, 2011).
29. Mukhopadhyay, P. *et al.* Fatty acid amide hydrolase is a key regulator of endocannabinoid-induced myocardial tissue injury. *Free Radic. Biol. Med.* **50**, 179–195 (2011).
30. Lenglet, S. *et al.* Fatty Acid Amide Hydrolase Deficiency Enhances Intraplaque Neutrophil Recruitment in Atherosclerotic Mice. *Arterioscler. Thromb. Vasc. Biol.* **33**, 215–223 (2013).
31. Quercioli, A. *et al.* Coronary Vasomotor Control in Obesity and Morbid Obesity. *JACC Cardiovasc. Imaging* **5**, 805–815 (2012).
32. Quercioli, A. *et al.* Elevated endocannabinoid plasma levels are associated with coronary circulatory dysfunction in obesity. *Eur. Heart J.* **32**, 1369–1378 (2011).
33. Cappellano, G. *et al.* Different Expression and Function of the Endocannabinoid System in Human Epicardial Adipose Tissue in Relation to Heart Disease. *Can. J. Cardiol.* **29**, 499–509 (2013).
34. Sugamura, K. *et al.* Activated Endocannabinoid System in Coronary Artery Disease and Antiinflammatory Effects of Cannabinoid 1 Receptor Blockade on Macrophages. *Circulation* **119**, 28–36 (2009).
35. Liu, R. & Zhang, Y. G1359A polymorphism in the cannabinoid receptor-1 gene is associated with coronary artery disease in the Chinese Han population. *Clin. Lab.* **57**, 689–93 (2011).
36. Niphakis, M. J. & Cravatt, B. F. Enzyme Inhibitor Discovery by Activity-Based Protein Profiling. *Annu. Rev. Biochem.* **83**, 341–377 (2014).
37. Baggelaar, M. P. *et al.* Highly Selective, Reversible Inhibitor Identified by Comparative Chemoproteomics Modulates Diacylglycerol Lipase Activity in Neurons. *J. Am. Chem. Soc.* **137**, 8851–8857 (2015).
38. Liu, Y., Patricelli, M. P. & Cravatt, B. F. Activity-based protein profiling: The serine hydrolases. *Proc. Natl. Acad. Sci.* **96**, 14694–14699 (1999).
39. Bátkai, S. *et al.* Cannabinoid-2 receptor mediates protection against hepatic ischemia/reperfusion injury. *FASEB J.* **21**, 1788–1800 (2007).
40. Schmid, P. C. *et al.* Occurrence and postmortem generation of anandamide and other long-chain *N*-acylethanolamines in mammalian brain. *FEBS Lett.* **375**, 117–120 (1995).
41. Epps, D. E., Schmid, P. C., Natarajan, V. & Schmid, H. H. O. *N*-Acylethanolamine accumulation in infarcted myocardium. *Biochem. Biophys. Res. Commun.* **90**, 628–33 (1979).
42. Epps, D. E., Natarajan, V., Schmid, P. C. & Schmid, H. H. O. Accumulation of *N*-acylethanolamine glycerophospholipids in infarcted myocardium. *Biochim. Biophys. Acta (BBA)/Lipids Lipid Metab.* **618**, 420–430 (1980).
43. Natarajan, V., Reddy, P. V., Schmid, P. C. & Schmid, H. H. O. On the biosynthesis and metabolism of *N*-acylethanolamine phospholipids in infarcted dog heart. *Biochim. Biophys. Acta (BBA)/Lipids Lipid Metab.* **664**, 445–448 (1981).
44. Natarajan, V., Reddy, P. V., Schmid, P. C. & Schmid, H. H. O. *N*-acylation of ethanolamine phospholipids in canine myocardium. *Biochim. Biophys. Acta (BBA)/Lipids Lipid Metab.* **712**, 342–355 (1982).

45. Baggelaar, M. P. *et al.* Development of an activity-based probe and in silico design reveal highly selective inhibitors for diacylglycerol lipase- $\alpha$  in brain. *Angew. Chemie - Int. Ed.* **52**, 12081–12085 (2013).
46. Ogasawara, D. *et al.* Rapid and profound rewiring of brain lipid signaling networks by acute diacylglycerol lipase inhibition. *Proc. Natl. Acad. Sci.* **113**, 26–33 (2016).
47. Janssen, A. P. A. *et al.* Development of a Multiplexed Activity-Based Protein Profiling Assay to Evaluate Activity of Endocannabinoid Hydrolase Inhibitors. *ACS Chem. Biol.* **13**, 2406–2413 (2018).
48. Varga, Z. V. *et al.* Alternative splicing of NOX4 in the failing human heart. *Front. Physiol.* **8**, 935 (2017).
49. Kantae, V. *et al.* Endocannabinoid tone is higher in healthy lean South Asian than white Caucasian men. *Sci. Rep.* **7**, (2017).
50. van Rooden, E. J. *et al.* Mapping in vivo target interaction profiles of covalent inhibitors using chemical proteomics with label-free quantification. *Nat. Protoc.* **13**, 752–767 (2018).
51. Liao, Z., Wan, Y., Thomas, S. N. & Yang, A. J. IsoQuant: A software tool for stable isotope labeling by amino acids in cell culture-based mass spectrometry quantitation. *Anal. Chem.* **84**, 4535–4543 (2012).



# 3

A.C.M. van Esbroeck  
A.F. Stevens  
V. Kantae  
L.T. Lelieveld  
E.J. van Rooden  
B.I. Florea  
R.C. van Wijk  
A.C. Harms  
P.H. van der Graaf  
J.M.F.G. Aerts  
T. Hankemeier  
H.S. Overkleeft  
M. van der Stelt

## Applications of activity-based protein profiling in developing zebrafish

**ABSTRACT** | The zebrafish (*Danio rerio*) is increasingly used as a pre-clinical vertebrate model in drug discovery and development. Here, an activity-based protein profiling (ABPP) method for broad-spectrum profiling of serine hydrolases and kinases in zebrafish larvae is presented. ABPP coupled to mass spectrometry analysis enabled the identification and mapping of 45 hydrolases and 51 kinases throughout early zebrafish development (0-5 days post fertilization), showing a variety of activity profiles. As an application, fatty acid amide hydrolase (FAAH) inhibitor PF04457845 was used in a competitive ABPP setup. FAAH2a was the only inhibited hydrolase among the hydrolases detected by chemical proteomics and downstream inhibition effects were confirmed by lipidomics analysis. With the increasing popularity of zebrafish as a vertebrate animal model and their use in phenotypic drug discovery, the combined approach of comparative and competitive ABPP may serve as a valuable tool in the drug discovery process, complementary to existing methods.

## Introduction

The zebrafish (*Danio rerio*) is a popular model system for embryonic development<sup>1,2</sup> and is increasingly used as a pre-clinical vertebrate model in drug discovery<sup>3,4</sup>. The zebrafish is evolutionary more distinct from humans than rodents are. Nonetheless, 71% of all human proteins and 82% of all disease-causing proteins have zebrafish orthologues<sup>5</sup>. Pharmacological effects of compounds are often conserved, as active sites or ligand binding domains tend to be more homologous<sup>3</sup>. A variety of genetic modification strategies in zebrafish has facilitated the generation of disease models, closely mimicking human diseases. Combined with several other advantages, including small size, rapid development, optical transparency and cost-effective use, the zebrafish is considered an attractive model organism, which is complementary to existing rodent models<sup>6</sup>. Its use has paved the way to whole-animal (semi-)high-throughput screening in phenotypic target discovery and toxicological screening<sup>6-8</sup>. However, target identification and target engagement studies remain challenging. Most biochemical zebrafish studies, especially in embryonic development, rely on protein<sup>9,10</sup> and gene expression<sup>11,12</sup> profiles. Despite the fact that gene and protein expression do not directly translate to protein activity, the activity profile is often not taken into account and the enzymatic state of a protein is not considered.

Activity-based protein profiling (ABPP) may aid in gaining a more complete view on the early development of the zebrafish and may help establish its validity as a model organism in the drug discovery process. ABPP uses active-site directed probes to assess the functional state of an entire enzyme class in a complex protein sample. Fluorescent reporter tags enable rapid sample analysis by sodium dodecyl sulfate polyacrylamide gel electrophoresis (SDS-PAGE) and in-gel fluorescence scanning, whereas affinity tags can be used for target enrichment and subsequent identification by mass spectrometry (MS)<sup>13,14</sup>. The method can be used for inhibitor profiling in a competitive setup. It enables target engagement studies and provides information on the selectivity profile of small molecule modulators within the investigated protein class<sup>15,16</sup>. Alternatively, a comparative setup can be used to map the activity landscape of different biological samples or states<sup>17</sup>, e.g. different stages of development, which may enable discovery of biological markers and drug targets<sup>15</sup>.

Two important protein classes, the serine hydrolases and kinases, can be targeted by activity-based probes. The serine hydrolases represent approximately 1% of all proteins in mammals and are characterized by a well conserved GXSXG amino acid motif and are involved in a broad spectrum of physiological processes, including signaling and metabolism<sup>14</sup>. Their active-site serine can interact covalently with fluorophosphonate (FP)-based and  $\beta$ -lactone-based probes, such as FP-rhodamine (FP-TAMRA)<sup>14,15</sup> and MB064<sup>18,19</sup>. The kinases, a large protein family with over 500 members, are known for their pivotal roles in cell signaling processes, differentiation, proliferation, and disease<sup>20,21</sup>. A conserved lysine in the kinase active-site offers a reactive group for kinase-targeting probes such as XO44<sup>22</sup>. This probe contains an alkyne moiety which



serves as a ligation handle to introduce a reporter group via a copper(I)-catalyzed azide-alkyne cycloaddition (“click” chemistry)<sup>23</sup>. Serine hydrolases and kinases have been demonstrated as drug targets by successful development of inhibitors and their therapeutic use in various diseases, including cancer, inflammation and Alzheimer’s<sup>24,25</sup>. For example, PF04457845, a fatty acid amide hydrolase inhibitor (FAAH), has entered clinical trials for the treatment of neurological disorders<sup>26,27</sup> and kinase inhibitors such as Imatinib and Dasatinib are powerful drugs in cancer treatment<sup>28</sup>.

In this study, a comparative ABPP assay was developed to map the serine hydrolase and kinase activity landscape during early zebrafish development (0-5 days post fertilization (dpf)). The assay was subsequently used in a competitive ABPP setup, using PF04457845 as a model drug. PF04457845 targets FAAH<sup>27,29</sup>, a membrane-bound serine hydrolase that degrades the endocannabinoid anandamide (AEA) and related amidated lipids<sup>30–33</sup>. Treatment of zebrafish larvae with PF04457845 enabled rapid mapping of the *in vivo* inhibitor interaction profile in a similar fashion as was reported for *in vitro* and *in situ* model systems<sup>16</sup>.

## Results & Discussion

### Comparative ABPP: Mapping zebrafish development

ABPP has previously been used to map the serine hydrolase landscape e.g. in mouse tissue<sup>17</sup>. Here, an ABPP assay was developed to facilitate the use of zebrafish larvae. It was anticipated that the number of proteins expressed would increase over the course of development. Therefore, clear lysate, membrane, and cytosol fractions were prepared from a large batch of 5 dpf larvae and fractions were analyzed by gel-based ABPP using hydrolase probes MB064 and FP-TAMRA (Figure 1A). Extensive labeling was observed, but band overlap impeded band identification by competitive ABPP (data not shown). Chemical proteomics with their biotinylated counterparts, MB108 and FP-biotin respectively, resulted in the identification of 61 different hydrolases (Figure 1B, Supplementary Table S1), of which 46, 33, and 48 were found in the lysate, cytosol, and membrane fractions respectively. Targets were identified as those having  $\geq 2$ -fold enrichment as compared to heat-inactivated controls and a peptide count  $\geq 2$  with at least 1 unique peptide. In addition, targets were filtered against a putative probe-target list developed for human/mouse-based experiments<sup>34</sup> and zebrafish gene homologues were included. Several of the enriched targets contained a serine hydrolase motif (GXSG)<sup>35</sup>, but were not part of the putative hydrolase target list. These hydrolases are indicated as additional zebrafish targets (Supplementary Table S1).

Several members of the  $\alpha,\beta$ -hydrolase domain containing protein (ABHD) family were detected, as well as a variety of carboxylic ester hydrolases (CEL, CES), and members of the endocannabinoid metabolic pathways such as monoacylglycerol lipase (MGLL) and the fatty acid amide hydrolases (FAAH, FAAH2a, FAAH2b). Of note, even though whole-animal proteomic analysis provides a rapid general overview of the

activity profile, poorly abundant proteins or tissue-specific activities may be lost in the proteomic analysis.

To increase sample throughput and improve experimental ease, the profiling process was streamlined by reducing sample size and simplifying sample preparation. Whole lysates were prepared from samples containing a varying number of larvae per replicate. Inconsistent labeling was observed in the gel-based assay when a single larva was used, whereas using 5 larvae was sufficient to obtain a reproducible labeling pattern between biological replicates (data not shown). The optimized assay conditions were employed in a comparative ABPP setup and enabled assessment of the hydrolase activity landscape throughout development. Larvae were obtained immediately after fertilization at 1, 2, 3, 4 or 5 dpf (5 larvae/replicate). Gel-based analysis of whole lysates labeled with MB064 and FP-TAMRA revealed that both the number of hydrolases and the activity of most hydrolases increased over time (Figure 2). Similarly, coomassie staining showed an overall increase in the number of proteins from 1 dpf onwards. Vitellogenin, one of the main constituents of the yolk sac, was observed as two thick bands at 70 and 120 kDa that decreased over time, in accordance with the use of the yolk as nutrient source<sup>1</sup>.

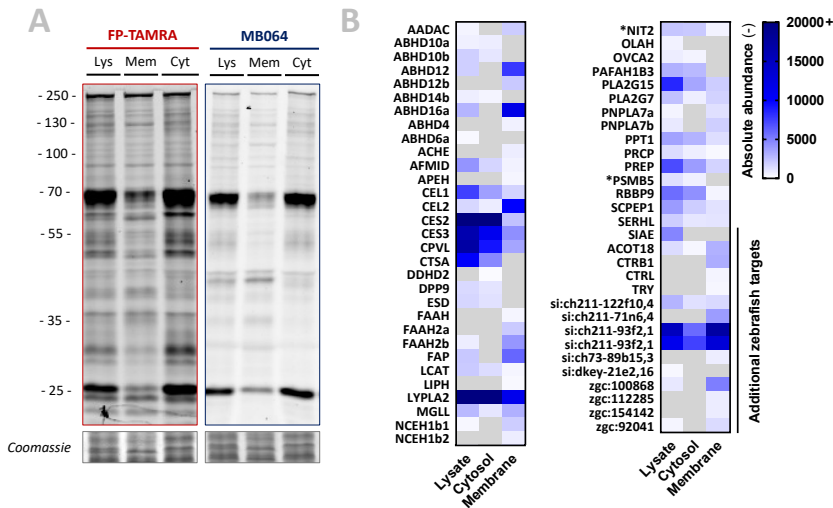


**Figure 1 | The serine hydrolase activity profile in zebrafish larvae (5 dpf).** Clear lysate (lys), membrane (mem) and cytosol (cyt) fractions from zebrafish larvae (5 dpf) were analyzed by gel-based ABPP and chemical proteomics. **(A)** Proteins were labeled with MB064 (2  $\mu$ M) or FP-TAMRA (500 nM) (20 min, 28  $^{\circ}$ C) and 10  $\mu$ g protein was resolved by SDS-PAGE. Coomassie served as a protein loading control. **(B)** Samples (200  $\mu$ g protein) were labeled with FP-Biotin and MB108 (10  $\mu$ M each, 30 min, 28  $^{\circ}$ C) and analyzed by chemical proteomics. Absolute abundance is summarized in a heat map (blue scale), proteins that were not detected are depicted in grey (n=3). Targets with a non-serine nucleophile are indicated with \*, additional zebrafish targets contain a GXSG motif but were not included in the putative hydrolase target list.

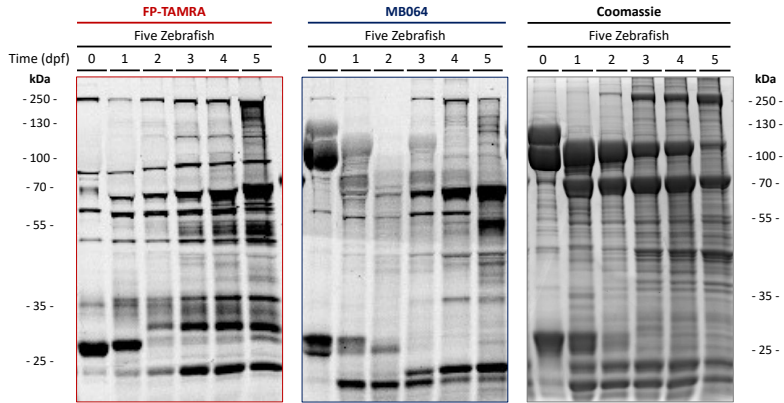


**Figure 2 | Comparative ABPP analysis of serine hydrolases during embryonic development.** Whole lysate of zebrafish larvae from different development stages (0-5 dpf, 5 larvae/sample) was labeled with FP-TAMRA (500 nM) or MB064 (2  $\mu$ M) (20 min, 28  $^{\circ}$ C) and resolved by SDS-PAGE. Coomassie served as a protein loading control.

Next, chemical proteomics was used to identify the hydrolase targets. Whole lysates (5 larvae/replicate, 0-5 dpf) were labeled with probes MB108 and FP-biotin and analyzed by LC-MS after affinity purification and trypsin-digestion (Figure 3A, Supplementary Figure S1, Supplementary Table S1). In total, 45 hydrolases were identified. In line with the gel-based data, the number of hydrolases detected increased over time, as well as their activity.

The activity of several hydrolases coincided with development of the organs in which they are generally highly expressed. For example, a rapid increase in carboxylic esterase 2 and 3 (CES2, CES3) and arylacetamide deacetylase (AADAC) abundance was observed from day 3 on (Figure 3). *ces2*, *ces3* and *aadac* are generally highly expressed in the liver<sup>36,37</sup>, of which the growth phase (> 2 dpf)<sup>38</sup> coincides with the increase in CES and AADAC activity as observed by ABPP. Similarly, activity of the pancreatic enzymes chymotrypsin (*zgc:92041*)<sup>36,37</sup> and carboxylic ester hydrolase 1 and 2 (CEL.1, CEL.2)<sup>36,37</sup> appeared at the end of pancreatic development (> 3 dpf)<sup>39</sup>.

Several other hydrolases (including acylaminoacyl-peptide hydrolase (APEH), S-formylglutathione hydrolase (ESD), OVCA2 esterase (OVCA2) and platelet-activating factor acetylhydrolase isoform 1b gamma subunit (PAFAH1b3)) had a more constant activity. Their reported (gene) expression is more uniform across different tissue types<sup>36,37</sup>, thus making their activity profiles less sensitive to development of a specific tissue type.

FAAH2b showed the most outstanding activity profile, as it was the only hydrolase which had a reduction in activity during development. FAAH2b is one of the metabolic enzymes in the endocannabinoid system. This system is responsible for the physiological effects of cannabis and is involved in a number of biological processes. In an mRNA-based study, *faah2b* expression was detected directly after fertilization, followed by a

rapid reduction and recovery at 4-5 dpf<sup>40</sup>. High FAAH2b activity levels during fertilization may be required for the hydrolysis of the endocannabinoid AEA and other *N*-acylethanolamines (NAEs). Functional cannabinoid receptors present in the sperm can be activated upon AEA release from female follicle fluids or eggs, thereby hampering fertilization<sup>41,42</sup>. Therefore, rapid degradation of AEA may be beneficial in the fertilization process.

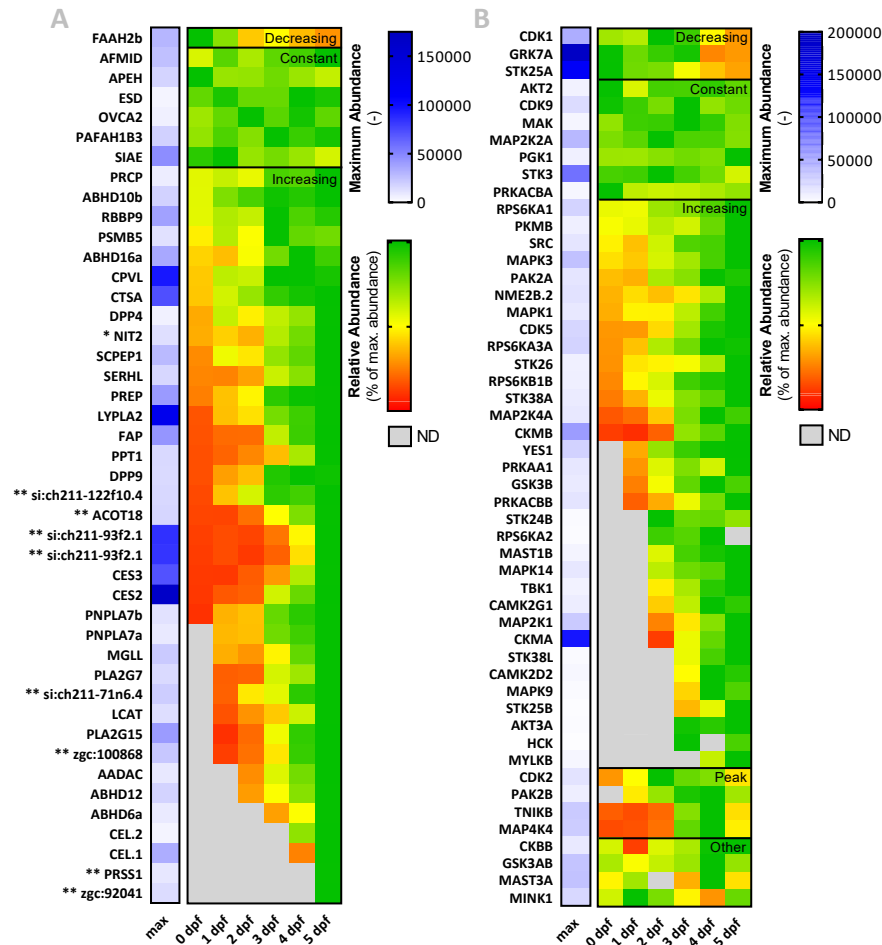


**Figure 3 | Serine hydrolase and kinase activity landscape during zebrafish development (0-5 dpf).** Heatmap summary of activity-based proteomics of (serine) hydrolases (A) and kinases (B). (A) Zebrafish whole lysates from different development stages (0-5 dpf, 5 larvae/sample) were treated with MB108 and FP-Biotin (10  $\mu$ M each, 30 min, 28  $^{\circ}$ C), followed by chemical proteomics analysis. \* Indicates targets with a non-serine nucleophile, \*\* indicates additional zebrafish targets containing a GX SXG motif, which were not included in the putative hydrolase target list. (B) Zebrafish whole lysates from different development stages (0-5 dpf, 5 larvae/sample) were treated with XO44 (10  $\mu$ M, 60 min, 28  $^{\circ}$ C) and conjugated to biotin-azide (40  $\mu$ M, 60 min, 28  $^{\circ}$ C), followed by chemical proteomics analysis. (A-B) Data is represented as absolute abundance at the time point with maximum abundance (blue scale) (individual data points in Supplementary Figure S1-2). Relative abundance is expressed as a percentage of maximum abundance per protein (green-red scale) or as not detected (grey) (mean, n=6). Outliers as determined by ROUT's outlier test (5%) have been excluded from calculations.

Several other endocannabinoid metabolic enzymes were also detected including the 2-arachidonoyl glycerol (2-AG) hydrolytic enzymes MGLL, ABHD12 and ABHD6a, starting at 1, 2 and 3 dpf, respectively, and increased over time. A similar increase in mRNA expression has been observed for *abhd6a*<sup>43</sup>. In contradiction with the chemical proteomics data, *mgll* expression peaked at 8 hpf, but was stably expressed from 1 dpf onward, while *abhd12* expression decreased from 2 dpf onwards in the same study<sup>43</sup>. Thus, gene expression and protein activity are not always directly correlated.

The ABPP assay was extended with kinase targeting probe XO44<sup>22</sup>, which interacts with a well-conserved reactive lysine in the kinase active site (Figure 3B, Supplementary Figure S2, Supplementary Table S2). Lysates were incubated with the probe, which was subsequently conjugated to a biotin reporter to enable enrichment and proteomic analysis. In total, 51 kinases were identified, having  $\geq 2$ -fold enrichment as compared to vehicle-treated controls, a peptide count  $\geq 2$  and at least 1 unique peptide. In addition, targets (or their human orthologues) had to be annotated as kinases in the Uniprot protein database. Of note, in contrast to the hydrolase probes, XO44 labels available kinase active-sites dependent on their affinity, but not necessarily on their active state.

The number of detected kinases increased throughout development and in general their abundance increased time dependently. For example, cyclin dependent kinase 5 (CDK5), serine/threonine kinase 38a (STK38A) and mitogen-activated protein kinase 1 and 3 (MAPK1, MAPK3) abundance steadily increased over time from fertilization onward. However, also different labeling profiles were observed. STK25B and MAPK14, for example, were detected at later stages and increased from there on, while STK24B remained stable once expressed. In contrast, STK25A decreased time dependently from 0 dpf onwards and CDK1 was stably expressed until 3 dpf and subsequently reduced.

A more distinct labeling profile was observed for p21 protein (CDC42/rac)-activated kinase 2b (PAK2b) and CDK2 which peaked at 3-4 dpf and 2 dpf respectively. Brain-subtype creatine kinase (CKBB) was abundant after fertilization, followed by a strong decrease at 1 dpf and a subsequent recovery and increase. These profiles suggest tight regulation of activity throughout the embryonic phase and may be related to important developmental processes. In human embryonic stem cells CDK2 plays a crucial role in balancing cell proliferation and cell death. Its downregulation induces a loss of pluripotency as well as differentiation toward extraembryonic lineages<sup>44</sup>. The function of PAK2b, or its human homologue PAK2, in development has not yet been described.

Several kinases also showed a steady abundance over time, which may indicate a more general role or a less tight regulation. For example, the metabolic kinase phosphoglycerate kinase (PGK), an ATP-generating enzyme in the glycolytic pathway<sup>45</sup>, is present at a very constant level, which corresponds with its house-keeping character. Similarly, v-akt murine thymoma viral oncogene homolog 2 (AKT2) is stably active from day 1 onward. CRISPR/Cas9 mediated disruption of *akt2* expression has been shown to

cause developmental deficits and increase lethality in zebrafish larvae, thereby stressing its importance throughout development<sup>46</sup>.

### Competitive ABPP: PF04457845 profiling

Having established the activity profile of serine hydrolases, a competitive ABPP assay was developed to enable rapid *in vivo* target engagement assessment and off-target profiling. Zebrafish larvae (5 dpf) were exposed to vehicle (DMSO, 0.1%) or FAAH inhibitor PF04457845 (1  $\mu$ M, 8 h) in their swimming medium. The bioavailability of the inhibitor was assessed by measuring the drug concentration in the blood using LC-MS analysis. PF04457845 was detected at a concentration of 0.5  $\mu$ M (n=1), thereby validating internal drug exposure in the treated larvae. After treatment, lysates were analyzed by gel-based ABPP using fluorescent probes MB064 and FP-TAMRA (Figure 4A-B) or chemical proteomics using their biotinylated counterparts MB108 and FP-biotin respectively (Figure 4C). PF04457845 inhibited fatty acid amide hydrolase 2a (FAAH2a), a FAAH analogue, without affecting the other 58 detected hydrolases. This is in line with human *in vitro* and *in situ* studies in which PF04457845 only targeted FAAH and FAAH2<sup>16</sup>. Of note, PF04457845's intended target FAAH falls below the detection limit in whole lysate fractions and inhibition could thus not be determined.

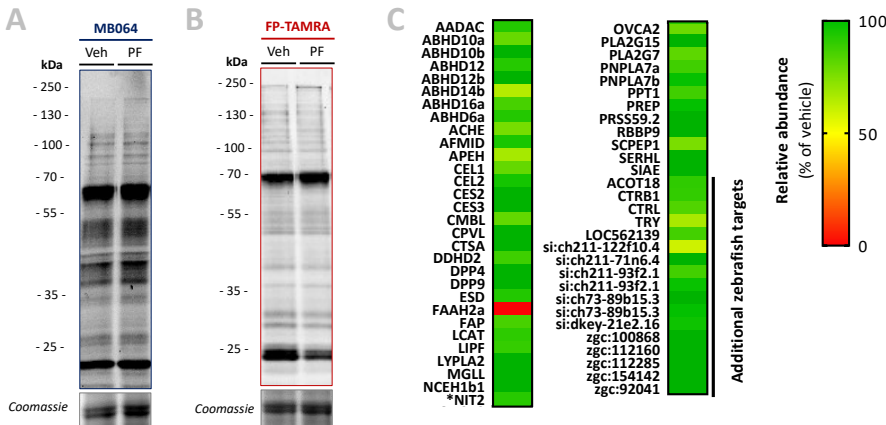


**Figure 4 | Competitive ABPP of zebrafish larvae *in vivo* treated with FAAH-inhibitor PF04457845.** (A-B) Gel-based activity profiling of zebrafish larvae (5 dpf) treated *in vivo* with vehicle or PF04457845 (1  $\mu$ M, 8 h, 28 °C). Clear lysate was labeled with (A) MB064 (1  $\mu$ M) or (B) FP-TAMRA (500 nM) (20 min, 28 °C) and 12.5  $\mu$ g protein was resolved by SDS-PAGE. Coomassie is shown as a loading control. (C) Heatmap summary of chemical proteomics analysis of zebrafish larvae (5 dpf, 300  $\mu$ g protein) treated *in vivo* with vehicle or PF04457845 (1  $\mu$ M, 8 h, 28 °C) with probes MB108 and FP-biotin (10  $\mu$ M each, 30 min, 28 °C). Data is expressed relative to vehicle treated (mean, n=4). Targets with a non-serine nucleophile are indicated with \*, additional zebrafish targets contain a GXSG motif but were not included in the putative hydrolase target list.

FAAH<sup>30,32</sup> and FAAH2a<sup>47,48</sup> both hydrolyze the endocannabinoid AEA<sup>49</sup> as well as other *N*-acylethanolamines (NAEs). To assess the functional effect of PF04457845 on FAAH(2), endocannabinoid levels were investigated by LC-MS (Figure 5A). The larvae were exposed to the drug in their swimming medium (1  $\mu$ M PF04457845, 2-24 h). The

levels of FAAH substrate AEA increased after 2 hours of treatment and reached a steady state after 5 hours, thus indicating that PF04457845 uptake was sufficient to inhibit FAAH/FAAH2 *in vivo*. The levels of a second endocannabinoid 2-AG were not affected by the drug (Figure 5A). Semi-targeted lipidomics was performed to assess the effects of PF04457845 on the overall lipid profile. In total, 223 lipids from 15 different lipid classes were detected in 5 dpf zebrafish larvae (Figure 5B). PF04457845 exposure (8 h) increased NAE levels, while other lipid classes remained unchanged. These data correspond with the clean interaction profile of PF04457845 as determined by ABPP.

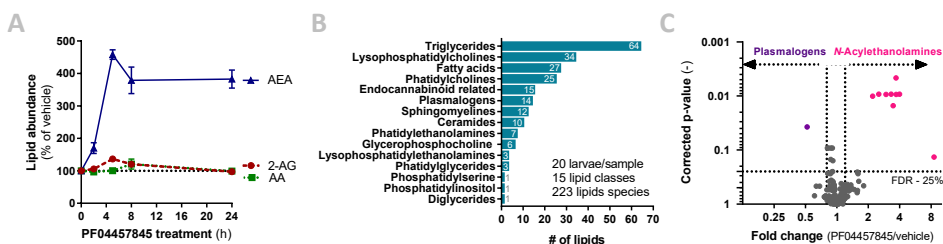


**Figure 5 | Lipidomics analysis of zebrafish larvae *in vivo* treated with FAAH inhibitor PF04457845.** (A) Time response curve of endocannabinoids (AEA, 2-AG) and metabolite arachidonic acid (AA). Zebrafish larvae (5 dpf) were treated *in vivo* with vehicle or PF04457845 (1  $\mu$ M, 2-24 h). Endocannabinoid levels were measured by LC-MS and expressed relative to vehicle-treated controls at the corresponding time point (mean  $\pm$  SEM,  $n=3$ ). (B-C) Zebrafish larvae (5 dpf) were treated with vehicle or PF04457845 (1  $\mu$ M, 8 h) and lipid levels were analyzed by LC-MS. (B) Total number of lipid species detected in zebrafish larvae sorted by lipid class. (C) Volcano plot summary of lipidomics data. Lipids with a fold change (FC) threshold of  $\geq 1.20$  or  $\leq 0.80$  and Benjamini-Hochberg false discovery rate (FDR)  $\leq 25\%$ , circles colored by lipid class (mean fold change,  $n=3$ ).

## Conclusion

In summary, a proteomics-based ABPP method was developed and enabled rapid mapping of the activity landscape of two large protein families in zebrafish larvae. Over 50 serine hydrolases were targeteded using broad-spectrum probes FP-biotin and MB108, as well as 51 kinases using the reactive-lysine targeting probe XO44. This enabled mapping of the hydrolase activity and kinase landscape throughout early zebrafish development (0-5 dpf). In addition, FAAH inhibitor PF04457845 was used to showcase zebrafish larvae as a simple *in vivo* model for drug discovery.

Phenotypic (semi-high throughput) drug screening is gaining popularity as it enables discovery of therapeutic drugs, even without having a validated drug-target<sup>4,50</sup>. The comparative chemical proteomics workflow may aid the discovery of potential serine hydrolase or kinase drug targets by enabling activity profile assessment between observed phenotypes. The competitive setup extends the assay, as it enables target identification and off-target screening. In addition, the comparative assay serves as a complementary tool to study developmental processes at the protein activity level, circumventing current limitations such as poor antibody availability for zebrafish proteins and limited translatability of mRNA levels to protein expression and activity.

## Experimental procedures

### Materials, probes and inhibitors

Fluorophosphonate-TAMRA (FP-TAMRA) and MB064, were synthesized in house as previously described<sup>18,51</sup>. XO44 was synthesized according to literature procedures<sup>22</sup>. All synthesized compounds were at least 95% pure and were analyzed by LC-MS, NMR, and HRMS. Stocks are prepared in DMSO. Other chemicals were purchased from Sigma Aldrich, unless indicated otherwise.

### Zebrafish sample collection

#### *Zebrafish husbandry*

Wildtype zebrafish were housed at Leiden University, the Netherlands in compliance with the local animal welfare regulations and were maintained according to standard protocols (zfin.org). Embryos were collected from family crosses of AB/TL wild-type strain (license number 10612, Leiden University) and were grown at 28.5 °C in embryo medium (60 µg/mL Instant Ocean sea salts (Sera Marin), methylene blue) in the dark. All experiments were performed using zebrafish embryos and larvae before the feeding stage, as specified by the EU animal protection Directive 2010/63/EU.

#### *Sample collection development stages*

Fertilized embryos were transferred to a petri dish in embryo medium and were maintained at 28.5 °C in the dark until 5 dpf. At 0, 1, 2, 3, 4, or 5 dpf embryos/larvae were collected. Embryos/larvae were washed three times with embryo medium. For each replicate, five embryos/larvae were transferred to a 1.5 mL Eppendorf tube using a Pasteur pipet. Alternatively, a large number of zebrafish larvae (> 100) was washed and transferred to a 1.5 mL Eppendorf tube. In either case, excess liquid was removed and the embryos/larvae were flash frozen in liquid nitrogen and stored at -80 °C until further use.

#### *PF04457845 in vivo treatment*

Embryos were raised in an incubator at 28.5 °C. At 5 dpf, larvae were treated with vehicle (0.05% DMSO) or PF04457845 (1 µM, 2-24 h, as indicated). For lipid extraction, three replicates of 20 larvae each were collected, washed three times with 80/20 embryo medium/methanol (v/v). For ABPP four replicates of ~60 larvae each were collected, without additional washing. Excess liquid was removed and the larvae were flash frozen in liquid nitrogen and stored at -80 °C until further use.

### Activity-based protein profiling

#### *Sample preparation*

Zebrafish larvae were thawed on ice and homogenized in a sufficient amount of sucrose lysis buffer (250 mM sucrose, 20 mM HEPES pH 7.2, 2 mM DTT, 1 mM MgCl<sub>2</sub>, 2 U/mL benzonase) or kinase lysis buffer (100 mM HEPES pH 8.0, 1.5 mM MgCl<sub>2</sub>, 1 mM EGTA pH 8.0, 150 mM NaCl, 1 mM Na<sub>3</sub>VO<sub>4</sub>, 0.1% (v/v) NP-40, 10 mM NaF, 1x mammalian protease inhibitor (M250, Amresco), 2 U/mL benzonase) with a pestle motor (whole lysate). Clear lysate was obtained as the supernatant fraction after two low-speed centrifugation steps (5 min, 1000 g, 4 °C) in which the cell debris was removed. Clear lysate was separated into cytosol and membrane fractions by ultracentrifugation (30,000 g, 60-90 min, 4 °C). The membrane pellet was resuspended in sucrose or kinase lysis buffer. Protein concentration of clear lysate, membrane, and cytosol fractions was determined by Bradford assay and samples were diluted (1-2 mg/mL) in their according buffers. Samples were flash frozen in liquid nitrogen and stored at -80 °C until further use.



For time-course experiments, the larvae (five per replicate) were homogenized in 100  $\mu$ L sucrose or kinase lysis buffer using a pestle motor. The entire sample ( $\pm$  100  $\mu$ L whole lysate) was used for proteomics experiments. For the gel-based assay, 20  $\mu$ L lysate was used per activity-based probe.

#### Gel-based ABPP

Protein samples were incubated with activity-based probes MB064 (2  $\mu$ M) or FP-TAMRA (500 nM). The reaction was quenched with Laemmli buffer (15 min, 50 °C) and samples were resolved by SDS-PAGE (10% acrylamide gel,  $\pm$  80 min, 180 V) along with protein marker (PageRuler™ Plus, Thermo Fisher). In-gel fluorescence was measured in the Cy3- and Cy5-channel (ChemiDoc™ MP, Bio-Rad) and gels were stained with Coomassie after scanning. Fluorescence was quantified and normalized to Coomassie staining using ImageLab™ software (Bio-Rad).

#### Label-free proteomics

The label-free chemical proteomics workflow was modified from Van Rooden *et al.*<sup>34</sup>. For serine hydrolase activity profiling, the lysates were incubated with serine hydrolase probe cocktail (10  $\mu$ M MB108, 10  $\mu$ M FP-biotin, 30 min, 28 °C, 300 rpm) and as a negative control a denatured protein sample (1% SDS, 5 min, 100 °C) was taken along. For kinase profiling, the lysates were incubated with kinase-probe XO44 (10  $\mu$ M, 30 min, 28 °C, 300 rpm). Treatment with vehicle (2% DMSO) was taken along as a negative control. Subsequently, the probe was conjugated to biotin-azide by addition of click mix (final concentration: 1 mM CuSO<sub>4</sub>·(H<sub>2</sub>O)<sub>5</sub>, 0.56 mM sodium ascorbate, 0.2 mM THPTA, 40  $\mu$ M biotin-azide) and subsequent incubation (60 min, 28 °C, 300 rpm).

Precipitation, alkylation and avidin enrichment were performed according to protocol<sup>34</sup>. Avidin beads were washed twice with SDS/PBS, followed by three PBS washes. On-bead digestion was performed overnight according to protocol and after sample preparation the dried peptides were stored at -20 °C until LC-MS analysis. Prior to measurement, samples were reconstituted in 40  $\mu$ L LC-MS sample solution and transferred to LC-MS vials. LC-MS data was analyzed by ProteinLynx Global SERVER™ (PLGS, Waters) and IsoQuant software<sup>52</sup> ([www.proteomeumb.org/MZw.html](http://www.proteomeumb.org/MZw.html)) (settings: minimal peptide score 5.5/6.0, false discovery rate 1%). Excel was used for further analysis, with the following cut-offs: unique peptides  $\geq$  1, identified peptides  $\geq$  2, ratio positive over negative control  $\geq$  2, part of hydrolase target list and/or containing a GXSGX serine hydrolase motif (additional zebrafish targets) (probe cocktail), or having the annotation kinase in the Uniprot database (XO44). Graphs were created using GraphPad Prism 7 (GraphPad).

### Lipidomics analysis: Endocannabinoids

#### Lipid extraction

Endocannabinoids and their congeners were quantified using LC-MS/MS analysis. The lipid extraction was performed on ice. In brief, 20 zebrafish larvae at 5 dpf were transferred to 1.5 mL Eppendorf tubes, spiked with deuterated internal standard mix for endocannabinoids (*N*-arachidonylethanolamine (AEA)-d8, *N*-arachidonoyldopamine (NADA)-d8, *N*-docosaheptaenoyl-ethanolamide (DHEA)-d4, 2-arachidonoylglycerol (2-AG)-d8, *N*-stearoyl-ethanolamine (SEA)-d3, *N*-palmitoyl-ethanolamine (PEA)-d4, *N*-linoleoyl-ethanolamine (LEA)-d3 and *N*-oleoyl-ethanolamine (OEA)-d4), followed by the addition of ammonium acetate buffer (100  $\mu$ L, 0.1 M, pH 4). After extraction with methyl *tert*-butyl ether (800  $\mu$ L), the tubes were thoroughly sonicated until the sample was homogenous. The samples were mixed for 6 min using a bullet blender at medium speed (Next Advance Inc.), followed by a centrifugation step (5,000 *g*, 12 min, 4 °C). Then 750  $\mu$ L of the upper methyl *tert*-butyl ether layer was transferred into a clean 1.5 mL Eppendorf tube. Samples were dried in a speed-vac (Eppendorf) followed by reconstitution in acetonitrile/H<sub>2</sub>O (30  $\mu$ L, 90/10, v/v). The reconstituted samples were centrifuged (14,000 *g*, 3 min, 4 °C) before transferring into LC-MS vials. 5  $\mu$ L of sample was injected for LC-MS analysis.

### LC-MS/MS analysis

A targeted analysis of 21 endocannabinoids and related NAEs was measured using an Acquity UPLC I class Binary solvent manager pump (Waters) in conjugation with AB SCIEX 6500 quadrupole-ion trap (QTRAP) (AB Sciex). Separation was performed with an Acquity HSS T3 column (1.2 x 100 mm, 1.8  $\mu$ m) maintained at 45 °C. The aqueous mobile phase A consisted of 2 mM ammonium formate and 10 mM formic acid, and the organic mobile phase B was acetonitrile. The flow rate was set to 0.4 mL/min; initial gradient conditions were 55% B held for 2 min and linearly ramped to 100% B over 6 min and held for 2 min; after 10 s, the system returned to initial conditions and held 2 min before next injection. Electrospray ionization-MS was operated in positive mode for measurement of 21 endocannabinoids and NAEs, and a selective Multiple Reaction Mode (sMRM) was used for quantification. Peak area integration was performed with MultiQuant (AB Sciex, Version 3.0.2) data analysis software. The obtained peak areas of targets were corrected by appropriate internal standards. Calculated response ratios, determined as the peak area ratios of the target analytes to the respective internal standards, were used to obtain absolute concentrations from their respective calibration curves.

**Table 1 | Target list of endocannabinoids and *N*-acylethanolamines and their validation parameters.** The method is validated in terms of linearity sensitivity (LOQ), process efficiency (matrix effect with recovery) and precision. Endogenous concentrations are expressed as mean  $\pm$  SEM.

Abbreviation	Metabolite name	Process efficiency (%)	Correlation coefficient ( $R^2$ )	Precision (% RSD)	Lipid level (fmol/larvae)
<b>2&amp;1AG (20:4)</b>	Arachidonoylglycerol	78	0.998	5	2270 $\pm$ 59
<b>AEA (20:4)</b>	Anandamide	85	0.999	12	0.5 $\pm$ 0.02
<b>DHEA (22:6)</b>	<i>N</i> -Docosahexaenoyl ethanolamide	49	0.999	4	42 $\pm$ 1.6
<b>LEA (18:2)</b>	<i>N</i> -Linoleoylethanolamide	79	0.999	3	0.38 $\pm$ 0.11
<b>OEA (18:1)</b>	<i>N</i> -Oleoylethanolamide	84	0.999	6	1.2 $\pm$ 0.28
<b>PEA (16:0)</b>	<i>N</i> -Palmitoylethanolamide	87	0.999	3	21.6 $\pm$ 0.9
<b>SEA (18:0)</b>	<i>N</i> -Stearoylethanolamide	91	0.999	2	11.7 $\pm$ 0.6
<b>DEA (22:4)</b>	<i>N</i> -Docosatetraenoyl ethanolamide	48	0.998	19	0.4 $\pm$ 0.02
<b>DGLEA (18:3)</b>	Dihomo- $\gamma$ -Linolenoyl ethanolamide	65	0.999	35	0.1 $\pm$ 0.01
<b>2-LG (18:2)</b>	2-Linoleoyl glycerol	63	0.999	8	6153 $\pm$ 493
<b>1-LG (18:2)</b>	1-Linoleoyl glycerol	74	0.981	7	773 $\pm$ 66
<b>2-OG (18:1)</b>	2-Oleoyl glycerol	73	0.999	3	17999 $\pm$ 1740
<b>1-OG (18:1)</b>	1-Oleoyl glycerol	N/A	0.986	3	2564 $\pm$ 191
<b>EPEA (20:5)</b>	<i>N</i> -Eicosapentaenoyl ethanolamide	65	0.999	5	7.3 $\pm$ 0.44
<b>POEA (16:1)</b>	<i>N</i> -Palmitoleoylethanolamide	99	0.999	4	0.8 $\pm$ 0.04
<b>PDEA (15:0)</b>	<i>N</i> -Pentadecanoylethanolamide	82	0.999	7	0.2 $\pm$ 0.01
<b>AA (20:4)</b>	Arachidonic Acid	122	0.998	7	80167 $\pm$ 5530

### Lipidomics analysis: Targeted lipidomics

#### Sample extraction

The endocannabinoid extraction protocol was followed, with the following adjustment. In addition to the endocannabinoid internal standards, non-endogenous lipid internal standards were added (lysophosphatidylcholine (LPC) 17:0, phosphatidylethanolamine (PE) 17:0/17:0, phosphatidylcholine (PC) 17:0/17:0, sphingomyelin (SM) d18:1/17:0, triglyceride (TG) 17:0/17:0/17:0, ceramide (Cer) d18:1/17:0 and fatty acid (FA) 17:0-d33). Each sample was injected on three different lipidomics platforms: endocannabinoids (5  $\mu$ L), positive lipids (2  $\mu$ L) and negative lipids (8  $\mu$ L).

#### LC-MS/MS analysis

The endocannabinoid analysis was followed as described above. Both lipidomics methods (positive and negative lipids) are adapted and modified from previously published work<sup>16</sup>. In brief, these methods are measured on an Acquity UPLC Binary solvent manager pump (Waters) coupled to a Synapt G2 electrospray ionization quadrupole time-of-flight (ESI-Q-TOF, Waters) high

resolution mass spectrometer using reference mass correction. The chromatographic separation was achieved on an Acquity HSS T3 column (1.2 x 100 mm, 1.8  $\mu$ m) maintained at 40 °C for both methods. The positive lipid run includes targets from different lipid classes including (lyso)phosphatidylcholines, triglycerides, ceramides. (Lyso)phosphatidylethanolamines and sphingomyelins were separated using a flow of 0.4 mL/min over a 16 min gradient. In positive mode, the mobile phase A consisted of 60/40 (v/v) acetonitrile/H<sub>2</sub>O with 10 mM ammonium formate, and the mobile phase B consisted of 10/90 (v/v) acetonitrile/isopropanol with 10 mM ammonium formate. The negative lipids constitute mainly free fatty acids and (lyso)phosphatidylcholines were separated with a flow of 0.4 mL/min over a 15 min gradient. In negative mode, the aqueous mobile phase A consisted of 5/95 (v/v) acetonitrile/H<sub>2</sub>O with 10 mM ammonium formate, and the organic mobile phase B consisted of 99% (v/v) methanol with 10 mM ammonium formate. The targets in both lipid methods were detected full scan (100-1000 m/z) in their respective ion charge mode.

### PF04457845 quantification

#### *Sample extraction*

PF04457845 was quantified using LC-MS/MS analysis in blood samples pooled from 20-25 treated zebrafish larvae at 5 dpf (1  $\mu$ M PF04457845, 8 h). The blood sample (total ~83 nL) was collected from anatomical locations of the larval circulation using a pulled needle (borosilicate glass capillary, original diameter: 0.5 mm, Sutter Instruments) in a micromanipulator, connected to a manual CellTram pump (Eppendorf) under 20x microscopic magnification (Leica). For determination of sample volume, an image was taken of each sample's blood content within the needle. To prevent coagulation, needles and collection tubes were coated with heparin. The sample extraction was performed on ice. 200  $\mu$ L of acetonitrile was added to the blood samples. The samples were vortexed and then centrifuged (13,000 *g*, 10 min). 150  $\mu$ L of supernatant was evaporated to dryness using a speedvac (Eppendorf) and reconstituted in 10  $\mu$ L of acetonitrile.

#### *LC-MS/MS analysis*

PF04457845 was measured using an Acquity UPLC I class Binary solvent manager pump (Waters) in conjugation with AB SCIEX 6500 quadrupole-ion trap (QTRAP) (AB Sciex). Separation was performed with Acquity HSS T3 column (1.2 x 100 mm, 1.8  $\mu$ m) maintained at 45 °C. The aqueous mobile phase A consisted of 2 mM ammonium formate and 10 mM formic acid, and the organic mobile phase B was acetonitrile. The flow rate was set to 0.5 mL/min; initial gradient conditions were 60% B held for 0.5 min and linearly ramped to 100% B over 2.5 min and held for 0.5 min; after 10 s the system returned to initial conditions and held 1.5 min before next injection. Electrospray ionization-MS was operated in positive mode for measurement of PF04457845 and a selective Multiple Reaction Mode (sMRM) was used for quantification. The ion masses monitored were Q1/Q3 456/335 (m/z). Peak area integration was performed with MultiQuant (AB Sciex, Version 3.0.2) data analysis software. The limit of detection (LOD) was 1 pM and the linear range used was from 1 to 1000 pM.

### Statistical methods

All statistical measures and methods are included in the respective Figure or Table captions. In brief, all data are shown as the mean  $\pm$  SEM where applicable. A Student's *t*-test (unpaired, two-tailed) was used to determine differences between two groups. All statistical analyses were conducted using Excel (Microsoft) or GraphPad Prism 7 (GraphPad), and a *p*-value < 0.05 was considered significant throughout unless indicated otherwise. For the lipidomics analysis a Benjamini-Hochberg correction was applied to obtain multicomparison corrected *p*-values and a false discovery rate of 25% was applied.

## Supplementary data

**Table S1 | Identified hydrolase targets in zebrafish.** Abbreviations and descriptions as annotated on uniprot.org.

\* Indicates targets with a GX SXG-domain that are not annotated, their molecular function is based on gene ontology.

Protein	Description	Protein	Description
<b>AADAC</b>	Arylacetamide deacetylase	<b>MGLL</b>	Monoglyceride lipase
<b>ABHD10a</b>	$\alpha$ - $\beta$ hydrolase domain containing 10a	<b>NCEH1B,1</b>	Neutral cholesterol ester hydrolase 1b, tandem duplicate 1
<b>ABHD10b</b>	$\alpha$ - $\beta$ hydrolase domain containing 10b	<b>NCEH1B,2</b>	Neutral cholesterol ester hydrolase 1b, tandem duplicate 2
<b>ABHD12</b> <i>si:ch211-117n7.7i</i>	$\alpha$ - $\beta$ hydrolase domain containing 12	<b>NIT2</b>	Omega-amidase NIT2
<b>ABHD14b</b>	$\alpha$ - $\beta$ hydrolase domain containing 14b	<b>OLAH</b>	Oleoyl-ACP hydrolase
<b>ABHD16a</b>	$\alpha$ - $\beta$ hydrolase domain containing 16a	<b>OVCA2</b>	Esterase OVCA2
<b>ABHD4</b>	$\alpha$ - $\beta$ hydrolase domain containing 4	<b>PAFAH1B3</b>	Platelet-activating factor acetylhydrolase isoform 1b $\gamma$ subunit
<b>ABHD6a</b>	$\alpha$ - $\beta$ hydrolase domain containing 6a	<b>PLA2G15</b>	Phospholipase A2 group XV
<b>ACHE</b>	Acetylcholinesterase	<b>PLA2G7</b>	Platelet-activating factor acetylhydrolase
<b>ACOT18</b>	Acyl-CoA thioesterase 18	<b>PNPLA6</b>	Patatin-like phospholipase domain-containing 6
<b>AFMID</b>	Kynurenine formamidase	<b>PNPLA7a</b>	Patatin-like phospholipase domain-containing 7a
<b>APEH</b>	Acylaminoacyl-peptide hydrolase	<b>PNPLA7b</b>	Patatin-like phospholipase domain-containing 7b
<b>CEL,1</b>	Carboxylic ester hydrolase	<b>PPT1</b>	Palmitoyl-protein thioesterase 1
<b>CEL,2</b>	Carboxylic ester hydrolase	<b>PPT2</b>	Palmitoyl-protein thioesterase 2
<b>CES2</b>	Carboxylic ester hydrolase	<b>PRCP</b>	Prolylcarboxypeptidase
<b>CES3</b>	Carboxylic ester hydrolase	<b>PREP</b>	Prolyl endopeptidase
<b>CMBL</b>	Carboxymethylenebutenolidase homolog	<b>PRSS1</b>	Trypsin
<b>CPVL</b>	Carboxypeptidase - vitellogenic-like	<b>PRSS59.1</b>	Protease serine 59 tandem duplicate 1
<b>CTRB1</b>	Chymotrypsinogen B1	<b>PSMB5</b>	Proteasome subunit beta type
<b>CTRL</b>	Chymotrypsin-like	<b>RBBP9</b>	Retinoblastoma-binding protein 9
<b>CTSA</b>	Cathepsin A	<b>SCPEP1</b>	Carboxypeptidase
<b>DPP4</b>	Dipeptidyl-peptidase 4	<b>SERHL</b>	Serine hydrolase-like protein
<b>DPP9</b>	Dipeptidyl-peptidase 9	<b>si:ch211-122f10.4</b>	* Serine-type carboxypeptidase activity
<b>ESD</b>	S-formylglutathione hydrolase	<b>si:ch211-71n6.4</b>	* Carboxylic ester hydrolase activity
<b>FAAH</b>	Fatty acid amide hydrolase	<b>si:ch211-93f2.1</b>	* Carboxylic ester hydrolase activity
<b>FAAH2A</b>	Fatty-acid amide hydrolase 2a	<b>si:ch73-89b15.3</b>	* Carboxylic ester hydrolase activity
<b>FAAH2B</b>	Fatty-acid amide hydrolase 2b	<b>si:dkey-21e2.16</b>	* Serine-type endopeptidase activity
<b>FAP</b>	Fibroblast activation protein $\alpha$	<b>SIAE</b>	Sialic acid acetyltransferase
<b>LCAT</b>	Lecithin-cholesterol acyltransferase	<b>TRY</b>	Trypsin
<b>LIPF</b>	Lipase member F	<b>zgc:100868</b>	* Serine-type endopeptidase activity
<b>LIPH</b>	Lipase member H	<b>zgc:112160</b>	* Serine-type endopeptidase activity
<b>LOC562139</b>	Chymotrypsinogen B1 like protein	<b>zgc:112285</b>	* Chymotrypsinogen B1 like protein
<b>LYPLA1</b>	Lysophospholipase I	<b>zgc:154142</b>	* Serine-type endopeptidase activity
<b>LYPLA2</b>	Lysophospholipase II	<b>zgc:92041</b>	* Serine-type endopeptidase activity

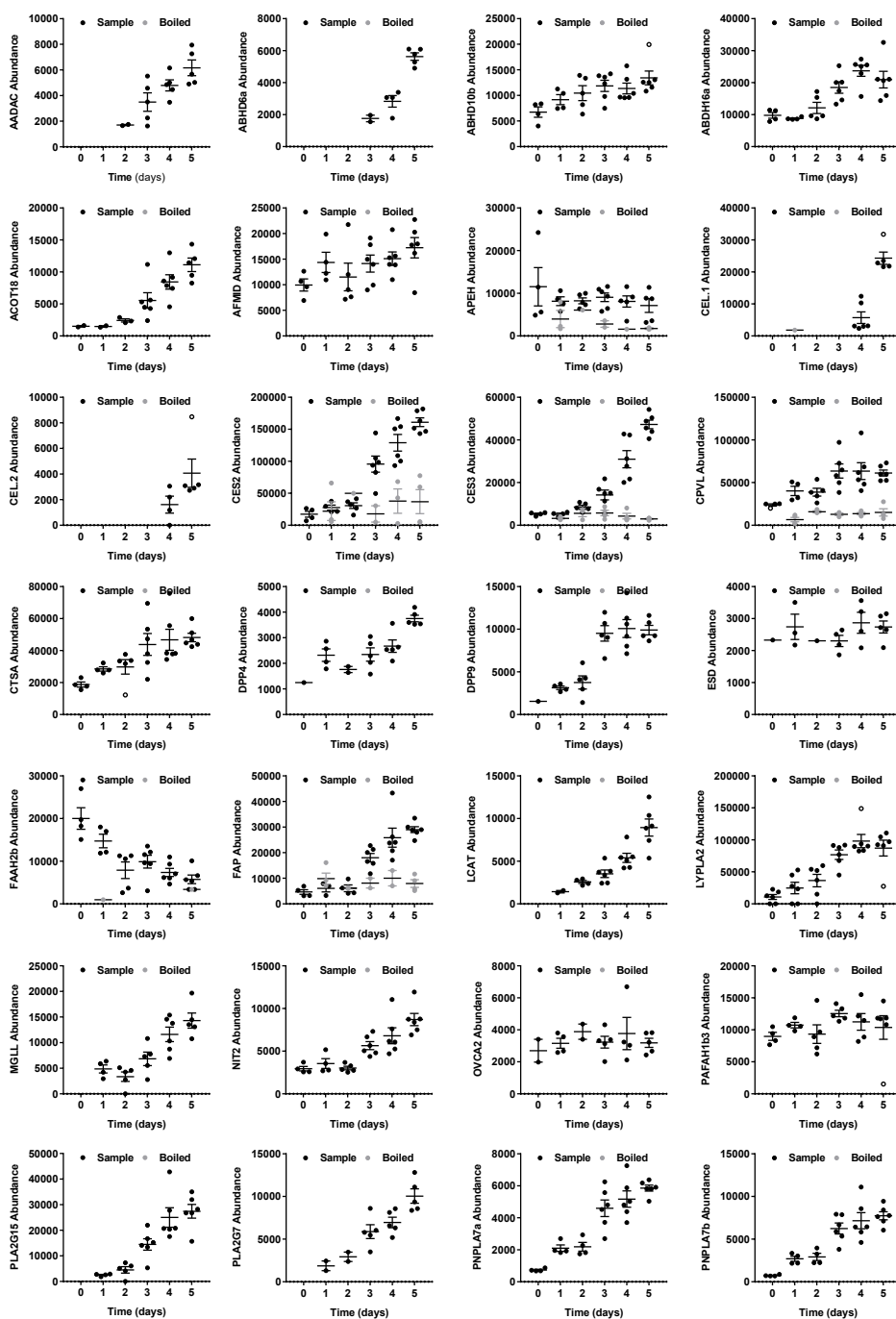
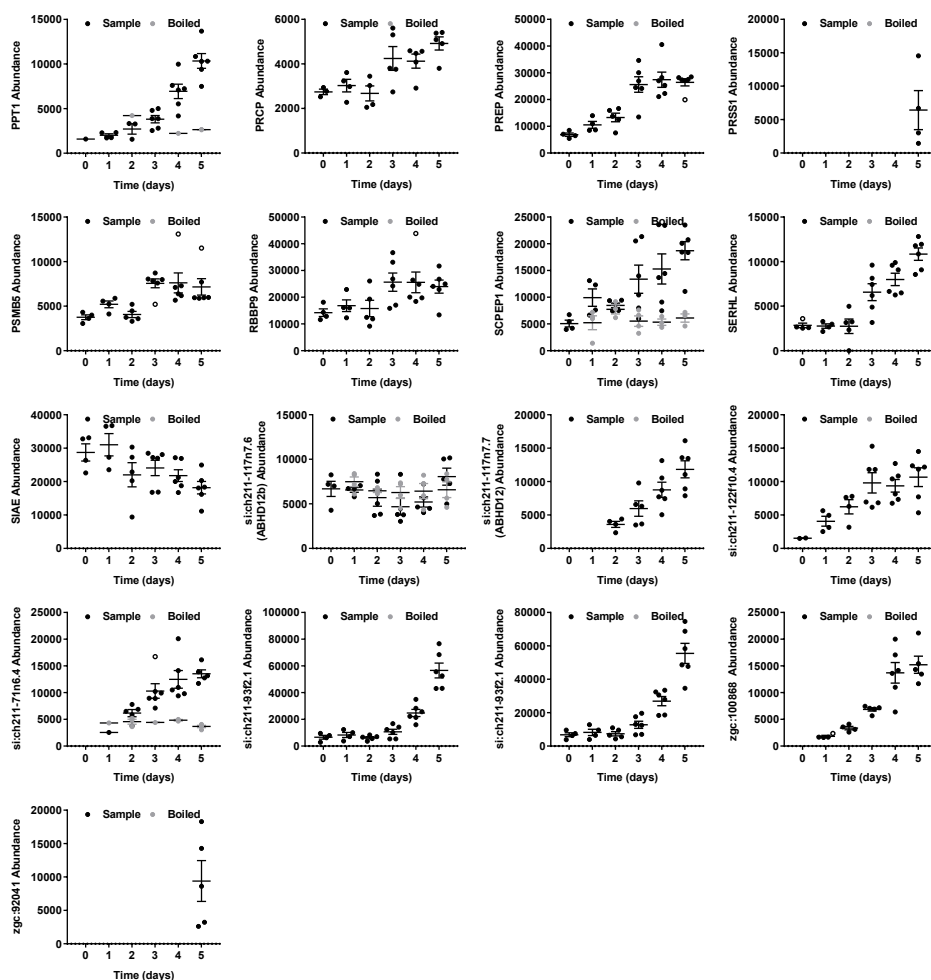


Figure S1 (1/2) | Chemical proteomics analysis of (serine) hydrolases during zebrafish development.



**Figure S1 (2/2) | Chemical proteomics analysis of (serine) hydrolases during zebrafish development.** Zebrafish whole lysates from different development stages (0-5 dpf, 5 larvae/sample) were treated with MB108 and FP-biotin (10  $\mu$ M each, 30 min, 28  $^{\circ}$ C), followed by chemical proteomics analysis. Samples boiled (1% SDS, 5 min, 95  $^{\circ}$ C) prior to probe incubation served as negative control for each time point. Cut-offs for target selection: ratio positive over negative control  $\geq 2$ , unique peptides  $\geq 1$ , identified peptides  $\geq 2$  for at least one time point. Targets must be part of hydrolase target list and/or containing a GX SXG serine hydrolase motif. Data is expressed as absolute abundance (mean  $\pm$  SEM and individual data points) for samples (black fill, n=6) or boiled controls (grey fill, n=4). Outliers as determined with a ROUT outlier test (5%) are depicted with open circles for non-boiled samples only. Undetected proteins in individual samples are not included in plots or calculations.

**Table S2 | Identified kinase targets in zebrafish.** Abbreviations and descriptions as annotated on uniprot.org.

Protein	Description	Protein	Description
<b>AKT2</b>	v-akt murine thymoma viral oncogene homolog 2	<b>MINK1</b>	Missshapen-like kinase 1
<b>AKT3A</b>	v-akt murine thymoma viral oncogene homolog 3a	<b>MYLKB</b>	Myosin light chain kinase b
<b>CAMK2D2</b>	Calcium/calmodulin-dependent protein kinase type II delta 2 chain	<b>NME2B.2</b>	NME/NM23 nucleoside diphosphate kinase 2b tandem duplicate 2
<b>CAMK2G1</b>	Calcium/calmodulin-dependent protein kinase (CaM kinase) II gamma 1	<b>PAK2A</b>	P21 protein (Cdc42/Rac)-activated kinase 2a
<b>CDK1</b>	Cell division control protein 2	<b>PAK2B</b>	p21 protein (Cdc42/Rac)-activated kinase 2b
<b>CDK2</b>	Cyclin-dependent kinase 2	<b>PGK1</b>	Phosphoglycerate kinase (Fragment)
<b>CDK5</b>	Cyclin-dependent kinase 5	<b>PKMB</b>	Pyruvate kinase
<b>CDK9</b>	Cyclin-dependent kinase 9	<b>PRKAA1</b>	Non-specific serine/threonine protein kinase
<b>CKBB</b>	Brain-subtype creatine kinase	<b>PRKACBA</b>	Protein kinase cAMP-dependent catalytic $\beta$ a
<b>CKMA</b>	Creatine kinase, muscle a	<b>PRKACBB</b>	Protein kinase cAMP-dependent catalytic $\beta$ b
<b>CKMB</b>	Ckmb protein	<b>RPS6KA1</b>	Ribosomal protein S6 kinase
<b>GRK7A</b>	Rhodopsin kinase 1	<b>RPS6KA2</b>	Ribosomal protein S6 kinase
<b>GSK3AB</b>	Glycogen synthase kinase 3 alpha b	<b>RPS6KA3A</b>	Ribosomal protein S6 kinase
<b>GSK3B</b>	Glycogen synthase kinase 3	<b>RPS6KB1B</b>	Ribosomal protein S6 kinase
<b>HCK</b>	Tyrosine-protein kinase	<b>SRC</b>	Proto-oncogene tyrosine-protein kinase Src
<b>MAK</b>	Male germ-cell associated kinase	<b>STK24B</b>	Serine/threonine kinase 24b
<b>MAP2K1</b>	Mitogen-activated protein kinase kinase 1	<b>STK25A</b>	Serine/threonine kinase 25a
<b>MAP2K2A</b>	Mitogen-activated protein kinase kinase 2	<b>STK25B</b>	Serine/threonine kinase 25b
<b>MAP2K4A</b>	Mitogen-activated protein kinase kinase 4A	<b>STK26</b>	Serine/threonine protein kinase 26
<b>MAP4K4</b>	Mitogen-activated protein kinase kinase kinase 4	<b>STK3</b>	Serine/threonine-protein kinase 3
<b>MAPK1</b>	Mitogen-activated protein kinase	<b>STK38A</b>	Serine/threonine kinase 38a
<b>MAPK3</b>	Mitogen-activated protein kinase	<b>STK38L</b>	Serine/threonine kinase 38-like
<b>MAPK9</b>	Mitogen-activated protein kinase	<b>TBK1</b>	TANK-binding kinase 1
<b>MAPK14</b>	Mitogen-activated protein kinase	<b>TNKB</b>	TRAF2 and NCK-interacting kinase b
<b>MAST1B</b>	Microtubule-associated serine/threonine kinase 1b	<b>YES1</b>	Tyrosine-protein kinase yes
<b>MAST3A</b>	Microtubule-associated serine/threonine kinase 3a		

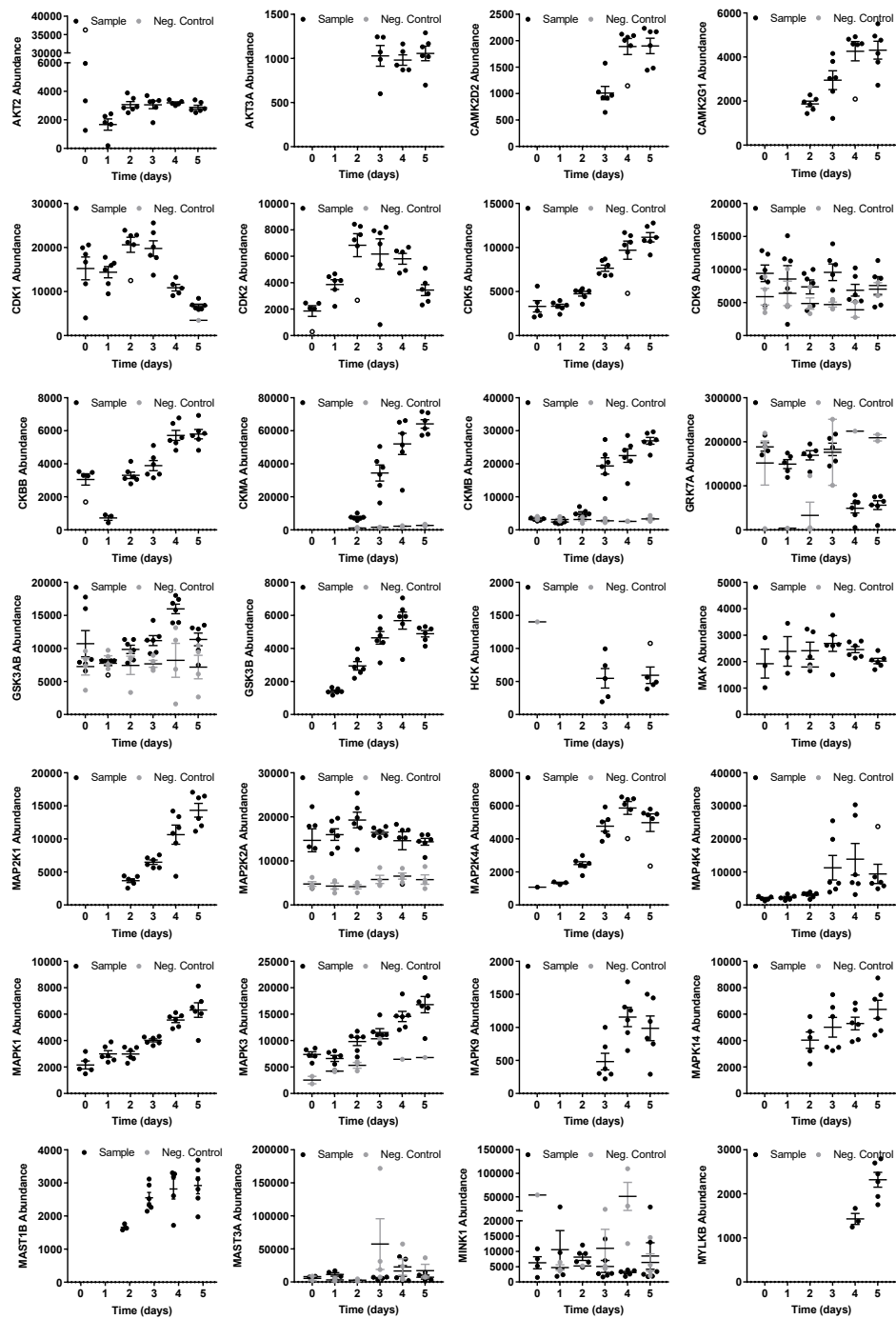
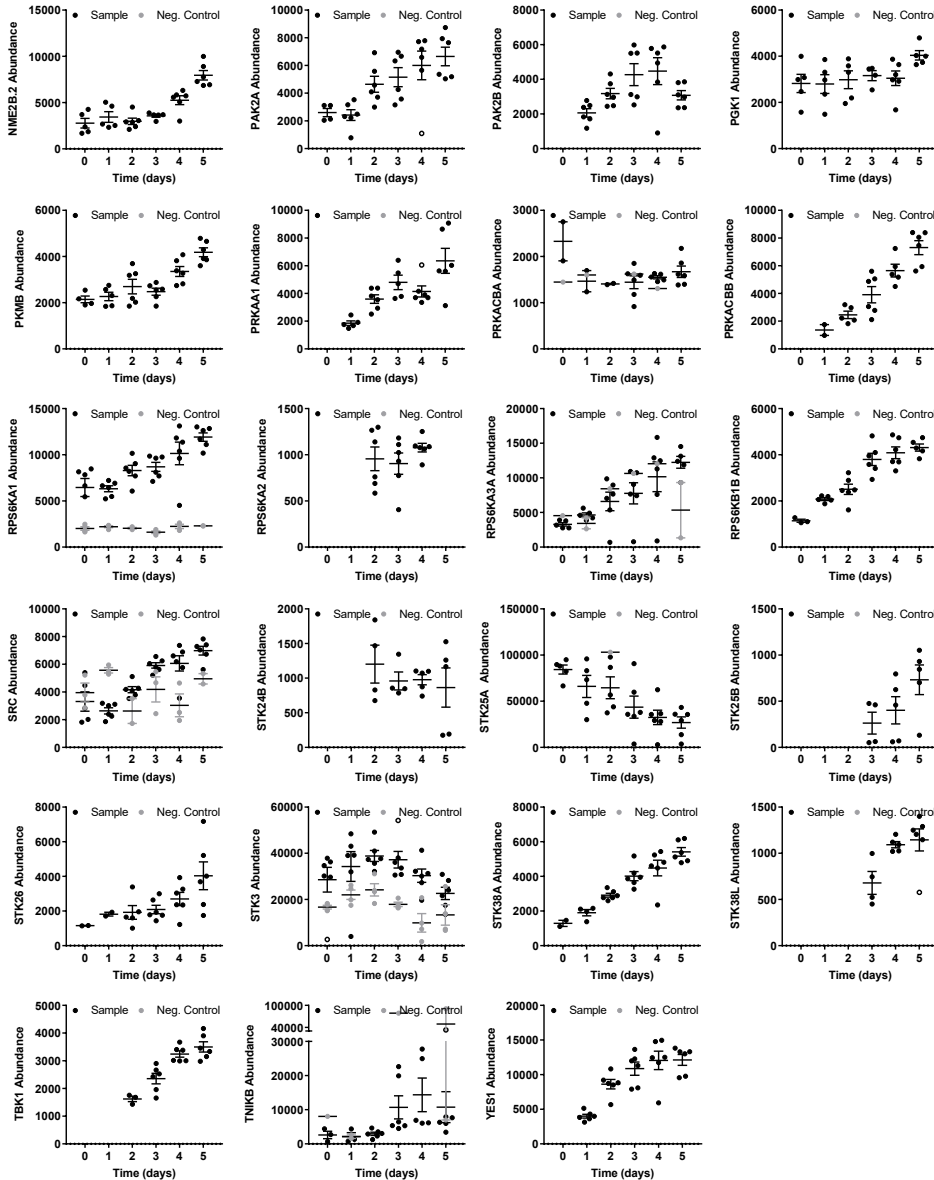


Figure S2 (1/2) | Chemical proteomics analysis of kinases during zebrafish development.





**Figure S2 (2/2) | Chemical proteomics analysis of kinases during zebrafish development.** Zebrafish whole lysates from different development stages (0-5 dpf, 5 larvae/sample) were treated with XO44 (10  $\mu$ M, 30 min, 28  $^{\circ}$ C) and subsequently conjugated to biotin-azide (40  $\mu$ M, 60 min, 28  $^{\circ}$ C), followed by chemical proteomics analysis. Vehicle treated sample served as negative control for each time point. Cut-offs for target selection: ratio positive over negative control  $\geq 2$ , unique peptides  $\geq 1$ , identified peptides  $\geq 2$  for at least one time point. Targets must be annotated as kinase in the Uniprot database. Data is expressed as absolute abundance (mean  $\pm$  SEM and individual data points) for samples (black fill, n=6) or vehicle treated controls (grey fill, n=4). Outliers as determined with a ROUT outlier test (5%) are depicted as open circles for non-boiled samples only. Undetected proteins in individual samples are not included in plots or calculations.

## References

1. Kimmel, C. B., Ballard, W. W., Kimmel, S. R., Ullmann, B. & Schilling, T. F. Stages of embryonic development of the zebrafish. *Dev. Dyn.* **203**, 253–310 (1995).
2. Link, B. A. & Megason, S. G. in *Source Book of Models for Biomedical Research* 103–112 (Humana Press, 2008). ISBN: 9781588299338.
3. MacRae, C. A. & Peterson, R. T. Zebrafish as tools for drug discovery. *Nat. Rev. Drug Discov.* **14**, 721–731 (2015).
4. Rennekamp, A. J. & Peterson, R. T. 15 Years of Zebrafish Chemical Screening. *Curr. Opin. Chem. Biol.* **24**, 58–70 (2015).
5. Howe, K. *et al.* The zebrafish reference genome sequence and its relationship to the human genome. *Nature* **496**, 498–503 (2013).
6. Lieschke, G. J. & Currie, P. D. Animal models of human disease: Zebrafish swim into view. *Nature Reviews Genetics* **8**, 353–367 (2007).
7. Bowman, T. V. & Zon, L. I. Swimming into the future of drug discovery: In vivo chemical screens in zebrafish. *ACS Chem. Biol.* **5**, 159–161 (2010).
8. Zon, L. I. & Peterson, R. T. In vivo drug discovery in the zebrafish. *Nature Reviews Drug Discovery* **4**, 35–44 (2005).
9. Tay, T. L. *et al.* Proteomic analysis of protein profiles during early development of the zebrafish, *Danio rerio*. *Proteomics* **6**, 3176–3188 (2006).
10. Alli Shaikh, A. *et al.* Functional mapping of the zebrafish early embryo proteome and transcriptome. *J. Proteome Res.* **13**, 5536–5550 (2014).
11. Kudoh, T. *et al.* A gene expression screen in zebrafish embryogenesis. *Genome Res.* **11**, 1979–1987 (2001).
12. White, R. J. *et al.* A high-resolution mRNA expression time course of embryonic development in zebrafish. *Elife* **6**, (2017).
13. van Rooden, E. J., Bakker, A. T., Overkleeft, H. S. & van der Stelt, M. Activity-Based Protein Profiling. *eLS* 1–9 (2018).
14. Liu, Y., Patricelli, M. P. & Cravatt, B. F. Activity-based protein profiling: The serine hydrolases. *Proc. Natl. Acad. Sci.* **96**, 14694–14699 (1999).
15. Niphakis, M. J. & Cravatt, B. F. Enzyme Inhibitor Discovery by Activity-Based Protein Profiling. *Annu. Rev. Biochem.* **83**, 341–377 (2014).
16. Van Esbroeck, A. C. M. *et al.* Activity-based protein profiling reveals off-target proteins of the FAAH inhibitor BIA 10-2474. *Science* **356**, 1084–1087 (2017).
17. Baggelaar, M. P. *et al.* Chemical Proteomics Maps Brain Region Specific Activity of Endocannabinoid Hydrolases. *ACS Chem. Biol.* **12**, 852–861 (2017).
18. Baggelaar, M. P. *et al.* Development of an activity-based probe and in silico design reveal highly selective inhibitors for diacylglycerol lipase- $\alpha$  in brain. *Angew. Chemie - Int. Ed.* **52**, 12081–12085 (2013).
19. Baggelaar, M. P. *et al.* Highly Selective, Reversible Inhibitor Identified by Comparative Chemoproteomics Modulates Diacylglycerol Lipase Activity in Neurons. *J. Am. Chem. Soc.* **137**, 8851–8857 (2015).
20. Tarkiainen, T. H. *et al.* Stability over time of short-term heart rate variability. *Clin. Auton. Res.* **15**, 394–399 (2005).
21. Manning, G., Whyte, D. B., Martinez, R., Hunter, T. & Sudarsanam, S. The protein kinase complement of the human genome. *Science* **298**, 1912–34 (2002).
22. Zhao, Q. *et al.* Broad-spectrum kinase profiling in live cells with lysine-targeted sulfonyl fluoride probes. *J. Am. Chem. Soc.* **139**, 680–685 (2017).
23. Rostovtsev, V. V., Green, L. G., Fokin, V. V. & Sharpless, K. B. A stepwise Huisgen cycloaddition process: Copper(I)-catalyzed regioselective ‘ligation’ of azides and terminal alkynes. *Angew. Chemie - Int. Ed.* **41**, 2596–2599 (2002).

24. Bachovchin, D. A. & Cravatt, B. F. The pharmacological landscape and therapeutic potential of serine hydrolases. *Nat. Rev. Drug Discov.* **11**, 52–68 (2012).
25. Klaeger, S. *et al.* The target landscape of clinical kinase drugs. *Science* **358**, eaan4368 (2017).
26. Johnson, D. S. *et al.* Discovery of PF-04457845: A highly potent, orally bioavailable, and selective urea FAAH inhibitor. *ACS Med. Chem. Lett.* **2**, 91–96 (2011).
27. Huggins, J. P., Smart, T. S., Langman, S., Taylor, L. & Young, T. An efficient randomised, placebo-controlled clinical trial with the irreversible fatty acid amide hydrolase-1 inhibitor PF-04457845, which modulates endocannabinoids but fails to induce effective analgesia in patients with pain due to osteoarthritis of the. *Pain* **153**, 1837–1846 (2012).
28. Zhang, J., Yang, P. L. & Gray, N. S. Targeting cancer with small molecule kinase inhibitors. *Nature Reviews Cancer* **9**, 28–39 (2009).
29. Li, G. L. *et al.* Assessment of the pharmacology and tolerability of PF-04457845, an irreversible inhibitor of fatty acid amide hydrolase-1, in healthy subjects. *Br. J. Clin. Pharmacol.* **73**, 706–716 (2012).
30. Cravatt, B. F. *et al.* Molecular characterization of an enzyme that degrades neuromodulatory fatty-acid amides. *Nature* **384**, 83–87 (1996).
31. Kathuria, S. *et al.* Modulation of anxiety through blockade of anandamide hydrolysis. *Nat. Med.* **9**, 76–81 (2003).
32. Devane, W. A. *et al.* Isolation and structure of a brain constituent that binds to the cannabinoid receptor. *Science* **258**, 1946–1949 (1992).
33. Long, J. Z. *et al.* Dual blockade of FAAH and MAGL identifies behavioral processes regulated by endocannabinoid crosstalk in vivo. *Proc. Natl. Acad. Sci. U. S. A.* **106**, 20270–5 (2009).
34. van Rooden, E. J. *et al.* Mapping in vivo target interaction profiles of covalent inhibitors using chemical proteomics with label-free quantification. *Nat. Protoc.* **13**, 752–767 (2018).
35. Long, J. Z. & Cravatt, B. F. The metabolic serine hydrolases and their functions in mammalian physiology and disease. *Chem. Rev.* **111**, 6022–6063 (2011).
36. Wu, C. *et al.* BioGPS: An extensible and customizable portal for querying and organizing gene annotation resources. *Genome Biol.* **10**, 130 (2009).
37. BioGPS - your Gene Portal System. Available at: <http://biogps.org/>. (Accessed: 1st December 2018)
38. Tao, T. & Peng, J. Liver development in zebrafish (*Danio rerio*). *Journal of Genetics and Genomics* **36**, 325–334 (2009).
39. Tiso, N., Moro, E. & Argenton, F. Zebrafish pancreas development. *Mol. Cell. Endocrinol.* **312**, 24–30 (2009).
40. Krug, R. G. *et al.* The endocannabinoid gene faah2a modulates stress-associated behavior in zebrafish. *PLoS One* **13**, e0190897 (2018).
41. Schuel, H. *et al.* Cannabinoids inhibit fertilization in sea urchins by reducing the fertilizing capacity of sperm. *Pharmacol. Biochem. Behav.* **40**, 609–615 (1991).
42. Schuel, H. *et al.* N-Acylethanolamines in human reproductive fluids. in *Chemistry and Physics of Lipids* **121**, 211–227 (2002).
43. Oltrabella, F., Melgoza, A., Nguyen, B. & Guo, S. Role of the endocannabinoid system in vertebrates: Emphasis on the zebrafish model. *Dev. Growth Differ.* **59**, 194–210 (2017).
44. Neganova, I., Zhang, X., Atkinson, S. & Lako, M. Expression and functional analysis of G1 to S regulatory components reveals an important role for CDK2 in cell cycle regulation in human embryonic stem cells. *Oncogene* **28**, 20–30 (2009).
45. Watson, H. C. *et al.* Sequence and structure of yeast phosphoglycerate kinase. *EMBO J.* **1**, 1635–1640 (1982).
46. Zhang, D., Wang, J., Zhou, C. & Xiao, W. Zebrafish akt2 is essential for survival, growth, bone development, and glucose homeostasis. *Mech. Dev.* **143**, 42–52 (2017).

47. Wei, B. Q., Mikkelsen, T. S., McKinney, M. K., Lander, E. S. & Cravatt, B. F. A second fatty acid amide hydrolase with variable distribution among placental mammals. *J. Biol. Chem.* **281**, 36569–36578 (2006).
48. McPartland, J. M., Glass, M., Matias, I., Norris, R. W. & Kilpatrick, C. W. A shifted repertoire of endocannabinoid genes in the zebrafish (*Danio rerio*). *Mol. Genet. Genomics* **277**, 555–570 (2007).
49. Di Marzo, V. Endocannabinoid signaling in the brain: biosynthetic mechanisms in the limelight. *Nat. Neurosci.* **14**, 9–15 (2011).
50. Kithcart, A. & MacRae, C. A. Using Zebrafish for High-Throughput Screening of Novel Cardiovascular Drugs. *JACC Basic to Transl. Sci.* **2**, 1–12 (2017).
51. Janssen, A. P. A. *et al.* Development of a Multiplexed Activity-Based Protein Profiling Assay to Evaluate Activity of Endocannabinoid Hydrolase Inhibitors. *ACS Chem. Biol.* **13**, 2406–2413 (2018).
52. Liao, Z., Wan, Y., Thomas, S. N. & Yang, A. J. IsoQuant: A software tool for stable isotope labeling by amino acids in cell culture-based mass spectrometry quantitation. *Anal. Chem.* **84**, 4535–4543 (2012).

# 4

A.C.M. van Esbroeck  
A.P.A. Janssen  
A.B. Cognetta III  
D. Ogasawara  
G. Shpak  
M. van der Kroeg  
V. Kantae  
M.P. Baggelaar  
F.M.S. de Vrij  
H. Deng  
M. Allarà  
F. Fezza  
Z. Lin  
T. van der Wel  
M. Soethoudt  
E.D. Mock  
H. den Dulk  
I.L. Baak  
B.I. Florea  
G. Hendriks  
L. de Petrocellis  
H.S. Overkleeft  
T. Hankemeier  
C.I. de Zeeuw  
V. Di Marzo  
M. Maccarrone  
B.F. Cravatt  
S.A. Kushner  
M. van der Stelt

## Activity-based protein profiling reveals off-target proteins of FAAH inhibitor BIA 10-2474

**ABSTRACT** | A recent phase I trial of the fatty acid amide hydrolase (FAAH) inhibitor BIA 10-2474 led to the death of one volunteer and produced mild-to-severe neurological symptoms in four others. Although the cause of the clinical neurotoxicity is unknown, it has been postulated that, given the clinical safety profile of other tested FAAH inhibitors, off-target activities of BIA 10-2474 may have played a role. The BIA 10-2474 interaction landscape was determined by activity-based proteomics and revealed that the drug inhibits several lipases that are not targeted by PF04457845, a highly selective and clinically tested FAAH inhibitor. BIA 10-2474, but not PF04457845, produced substantial alterations in lipid networks in human cortical neurons, suggesting that promiscuous lipase inhibitors have the potential to cause metabolic dysregulation in the nervous system.

## Introduction

Severe adverse effects of drug candidates are rarely observed in phase I clinical trials, due to extensive preclinical toxicological profiling in animals and precautions taken into account in the design of first-in-human studies. However, in January 2016, a first-in-human study of the fatty acid amide hydrolase (FAAH) inhibitor BIA 10-2474 led to the death of one volunteer and the hospitalization of four others<sup>1–4</sup>. All patients manifested mild-to-severe neurological symptoms<sup>3</sup>. In rodents, no obvious toxicological results were found with BIA 10-2474 that could predict the observed human clinical neurotoxicity. In a study on dogs treated for 13 weeks with BIA 10-2474, a dose-dependent pulmonary toxicity was observed and two dogs from the subgroup receiving the highest dose were sacrificed<sup>4</sup>. An initial toxicology study in primates showed that the highest administered dose led to axonal dystrophy in the spinal bulb. A follow-up primate study led to the death of one animal and the sacrifice of several others for undisclosed ethical reasons<sup>4</sup>. However, these findings were not considered to be sufficiently concerning to abandon the first-in-human studies due to the large therapeutic window in preclinical studies of BIA 10-2474.

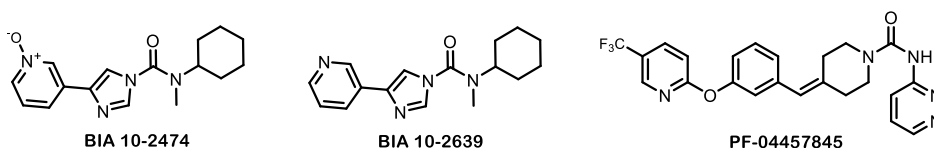


**Figure 1 | Chemical structures of FAAH inhibitor BIA 10-2474, its metabolite BIA 10-2639, and clinically safe FAAH inhibitor PF04457845.**

The BIA 10-2474 target enzyme FAAH is a membrane-bound serine hydrolase that degrades the endocannabinoid anandamide and related amidated lipids<sup>5–8</sup>. Three explanations for the clinical neurotoxicity of BIA 10-2474 have been proposed: (I) errors may have occurred in the clinical trial itself, either in the manufacturing or handling of the compound or in the conduct of the trial; (II) through its inhibitory effects on FAAH, BIA 10-2474 may have produced high levels of long-chain fatty acid amides (e.g. anandamide) and their oxygenated metabolites, which could potentially overstimulate cannabinoid CB1R<sup>8</sup>, TRPV1<sup>9</sup>, and/or NMDA receptors<sup>10</sup>; or (III) BIA 10-2474 and/or its metabolites might have off-target activities. The first hypothesis was dismissed by the French authorities<sup>4</sup>. The second hypothesis is considered unlikely because other FAAH inhibitors, such as PF04457845, have exhibited favorable safety profiles in phase I and II clinical trials<sup>11,12</sup>. The third hypothesis has not been directly evaluated, because little or no information was available regarding the protein interaction profile of BIA 10-2474<sup>1</sup>.

BIA 10-2474 (Figure 1) contains an electrophilic imidazole urea that may react with the nucleophilic serine of FAAH and other serine hydrolases to form covalent and irreversible adducts. Based on previously developed chemical proteomic methods to map the interaction landscapes of (ir)reversible serine hydrolase inhibitors<sup>13–15</sup>, it was anticipated that the serine hydrolase targets of BIA 10-2474 could be identified and

compared to the selectivity profiles of clinical FAAH inhibitor PF04457845 (Figure 1), which has progressed to phase II trials without any serious adverse events<sup>16</sup>. BIA 10-2639, a confirmed metabolite in which the *N*-oxide is reduced to a pyridine (Figure 1)<sup>4</sup> was investigated to compare inhibitor and metabolite activity.

The interaction landscape of BIA 10-2474 was investigated by activity-based protein profiling (ABPP), a chemical proteomic method that employs active site-directed chemical probes to record the functional state of entire enzyme classes directly in native biological systems<sup>13–15</sup>. When coupled to fluorescent reporter groups, activity-based probes (ABPs) enable convenient visualization of enzyme activities in complex proteomes by SDS-PAGE (sodium dodecyl sulfate polyacrylamide gel electrophoresis) and in-gel fluorescence scanning. When coupled to a biotin reporter group, ABPs enable affinity enrichment and identification of enzyme activities by mass spectrometry (MS)-based proteomics. In either format, ABPP serves as a versatile method to assess target engagement and proteome-wide selectivity for small-molecule inhibitors as pre-incubation of the proteome with an inhibitor will reduce the ABP labeling of proteins targeted by the inhibitor.

## Results

### BIA 10-2474 is a weak irreversible inhibitor of FAAH and ABHD6 *in vitro*

Competitive and comparative gel-based ABPP was performed using two different probes: the broad spectrum serine hydrolase-directed fluorophosphonate-rhodamine (FP-TAMRA) and the tailored  $\beta$ -lactone probe MB064 that preferentially reacts with endocannabinoid related hydrolases diacylglycerol lipase  $\alpha$  (DAGL $\alpha$ ),  $\alpha/\beta$  hydrolase domain containing protein 6 (ABHD6) and 12 (ABHD12), along with a handful of other enzymes<sup>14</sup>. Together, FP-TAMRA and MB064 provided a target engagement assay for FAAH and a broad array (>50) of other brain serine hydrolases.

Human frontal cortex (GFi3) and cerebellum samples were acquired from three male donors (aged 49, 50, and 80 years old with a post-mortem delay of 4–8 h) without any history of neuropsychiatric illness or postmortem evidence of neuropathology. ABPP studies revealed that the membrane and soluble serine hydrolase content were overlapping but varied between these brain regions (Supplementary Figure S1). The identity of FAAH and other endocannabinoid hydrolases including DAGL $\alpha$  and ABHD6 was confirmed with reference inhibitors by competitive ABPP (Supplementary Figure S2). In total, 49 and 56 fluorescent bands corresponding to putative serine hydrolases were detected in frontal cortex (Figure 2A–D) and cerebellum (Supplementary Figure S3A–D) respectively.

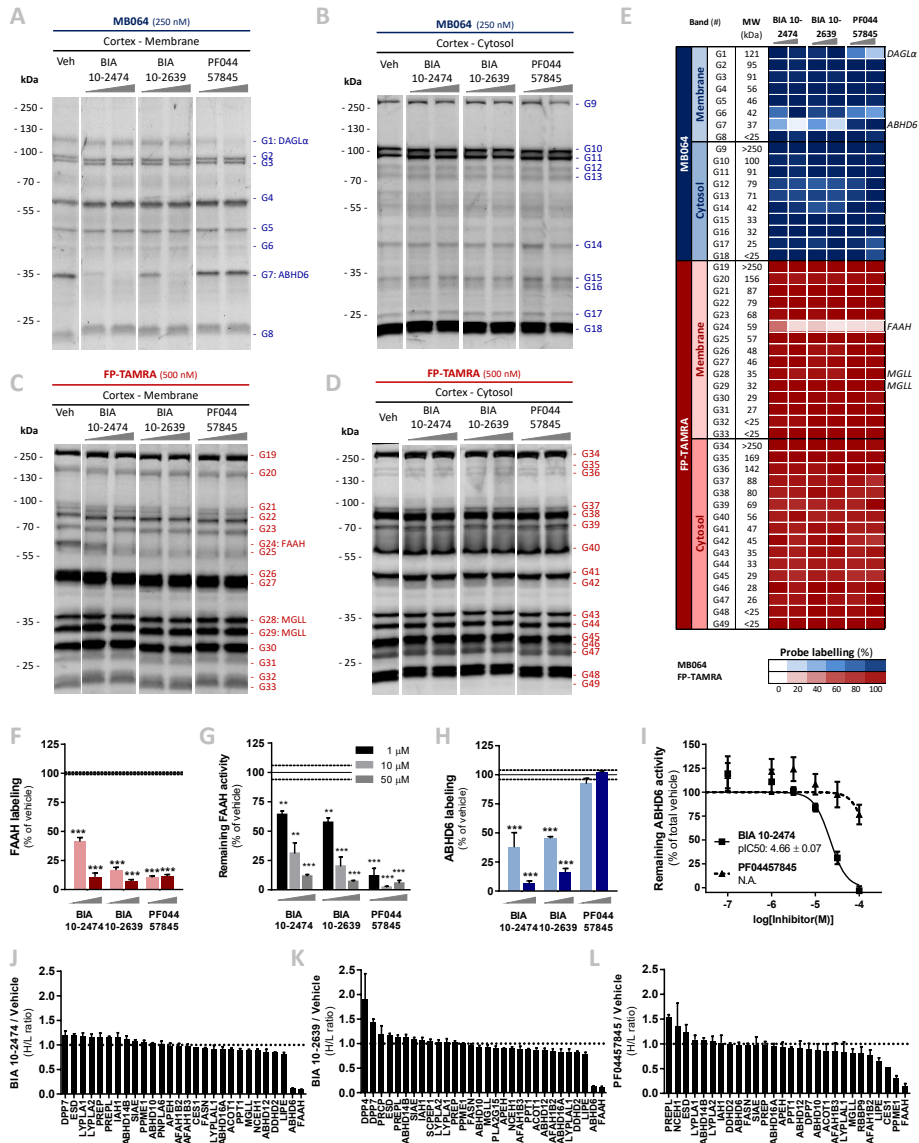


**Figure 2 | Identification of FAAH and ABHD6 as *in vitro* targets of BIA 10-2474 by competitive ABPP on serine hydrolases.** (A-F, H) Gel-based ABPP analysis of human cortex (GF13) proteome incubated *in vitro* with vehicle or inhibitor BIA 10-2474, BIA 10-2639 or PF04457845 (10/50  $\mu$ M, 30 min, 37  $^{\circ}$ C) and subsequently labeled with MB064 (250 nM) (A, B) or FP-TAMRA (500 nM) (C, D) (20 min, rt). The serine hydrolase activities were quantified, normalized for protein loading and expressed relative to control. Heat-map summary of all 49 quantified bands (E) and bar-graph depiction of BIA 10-2474 (off)-targets FAAH (F) and ABHD6 (H). (G) FAAH activity relative to vehicle treated control after incubation with BIA 10-2474, BIA 10-2639 or PF04457845 (1/10/50  $\mu$ M, 15 min, rt) as measured in a radiometric [ $^{14}$ C]-anandamide assay on purified recombinant FAAH. (I) Dose response curve of BIA 10-2474 and PF04457845 on recombinant ABHD6, as measured in a natural substrate assay. (J-L) Chemical proteomics analysis of human cortex (GF13) proteome, treated with BIA 10-2474 (J), BIA 10-2639 (K), or PF04457845 (L) (50  $\mu$ M, 30 min, 37  $^{\circ}$ C) using probes MB108 or FP-biotin (10  $\mu$ M, 60 min, rt). Data is expressed as a H/L ratio as compared to vehicle treated sample. (E-L) Data is expressed as mean  $\pm$  SEM (E-H, J-L: n=3, K: n=4) with \* p < 0.05, \*\* p < 0.01, \*\*\* p < 0.001 (two-tailed t-test).



The clinical trial subjects who developed neurological symptoms were exposed to a dosage of BIA 10-2474 that was 10 to 50 times higher than that required for blockade of FAAH activity in the clinical trial participants<sup>4</sup>. Inhibitor activity against FAAH and other serine hydrolases was therefore evaluated at two high concentrations (10 and 50  $\mu\text{M}$ ) in human brain soluble and membrane proteomes by gel-based competitive ABPP. Representative gel-based ABPP data are shown (Figure 2A-D, Figure 2A-D) alongside a heat map that summarizes the inhibitor-serine hydrolase interaction landscape (Figure 2E, Supplementary Figure S3E).

BIA 10-2474, BIA 10-2639, and PF04457845 all inhibited FAAH, with BIA 10-2474 showing the weakest inhibitory effect (Figure 2F). In a radioactive substrate assay using [<sup>14</sup>C]-anandamide, the weak inhibitory activity of BIA 10-2474 and BIA 10-2639 was confirmed with  $\text{IC}_{50}$  values  $> 1 \mu\text{M}$  as compared to  $\pm 0.01 \mu\text{M}$  for PF04457845 (Figure 2G). Notably, BIA 10-2474 as well as its metabolite exhibited distinct off-target activity towards ABHD6 in the gel-based assay (Figure 2H), which was not observed for PF04457845. Moreover, BIA 10-2474 and its metabolite did not reduce the labeling of endocannabinoid hydrolases monoacylglycerol lipase (MGLL) and DAGL $\alpha$  (Figure 2E, Supplementary Figure S3E).

The brain off-target profiles of FAAH inhibitors were confirmed and extended by performing ABPP coupled to high-resolution quantitative mass spectrometry (MS). This methodology allows for a more accurate quantification by avoiding the band overlap observed with the gel-based assays and enables screening of the inhibitors over a broader range of serine hydrolases. Quantitative MS confirmed complete inhibition of FAAH and validated ABHD6 as an off-target of BIA 10-2474 and its metabolite, but not of PF04457845 (Figure 2J-L). PPME1 was identified as a potential off-target of PF04457845 with a heavy/light ratio  $< 0.5$  (Figure 2L).

To confirm that the off-target ABHD6 identified by ABPP was inhibited in its catalytic activity, its activity was measured in a real-time fluorescence-based natural substrate assay<sup>17</sup>. BIA 10-2474 inhibited recombinant ABHD6-mediated hydrolysis of 2-AG with an  $\text{IC}_{50}$  of  $22 \pm 4 \mu\text{M}$  ( $n=4$ ), whereas PF04457845 was inactive ( $\text{IC}_{50} > 100 \mu\text{M}$ ) (Figure 2I). Notably, BIA 10-2474, BIA 10-2639 and PF04457845 did not cross-react with other proteins of the endocannabinoid system including DAGL $\alpha$ , DAGL $\beta$ , MGLL and *N*-acyl phosphatidylethanolamine phospholipase D (NAPE-PLD), nor with the endocannabinoid-binding TRP ion channels (Supplementary Tables S1, S2).

The BIA 10-2474 interaction profiling was extended with three compounds in which an alkyne functionality was introduced at different positions in the molecule (AJ167, AJ179, AJ198) (Supplementary Figure S4A)<sup>18</sup>. The alkyne group serves as a ligation handle to introduce fluorescent reporter groups via copper(I)-catalyzed azide-alkyne cycloaddition (“click”) chemistry<sup>19</sup>. Few additional labeled proteins were detected in human cortical and cerebellar proteomes (Supplementary Figure S4E-G) for which no competition was observed upon pre-incubation with BIA 10-2474, indicating limited

cross-reactivity of BIA 10-2474 with non-serine hydrolases in the brain proteome. Importantly, these experiments definitively prove covalent binding of AJ179 and AJ198 to FAAH (Supplementary Figure S4B-C, E-F), which was maintained even under denaturing SDS-PAGE conditions, thereby supporting an irreversible reaction mechanism for BIA 10-2474.

### BIA 10-2474 inhibitory potency is drastically improved *in situ*

As noted above, in the biochemical substrate assay using recombinant FAAH and gel-based ABPP experiments with human brain lysates, BIA 10-2474 exhibited weaker *in vitro* potency for FAAH compared to PF04457845. Notably, this difference was attenuated *in situ*, as our gel-based ABPP experiments revealed that BIA 10-2474 inhibited FAAH, as well as other serine hydrolases (e.g., ABHD6 and FAAH2, which is a human-specific orthologue of FAAH<sup>20</sup>) with substantially increased potency in human cells (Figure 3). The reason for the increased cellular activity of BIA 10-2474 is at present unclear, but it was consistently observed in multiple cell types (data not shown) and with multiple protein targets of the compound, which may suggest that cellular accumulation of the compound results in greater than expected inhibitory activity against FAAH and other serine hydrolases. Previous chemical proteomic studies have uncovered similar effects for covalent kinase inhibitors<sup>21</sup>.

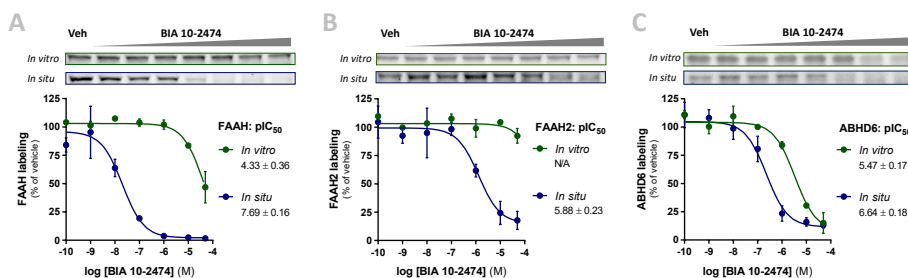


**Figure 3 | BIA 10-2474 inhibitory potency towards FAAH, FAAH2, and ABHD6 is increased *in situ*.** (A-C) Dose response curves of BIA 10-2474 against FAAH, ABHD6 and FAAH2 *in vitro* and *in situ*. HEK293-T cells transiently overexpressing FAAH (A) or FAAH2 (B), or endogenously expressing ABHD6 (C) were treated *in situ* with vehicle or BIA 10-2474 (0.1 nM – 50  $\mu$ M, 2 h, 37  $^{\circ}$ C), harvested and subsequently prepped as whole lysates (*in situ* samples, blue). Alternatively, membrane fractions from HEK293-T cells overexpressing recombinant FAAH and FAAH2 were mixed and *in vitro* incubated with vehicle of BIA 10-2474 (0.1 nM – 50  $\mu$ M, 30 min, 37  $^{\circ}$ C) (*in vitro* samples, green). Subsequently, all samples were labeled with activity-based probe FP-TAMRA (500 nM, 20 min, RT). Remaining probe labeling was quantified, normalized for protein loading and expressed relative to vehicle treated sample. Data is expressed as mean  $\pm$  SEM (Vehicle: n=6, BIA: n=3) and pIC<sub>50</sub>  $\pm$  SD.

### BIA 10-2474 disrupts the neural lipid network by targeting multiple hydrolases

In light of the increased *in situ* potency of BIA 10-2474, its off-target profile was investigated in human cortical neurons using gel-based ABPP studies. Apart from FAAH and ABHD6, three additional targets were identified with molecular weights of approximately 150, 62 and 47 kDa respectively (Figure 4A). Using chemical proteomics,

these off-targets were confirmed and identified as patatin-like phospholipase domain containing protein 6 (PNPLA6, also known as neuropathy target esterase (NTE)), carboxyl esterase 2 (CES2) and phospholipase 2 group XV (PLA2G15, also known as phospholipase A2 (LPLA2)) with a heavy/light ratio < 0.5 (Figure 4B).

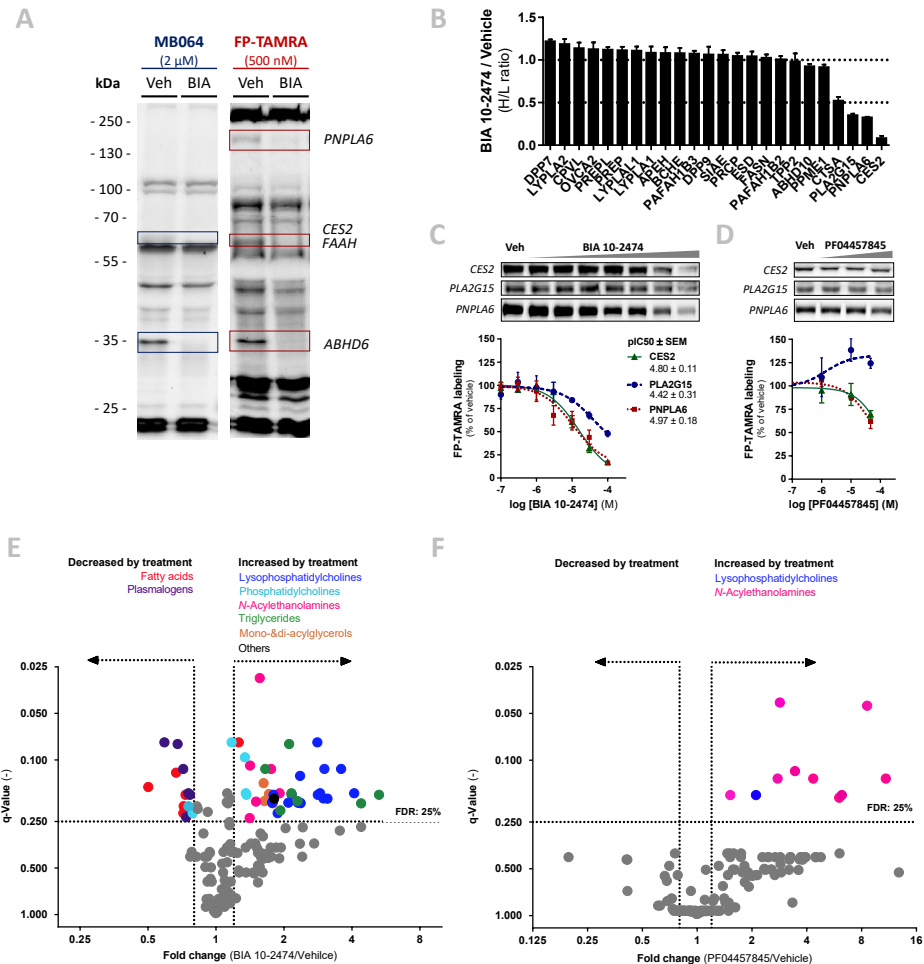


**Figure 4 | *In situ* treatment of human neuronal cultures with BIA 10-2474 reveals additional off-targets and results in disruption of lipid homeostasis.** (A-B) Human neuronal cultures were treated *in situ* with vehicle or BIA 10-2474 (50  $\mu$ M, 24 h, 37  $^{\circ}$ C). Lysates were labeled with activity-based probes MB064 (2  $\mu$ M) or FP-TAMRA (500 nM) (20 min, rt) for gel-based ABPP (A) or with MB108 or FP-biotin (10  $\mu$ M, 60 min, rt) for chemical proteomics (B). (C-D) Dose response curves of BIA 10-2474 against CES2, PLA2G15 or PNPLA6 *in situ*. HEK293-T cells transiently overexpressing CES2, PLA2G15, or PNPLA6 were treated *in situ* with vehicle, BIA 10-2474 (0.1-100  $\mu$ M) (C), or PF04457845 (0.1 – 50  $\mu$ M) (D) (24 h, 37  $^{\circ}$ C). Whole lysates were labeled with activity-based probe FP-TAMRA (500 nM, 20 min, rt). Remaining probe labeling was quantified, normalized for protein loading and expressed relative to vehicle treated sample. Data is expressed as mean  $\pm$  SEM (vehicle: n=6, treated: n=3) and pIC<sub>50</sub>  $\pm$  SD. (E-F) Volcano plot of lipidomics analysis of human neurons treated *in situ* with vehicle, BIA 10-2474 (50  $\mu$ M) (E), or PF04457845 (1  $\mu$ M) (F) (48 h, 37  $^{\circ}$ C). Lipids with a fold change (FC) threshold of  $\geq 1.20$  or  $\leq 0.80$  and Benjamini–Hochberg false discovery rate (FDR)  $\leq 25\%$  are represented by colored circles distinguished by lipid class (n=3).

Most of the interaction partners of BIA 10-2474 identified in this study are known to be involved in cellular lipid metabolism<sup>22,23</sup>. To confirm the interaction of BIA 10-2474 with its lipolytic serine hydrolase off-targets, these proteins were transiently overexpressed in HEK293-T cells and concentration-dependent *in situ* inhibition was assessed using gel-based ABPP (Figure 4C-D). BIA 10-2474, but not PF04457845, inhibits PNPLA6, CES2 and PLA2G15 with IC<sub>50</sub>-values of 11, 16 and 38  $\mu$ M respectively.

Based on the off-target profile of BIA 10-2474 it was postulated that prolonged exposure to BIA 10-2474 might result in alterations of human neuronal lipid metabolism. This hypothesis was tested by targeted lipidomics analysis of human cortical neurons treated with vehicle or BIA 10-2474. In total, 161 lipid species were quantified from which significant changes in several lipid classes were observed. Levels of *N*-acylethanolamines, triglycerides, monoacylglycerols, and (lyso)phosphatidylcholines were increased in BIA 10-2474-treated cells, while those of free fatty acids and plasmalogens were reduced, consistent with the inhibition of FAAH, FAAH2, ABHD6, CES2, PLA2G15, and PNPLA6 activities (Figure 4E). Prolonged treatment with PF04457845 only affected lipid levels of a lysophosphatidylcholine and increased several *N*-acylethanolamines, consistent with FAAH and FAAH2 inhibition (Figure 4F).

## Discussion

No information had previously been available regarding the protein interaction profile of BIA 10-2474 that could help in defining the cause of its clinical toxicity, and in particular to directly evaluate the possibility that the observed clinical neurotoxicity might have resulted from off-target activity<sup>1</sup>. Aided by chemical proteomic methods for mapping the interaction landscapes of serine hydrolase inhibitors<sup>13–15,24,25</sup>, the serine hydrolase target selectivity of BIA 10-2474 was compared to that of PF04457845, a widely used clinically safe FAAH inhibitor. Here, BIA 10-2474 was shown to be an irreversible, potent FAAH and FAAH2 inhibitor *in situ*, that increases cellular levels of long-chain fatty acid ethanolamines. Using human brain tissue lysates and cultured human cortical neurons and cell lines, multiple lipase off-targets of BIA 10-2474 (including ABHD6, CES2, PLA2G15 and PNPLA6) were discovered that were not targeted by PF04457845. By targeting these lipases, BIA 10-2474 disrupted the neural lipid metabolism, resulting in increased levels of *N*-acylethanolamines, monoacylglycerols, triglycerides, (lyso)phosphatidylcholines, and reductions in free fatty acids and plasmalogens. When considering the basis for BIA 10 2474's broader interaction profile with serine hydrolases compared to PF04457845, the greater intrinsic reactivity of BIA 10-2474, which is reflected in a much faster rate of methanolysis (data not shown), may have been a contributing factor.

FAAH2 is a human orthologue of FAAH, which also degrades long-chain fatty acid amides<sup>20</sup>. However, little is known about the neurobiological function of FAAH2. CES2 is a serine esterase involved in the hydrolysis of ester and amide bonds of xenobiotics and prodrugs, but also of endogenous lipids. It is highly expressed in the liver and in

endothelial cells. Hepatic CES2 is required for triglyceride homeostasis by modulating lipolysis, ER stress and lipogenesis<sup>26</sup>. PLA2G15 is a lysosomal phospholipase highly expressed in alveolar macrophages and microglial cells. Inhibition of PLA2G15 leads to accumulation of phosphatidylcholines and phosphatidylethanolamines, and has previously been implicated in drug-induced phospholipidosis<sup>27</sup>.

ABHD6 has a minor role in endocannabinoid 2-arachidonoylglycerol (2-AG) metabolism<sup>28</sup>, degrades bis(monoacylglycerol)phosphate<sup>29</sup>, and acts as a lysophosphatidyl hydrolase<sup>22,28</sup>. Independent of its catalytic function, ABHD6 exhibits a scaffolding function. Recently, proteomic experiments revealed that ABHD6 physically interacts with the C-terminal tail of the GluR1 subunit of the  $\alpha$ -amino-3-hydroxy-5-methyl-4-isoxazolepropionic acid receptor (AMPA), one of the major postsynaptic ionotropic glutamate receptors mediating excitatory synaptic neurotransmission in the central nervous system. Two independent groups have shown that ABHD6 is a potent negative regulator of cell surface trafficking of GluR1-containing AMPARs<sup>30,31</sup>. Some enzyme inhibitors are known to act as chemical chaperones increasing cellular protein levels by reducing proteolysis or enhancing protein biosynthesis and folding<sup>32</sup>. BIA 10-2474 might also act as a chemical chaperone to modulate ABHD6 protein levels, thereby possibly affecting AMPAR signaling in neuronal tissue.

PNPLA6 has previously been linked to neurodegeneration in humans resulting from organophosphate-based pesticides<sup>23,33</sup>. PNPLA6 is a (lyso)phospholipase that uses (lyso)phosphatidylcholine as a substrate and is highly expressed in endothelial cells, astrocytes, and neurons. Proper neuronal phosphatidylcholine homeostasis mediated by PNPLA6 is required for axonal maintenance<sup>34</sup>. PNPLA6 inhibition leads to neurodegeneration following an age-dependent neuropathy of increasing severity in older age. Notably, PNPLA6-mediated neurotoxicity following acute organophosphate exposure is species dependent, with less pronounced effects in rodents than humans. Mice with a homozygous germline deletion of PNPLA6 have embryonic lethality due to placental and vasculature defects, however, brain-specific deletion of PNPLA6 results in prominent neuronal pathology<sup>35</sup>. A threshold of > 70% PNPLA6 inhibition has been determined as responsible for developing neurodegeneration upon organophosphate exposure in chicken<sup>23,33</sup>. It is remarkable that many clinical symptoms arising from PNPLA6-mediated neurological sequelae following organophosphate exposure resemble the neuropathology observed in the clinical trial participants<sup>3</sup> who received a cumulative dose of 250-300 mg of BIA 10-2474, including precedent for human neurotoxicity, brain region sensitivity, age dependency, species selectivity, dosing threshold and time course of neuropathology. Additional experimental evidence and more detailed information from the Rennes' clinical trial will be required to firmly establish the relative causality of the identified BIA 10-2474 off-targets. Importantly, based on this work it cannot be excluded that non-covalent interactions of BIA 10-2474 may have contributed to the drug's neurotoxic effects.

## Conclusion

Taken together, this study shows that BIA 10-2474 is a covalent irreversible and non-selective serine hydrolase inhibitor and highlights the disruption of cellular lipid networks as an important potential mediator of the observed neurotoxicity. The described data do not reveal whether inhibition of one or more of the identified BIA 10-2474's off-target proteins (including FAAH2, ABHD6, PNPLA6, PLA2G15 and CES2) are responsible for the clinical neurotoxicity caused by this drug. However, the study does emphasize the general utility of ABPP as a versatile chemical proteomic method to assess on-target engagement and off-target activity of covalent drugs to guide therapeutic development. In retrospect, it appears likely that the implementation of a method such as ABPP might have permitted a safer clinical trial design for BIA 10-2474 by establishing a dose range in which FAAH was inhibited, but still below the threshold for engaging off-target interactions.

## Experimental procedures

### Materials, probes and inhibitors

Activity-based probe TAMRA-fluorophosphonate (FP-TAMRA) was purchased from ThermoFisher, MB064 and MB108 were synthesized in-house as previously described<sup>24</sup>. PF04457845 was synthesized in house, as well as purchased from Sigma Aldrich. Inhibitors BIA 10-2474, BIA 10-2639 and activity-based probes AJ167, AJ179, AJ198 were synthesized in-house as previously described<sup>18</sup>. All synthesized compounds were at least 95% pure and were analyzed by LC-MS, NMR and HRMS. Other chemicals, reagents, and primers were purchased from Sigma Aldrich unless indicated otherwise.

### Cloning

Full-length human cDNA of ABHD6, FAAH, PNPLA6, PLA2G15, CES2 (Source Bioscience) and FAAH2 (BioCat) was cloned into mammalian expression vector pcDNA3.1, containing genes for ampicillin and neomycin resistance. The inserts were cloned in frame with a C-terminal FLAG-tag and site-directed mutagenesis was used to remove restriction sites by silent point mutations. Plasmids were isolated from transformed XL-10 Z-competent cells (Maxi Prep kit: Qiagen) and sequenced at the Leiden Genome Technology Center. Sequences were analyzed and verified (CLC Main Workbench).

### Cell culture

#### *General*

HEK293-T (human embryonic kidney) cells were cultured at 37 °C under 7% CO<sub>2</sub> in DMEM containing phenol red, stable glutamine, 10% (v/v) new born calf serum (Thermo Fisher), and penicillin and streptomycin (200 µg/mL each; Duchefa). Medium was refreshed every 2-3 days and cells were passaged twice a week at 80-90% confluency by resuspension in fresh medium. Cell lines were purchased from ATCC and were regularly tested for mycoplasma contamination. Cultures were discarded after 2-3 months of use.

#### *Human neural cell culture*

Human iPSC-derived neural progenitor cells (NPCs) (Axol Biosciences, line ax0015) were plated on sterile coverslips in 12-well plates, coated with poly-L-ornithin/laminin (Sigma-Aldrich), in neural differentiation medium (Neurobasal medium, 1% N2 supplement, 2% B27-RA supplement, 1% MEM-NEAA, 20 ng/mL BDNF (ProSpec Bio)), 20 ng/mL GDNF (ProSpec Bio), 1 µM db-cAMP (Sigma-Aldrich), 200 µM ascorbic acid (Sigma-Aldrich), 2 µg/mL laminin, and 1% P/S), resulting in neural networks composed of neurons and glia. Cells were refreshed with neural differentiation medium 3 times per week. During weeks 1-4, medium was fully refreshed. After 4 weeks of neural differentiation, only half of the volume of medium per well was refreshed.

#### *Transient Transfection*

One day prior to transfection HEK293-T cells were seeded to 15 cm dishes or 12 wells plates (~62.500 cells/cm<sup>2</sup>). Prior to transfection, culture medium was aspirated and a minimal amount of medium was added. A 3:1 (m/m) mixture of polyethylenimine (PEI) (60 µg/dish or 1.875 µg/well) and plasmid DNA (20 µg/dish or 0.625 µg/well) was prepared in serum free culture medium and incubated (15 min, rt). Transfection was performed by dropwise addition of the PEI/DNA mixture to the cells. Transfection with the empty pcDNA3.1 vector was used to generate control samples. After 24 h, medium was refreshed. Medium was aspirated 48 or 72 h post-transfection and cells were harvested by resuspension in PBS. Cells were pelleted by

centrifugation (5 min, 1,000 g) and the pellet was washed with PBS. Supernatant was discarded and cell pellets were frozen in liquid nitrogen and stored at -80 °C until sample preparation.

#### *In situ treatment*

*In situ* treatment was initiated 24 h (for 24-48 h treatment) or 48 h (for 2 h treatment) post-transfection in 12 wells plates. Medium was aspirated and medium containing inhibitor or DMSO as vehicle was added (0.1 - 1.0% DMSO, DMSO concentration constant within each experiment). Final concentrations for inhibitors are indicated in the main text and figure legends. After 2, 4, 24, or 48 h exposure to treatment medium, medium was aspirated and cells were harvested and stored as described above until sample preparation (whole cell lysate).

### Sample preparation

#### *Whole cell lysate*

Cell pellets were thawed on ice, resuspended in cold lysis buffer (20 mM HEPES pH 7.2, 2 mM DTT, 250 mM sucrose, 1 mM MgCl<sub>2</sub>, 2.5 U/mL benzonase) and incubated on ice (15 min). The cell lysate was used for membrane preparation (below) or was diluted to appropriate concentration in cold storage buffer (20 mM Hepes, pH 7.2, 2 mM DTT) for use as whole lysate (HEK293-T: 2.0 mg/mL, neuronal cultures: 1.5 mg/mL). Protein concentrations were determined by a Quick Start™ Bradford Protein Assay (Bio-Rad) and diluted samples were flash frozen in liquid nitrogen and stored at -80 °C until further use.

#### *Tissue lysate*

Human Brain Tissue was supplied by the Netherlands Brain Bank and stored at - 80 °C until use. Tissues were thawed on ice, dounce homogenized in cold lysis buffer (20 mM HEPES pH 7.2, 2 mM DTT, 250 mM sucrose, 1 mM MgCl<sub>2</sub>, 2.5 U/mL benzonase) and incubated on ice (15 min), followed by two low-speed spins (3 min, 2500 g, 4 °C) to remove debris. The supernatant fraction was used for separation of the cytosolic and membrane fractions.

#### *Membrane preparation from lysate*

The membrane and cytosolic fractions of cell or tissue lysates were separated by ultracentrifugation (93,000 g, 45 min, 4 °C). The supernatant was collected (cytosolic fraction) and the membrane pellet was resuspended in cold storage buffer by thorough pipetting and passage through an insulin needle. Protein concentrations were determined by a Quick Start™ Bradford Protein Assay (Bio-Rad) and samples were diluted to 2.0 mg/mL with cold buffer (20 mM Hepes pH 7.2, 2 mM DTT), flash frozen in liquid nitrogen and stored at -80 °C until further use. FAAH and FAAH2 overexpression membranes were mixed in an appropriate ratio for ABPP (0.1 mg/mL : 1.0 mg/mL).

### Activity-based protein profiling

#### *Direct activity-based probes*

Gel-based ABPP was performed and analyzed with minor adaptations on previously reported procedures<sup>24</sup>. In brief, for *in vitro* inhibition, human brain proteome or cell lysate was incubated with vehicle (2.5% DMSO) or inhibitor (final concentrations indicated in figure legends) (30 min, 37 °C), followed by an incubation with the activity-based probe MB064 (250 nM, 2 μM) or FP-TAMRA (500 nM) (20 min, rt). Lysates from *in situ* treated cells were directly incubated with activity-based probes. Reactions were quenched with Laemmli buffer (30 min, rt) and proteins (brain: 20 μg, HEK293-T: 10 μg, neurons: 7.5 μg) were resolved by SDS-PAGE (10% acrylamide gel, 180 V, 75-80 min). In-gel fluorescence was scanned using Cy3 and Cy5 multichannel settings (605/50 and 695/55 filters, respectively) on a ChemiDoc imaging system (Bio-Rad) and stained with coomassie after scanning. Fluorescence was normalized to coomassie staining and quantified



with ImageLab™ software (Bio-Rad). Data was processed in Excel (Microsoft) and graphs and IC<sub>50</sub> fits were prepared with Graphpad Prism 7 (Graphpad).

### Two-step activity-based probes

The two-step labeling was adapted from previously developed methods<sup>36</sup>. In brief, human brain proteome (80 µg in 40 µL, cytosol or membrane fraction) was pre-incubated with vehicle or inhibitor (50 µM, 30 min, 37 °C), followed by an incubation with the alkyne probe (50 µM, 30 min, 37 °C) and subsequent conjugation to Cyanine-5-azide (Cy5-N<sub>3</sub>) by addition of 5 µL freshly prepared click mix (40 mM CuSO<sub>4</sub>·(H<sub>2</sub>O)<sub>5</sub>, 240 mM sodium ascorbate, 0.3 mM THPTA, 35 µM Cy5-N<sub>3</sub>) (60 min, rt). Proteins were precipitated by adding methanol (50 µL), chloroform (15 µL) and water (15 µL), mixed by brief vortexing and pelleted by centrifugation (10 min, 4000 rpm). The supernatant was removed and the pellet was washed twice with methanol (50 µL). The pellet was redissolved in Laemmli buffer (40 µL, 95 °C, 5 min) and 20 µg protein was resolved by SDS-PAGE (10% acrylamide gel, 180 V, 75-80 min). In-gel fluorescence was scanned using Cy3- and Cy5-multichannel settings (605/50 and 695/55 filters, respectively) on a ChemiDoc imaging system (Bio-Rad) and stained with coomassie after scanning.

### Activity-based proteomics

Activity-based proteomics was based on previously described procedures<sup>14</sup>. In summary, human GF13 proteome (250 µg protein from cytosolic or membrane fraction) or human neurons (90 µg protein from whole lysate, *in situ* vehicle or inhibitor treated) was incubated with vehicle (2% DMSO) or inhibitor (BIA 10-2474 or PF04457845, 50 µM, 30 min, 37 °C). The proteome was labeled with MB108 or FP-Biotin (10 µM, 60 min, rt). The labeling reaction was quenched and after a chloroform/methanol precipitation, the precipitated proteome was resuspended in 6 M Urea / 25 mM ammonium bicarbonate (15 min, rt). The proteome was reduced (10 µM DTT, 15 min, 65 °C), alkylated (iodoacetamide, 40 mM, 30 min, rt), and subsequently heated with SDS (0.2%, 5 min, 65 °C). Avidin-Agarose beads (50 µL of a 50% slurry / sample) were washed with PBS and incubated with the proteome (3 h, rt, shaking). Beads were isolated by centrifugation (2500 g, 2 min) and washed with SDS-PBS (0.5% w/v) once and three times with PBS. After transfer to a low-binding Eppendorf tube, proteins were digested with sequencing grade trypsin (Promega) (500 ng per sample) in 250 µL OB-Dig buffer (100 mM Tris pH 8.0, 100 mM NaCl, 1 mM CaCl<sub>2</sub>, 2% acetonitrile) (37 °C, O/N, 900 rpm). The pH was adjusted with formic acid to pH 3 and beads were removed by filtration. Peptides were isotopically labeled by on stage-tip dimethyl labeling, with subsequent addition of 20, 20, 30, 30, and 40 µL of light (vehicle, L) or medium (inhibitor, H) reagent to the stage-tips. The centrifugation speed during labeling was adjusted to have a flow through time of approximately 5 min (400 - 1000 g) per labeling step.

## Targeted lipidomics

### Sample extraction

Lipids were extracted from *in situ* treated human neurons (48 h, 50 µM BIA 10-2474, 1 µM PF04457845 or vehicle (0.25% DMSO)). The sample extraction was performed on ice. In brief, cell pellets with 1 million cells were transferred to 1.5 mL Eppendorf tubes, spiked with 10 µL each of deuterated internal standard mix for endocannabinoids (*N*-arachidonylethanolamide (AEA)-d8, *N*-arachidonoyldopamine (NADA)-d8, *N*-docosahexaenylethanolamide (DHEA)-d4, 2-arachidonoylglycerol (2-AG)-d8, *N*-stearoylethanolamine (SEA)-d3, *N*-palmitoylethanolamine (PEA)-d4, *N*-linoleoylethanolamine (LEA)-d3 and *N*-oleoylethanolamine (OEA)-d4), positive apolar lipids (lysophosphatidylcholines (LPC)17:0, phosphatidylethanolamines (PE)17:0/17:0, phosphatidylcholines (PC)17:0/17:0, sphingomyelins (SM) d18:1/17:0, triglycerides (TG) 17:0/17:0/17:0, ceramides (Cer) d18:1/17:0) and negative polar lipids (fatty acid (FA)17:0-d33), followed by the addition of ammonium acetate buffer (100 µL, 0.1 M, pH 4). After addition of methyl *tert*-butyl ether (1 mL), the tubes were thoroughly mixed for 4 min using a bullet blender

at medium speed (Next Advance), followed by a centrifugation step (5000 *g*, 12 min, 4 °C). Then 925 µL of the upper methyl tert-butyl ether layer was transferred into clean 1.5 mL Eppendorf tubes. Samples were dried in a speed-vac followed by reconstitution in acetonitrile/water (50 µL, 90/10, v/v). The reconstituted samples were centrifuged (14000 *g*, 3 min, 4 °C) before transferring into LC-MS vials. Each sample was injected on three different lipidomics platforms: endocannabinoids (5 µL), positive apolar lipids (2 µL) and for negative polar lipids (8 µL).

#### *LC-MS/MS Analysis for endocannabinoids*

A targeted analysis of 21 endocannabinoids and related *N*-acylethanolamines were measured using an Acquity UPLC I class Binary solvent manager pump (Waters) in conjugation with AB SCIEX 6500 quadrupole-ion trap (QTRAP) (AB Sciex). Separation was performed with Acquity HSS T3 column (1.2 x 100 mm, 1.8 µm) maintained at 45 °C. The aqueous mobile phase A consisted of 2 mM ammonium formate and 10 mM formic acid, and the organic mobile phase B was acetonitrile. The flow rate was set to 0.4 mL/min; initial gradient conditions were 55% B held for 2 min and linearly ramped to 100% B over 6 min and held for 2 min; after 10 s the system returned to initial conditions and held 2 min before next injection. Electrospray ionization-MS was operated in positive mode for measurement of 21 endocannabinoids and NAEs, and a selective Multiple Reaction Mode (sMRM) was used for quantification.

#### *LC-MS/MS analysis for positive apolar and negative polar lipids*

Both lipidomics methods are adapted and modified from previously published work<sup>37</sup>. In brief, these methods are measured on an Acquity UPLC Binary solvent manager pump (Waters) coupled to an Agilent 6530 electrospray ionization quadrupole time-of-flight (ESI-Q-TOF, Agilent, Jose, CA, USA) high resolution mass spectrometer using reference mass correction. The chromatographic separation was achieved on an Acquity HSS T3 column (1.2 x 100 mm, 1.8 µm) maintained at 40 °C for both methods. The positive polar lipids that include targets from different lipid classes including (lyso)phosphatidylcholines, triglycerides, ceramides. (Lyso)phosphatidylethanolamines and sphingomyelins were separated using a flow of 0.4 mL/min over a 16 min gradient. In positive mode, the aqueous mobile phase A consisted of 60/40 (v/v) acetonitrile/H<sub>2</sub>O with 10 mM ammonium formate, and the organic mobile phase B consisted of 10/90 (v/v) acetonitrile/isopropanol with 10 mM ammonium formate. The negative apolar lipids that constitute mainly free fatty acids and (lyso)phosphatidylcholines were separated with a flow of 0.4 mL/min over 15 min gradient. In negative mode, the aqueous mobile phase A consisted of 5/95 (v/v) acetonitrile/H<sub>2</sub>O with 10 mM ammonium formate, and the organic mobile phase B consisted of 99% (v/v) methanol with 10 mM Ammonium formate. The targets in both lipid methods were detected full scan (100-1000 *m/z*) in their respective ion charge mode.

### Activity assays

#### *Radiolabeled natural substrate assay FAAH*

The radiolabeled natural substrate based assay for human FAAH was performed as reported previously<sup>38</sup>. Anandamide (AEA) (Sigma Chemical) was purchased from Sigma Chemical Co., purified FAAH was obtained from Cayman Chemical, [<sup>14</sup>C-ethanolamine]-anandamide (60 Ci/mmol) was purchased from ARC. FAAH (2.5 µg per test) was pre-incubated with each compound (15 min, rt) and subsequently incubated with [<sup>14</sup>C-ethanolamine]anandamide (10 µM, 15 min, 37 °C, in 500 µL of 50 mM Tris-HCl pH 9). The reaction was stopped by the addition of 0.6 mL of ice-cold methanol/chloroform (2:1, v/v). The mixture was centrifuged (3000 *g*, 5 min), the upper aqueous layer was put in a vial containing liquid scintillation cocktail (Ultima Gold XR, Perkin Elmer Life Sciences) and radioactivity was quantified in a β-counter.

*Natural substrate-based fluorescence assay ABHD6*

The natural substrate ABHD6 assay was performed as previously published<sup>39</sup>.

*Natural substrate-based fluorescence assay DAGLα/β*

The natural DAG substrate assay was performed as reported previously<sup>17</sup>. Standard assay conditions: 0.2 U/mL glycerol kinase (GK), glycerol-3-phosphate oxidase (GPO) and horseradish peroxidase (HRP), 0.125 mM ATP, 10 μM Amplifu™Red, 5% DMSO in a total volume of 200 μL. The assay additionally contained 5 μg/mL MGLL-overexpressing membranes, 100 μM SAG and 0.0075% (w/v) Triton X-100, with a final protein concentration of 50 μg/mL. The mDAGLβ assay was performed as the hDAGLα assay, but assay buffer was supplemented with 5 mM CaCl<sub>2</sub> and the SAG concentration was 75 μM.

*Natural substrate-based fluorescence assay MGLL*

The natural substrate MGLL assay was performed as previously published<sup>17</sup>.

*Surrogate substrate assay NAPE-PLD*

The surrogate substrate assay was based on a previously reported method<sup>40</sup>. The membrane protein fraction of HEK293-T cells transiently overexpressing NAPE-PLD was diluted to 0.4 mg/mL in assay buffer (50 mM Tris-HCl pH 7.5, 0.02% Triton X-100, 150 mM NaCl). The substrate PED6 (10 mM, Invitrogen) was consecutively diluted in DMSO (25x) and in assay buffer (10x). The assay was performed in a dark Greiner 96 wells plate, end volume 100 μL. The membrane protein lysate (final concentration 0.04 mg/mL) was incubated with inhibitor or vehicle (30 min, 37 °C). A sample without membrane protein lysate was incorporated for background subtraction. Subsequently, substrate was added (PED6, final concentration: 1 μM) and the measurement is started immediately on a TECAN infinite M1000 pro (37 °C, scanning at 2 min intervals for 1 h: excitation 485 nm, emission 535 nm).

*Radioligand displacement assays for cannabinoid receptors*

[<sup>3</sup>H]CP55940 displacement assays to determine the affinity for the CB1R and CB2R were performed as previously described<sup>25,41</sup>, with the following changes. Ligands of interest were incubated (25 °C, 2 h) with membrane aliquots containing 1.5 μg (CHOK1hCB2<sub>bgal</sub>) membrane protein in 100 μL assay buffer (50 mM Tris-HCl, 5 mM MgCl<sub>2</sub>, 0.1% BSA, pH 7.4) with ~1.5 nM [<sup>3</sup>H]CP55940 per assay point. Non-specific binding was determined in the presence of 10 μM AM630. Filtration was performed on 96-well GF/C filters, each well presoaked for 30 min with 25 μL 0.25% PEI, using a 96-wells Filtermate harvester (PerkinElmer). Filter-bound radioactivity was determined by scintillation spectrometry using a Microbeta<sup>®</sup> 2450 microplate counter (PerkinElmer).

*Fluorescent Ca<sup>2+</sup> assays for TRP ion channels*

HEK293 (human embryonic kidney) cells stably overexpressing recombinant human TRPV1 or rat TRPA1, TRPV2, TRPV3, TRPV4, or TRPM8 were grown in 10 cm Petri dishes as mono-layers in minimum essential medium (MEM) supplemented with non-essential amino acids, 10% fetal bovine serum, 2 mM glutamine, and maintained at 5% CO<sub>2</sub> at 37 °C. Quantitative real time analysis was carried out to measure TRP gene over-expression in transfected-cells (data not shown). On the day of the experiment, cells were loaded with the methyl ester Fluo-4 AM in MEM (4 μM in DMSO containing 0.02% Pluronic F-127, Invitrogen (dark, 1 h, rt) washed twice with Tyrode's buffer (145 mM NaCl, 2.5 mM KCl, 1.5 mM CaCl<sub>2</sub>, 1.2 mM MgCl<sub>2</sub>, 10 mM d-glucose, and 10 mM HEPES, pH 7.4), resuspended in the same buffer and transferred (about 100,000 cells) to the quartz cuvette of the spectrofluorimeter (PerkinElmer LS50B equipped with PTP-1 Fluorescence Peltier System; PerkinElmer Life and Analytical Sciences) under continuous stirring. The effects on intracellular Ca<sup>2+</sup> concentration ([Ca<sup>2+</sup>]<sub>i</sub>) before and after the addition of various concentrations of test compounds was measured by cell fluorescence (excitation: 488 nm, emission: 516 nm, 25 °C).

The effects of compounds were normalized against the response to ionomycin (4  $\mu\text{M}$ ) in each experiment. The increases in fluorescence in wildtype HEK293 cells were used as baseline and subtracted from the values obtained from transfected cells. Efficacy was defined as the maximum response elicited by the compounds tested and was determined by comparing their effect with the analogous effect observed with 4  $\mu\text{M}$  ionomycin (Cayman), while the potency of the compounds ( $\text{EC}_{50}$ ) was determined as the concentration required to produce half-maximal increases in  $[\text{Ca}^{2+}]_i$ . Curve fitting (sigmoidal dose–response variable slope) and parameter estimation were performed with GraphPad Prism 6 (GraphPad).

Antagonist/desensitizing behavior was evaluated by adding the test compounds in the quartz cuvette 5 min before stimulation of cells with agonists. In the case of human TRPV1-expressing HEK293 cells the agonist used was capsaicin (0.1  $\mu\text{M}$ , in the case of SR141716A 10 nM was also used), which was able of elevating intracellular  $\text{Ca}^{2+}$  with a potency of  $\text{EC}_{50} = 5.3 \pm 0.4$  nM and efficacy =  $78.6 \pm 0.6\%$ .

For TRPV2, the rat TRPV2-HEK293 cells exhibited a sharp increase in  $[\text{Ca}^{2+}]_i$  upon application of lysophosphatidylcholine (LPC, 3  $\mu\text{M}$ ). The concentration for half-maximal activation was  $3.40 \pm 0.02$   $\mu\text{M}$  and efficacy was  $91.7 \pm 0.5\%$ . For TRPV3, rat TRPV3-expressing HEK293 cells were first sensitized with the non-selective agonist 2-aminoethoxydiphenyl borate (100  $\mu\text{M}$ ). Antagonist/desensitizing behavior was evaluated against thymol (100  $\mu\text{M}$ ), which showed an efficacy of  $34.7 \pm 0.2\%$  and a potency of  $\text{EC}_{50} = 84.1 \pm 1.6$   $\mu\text{M}$ . For TRPV4, the rat TRPV4-expressing HEK293 cells the agonist used was *N*-([1*S*]-1-[[4-((2*S*)-2-[[[(2,4-dichlorophenyl)sulfonyl]amino]-3-hydroxypropanoyl]-1-piperazinyl]carbonyl]-3-methylbutyl)-1-benzothiophene-2-carboxamide (GSK1016790A), (10 nM), which was able of elevating intracellular  $\text{Ca}^{2+}$  with a potency of  $\text{EC}_{50} = 0.46 \pm 0.07$   $\mu\text{M}$ , and an efficacy of  $51.9 \pm 1.7\%$ . For TRPM8, the rat TRPM8-expressing HEK293 cells, antagonist/desensitizing behavior was evaluated against icilin at 0.25  $\mu\text{M}$  and 0.10  $\mu\text{M}$ . For icilin, efficacy was  $75.1 \pm 1.1$  and potency  $\text{EC}_{50} = 0.11 \pm 0.01$   $\mu\text{M}$ . For HEK293 cells stably overexpressing recombinant rat TRPA1, the effects of TRPA1 agonists are expressed as a percentage of the effect obtained with 100  $\mu\text{M}$  allyl isothiocyanate (AITC), which showed a potency of  $\text{EC}_{50} = 1.41 \pm 0.04$   $\mu\text{M}$  and an efficacy of  $65.9 \pm 0.5$ .

The effect on  $[\text{Ca}^{2+}]_i$  exerted by agonist alone was taken as 100%. Data are expressed as the concentration exerting a half-maximal inhibition of agonist-induced  $[\text{Ca}^{2+}]_i$  elevation ( $\text{IC}_{50}$ ), which was calculated again using GraphPad Prism 6 (Graphpad). All determinations were performed at least in triplicate. Statistical analysis of the data was performed by analysis of variance at each point using ANOVA followed by the Bonferroni's test.

## Statistical methods

All statistical measures and methods are included in the respective figure or table captions. In brief: all data are shown as the mean  $\pm$  SEM where applicable. A Student's *t*-test (unpaired, two-tailed) was used to determine differences between two groups. All statistical analyses were conducted using Excel (Microsoft) or GraphPad Prism 6 (Graphpad), and a *p*-value < 0.05 was considered significant throughout unless indicated otherwise. For the lipid profiling study (Figure 4E-F), a Benjamini-Hochberg correction (25% false discovery rate) was applied.

## Supplementary data

**Table S1 | Remaining enzyme activities of endocannabinoid related enzymes.** DAGL $\alpha$ , DAGL $\beta$ , MGLL, ABHD6 and NAPE-PLD relative to DMSO as vehicle and [ $^3$ H]CP55940 displacement at overexpressing CB1R- and CB2R membranes (prefix h: human, prefix m: mouse).

Inhibitor		Remaining activity (% $\pm$ SD)					Radioligand displacement (% $\pm$ SEM)	
Protein:		hDAGL $\alpha$	mDAGL $\beta$	hMGLL	hABHD6	hNAPE-PLD	hCB1R	hCB2R
BIA 10-2474	10 $\mu$ M	102.7 $\pm$ 9.3	94.1 $\pm$ 4.3	117.9 $\pm$ 3.0	83.9 $\pm$ 8.2	96.9 $\pm$ 11.9	29.8 $\pm$ 1.5	6.0 $\pm$ 5.4
	30 $\mu$ M	113.4 $\pm$ 4.0	102.9 $\pm$ 1.9	-	31.2 $\pm$ 13.2	-	-	-
	50 $\mu$ M	-	-	-	-	95.9 $\pm$ 10.1	38.4 $\pm$ 2.3	16.7 $\pm$ 8.9
BIA 10-2639	10 $\mu$ M	107.6 $\pm$ 2.6	94.5 $\pm$ 1.7	-	111.2 $\pm$ 8.3	89.0 $\pm$ 7.2	36.8 $\pm$ 4.1	13.4 $\pm$ 8.0
	30 $\mu$ M	110.2 $\pm$ 3.2	102.1 $\pm$ 4.2	-	90.3 $\pm$ 11.2	-	-	-
	50 $\mu$ M	-	-	-	-	89.9 $\pm$ 2.6	44.0 $\pm$ 5.6	19.9 $\pm$ 5.4
PF04457845	10 $\mu$ M	99.2 $\pm$ 8.7	105.5 $\pm$ 0.5	-	108.3 $\pm$ 21.6	98.6 $\pm$ 6.7	59.9 $\pm$ 2.5	51.5 $\pm$ 4.6
	30 $\mu$ M	83.0 $\pm$ 8.4	106.2 $\pm$ 1.5	-	97.5 $\pm$ 26.7	-	-	-
	50 $\mu$ M	-	-	-	-	70.2 $\pm$ 6.8	103.8 $\pm$ 4.6	86.4 $\pm$ 1.3

**Table S2 | Efficacy and affinity of compounds for TRPV-, TRPA1- and TRPM8-channels.**

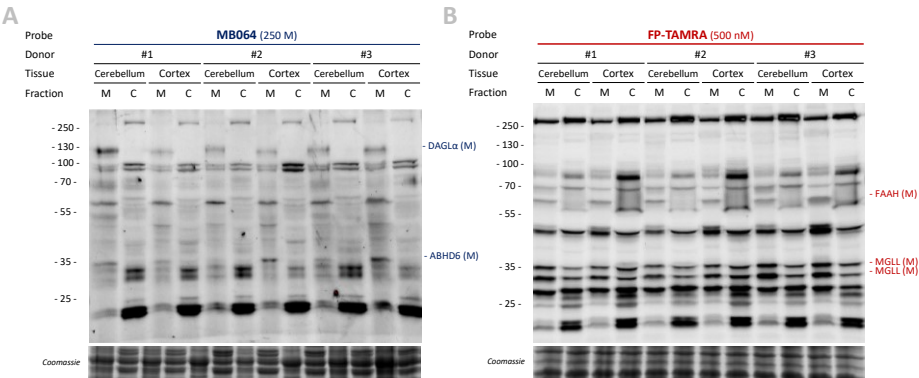
Inhibitor	TRPV1		TRPV2		TRPV3	
	Efficacy	IC <sub>50</sub>	Efficacy	IC <sub>50</sub>	Efficacy	IC <sub>50</sub>
	% Ionomycin 4 $\mu$ M	capsaicin 0.1 $\mu$ M	% Ionomycin 4 $\mu$ M	LPC 3 $\mu$ M	% Ionomycin 4 $\mu$ M	Thymol 100 $\mu$ M
BIA 10-474	< 10	> 20 $\mu$ M	< 10	> 20 $\mu$ M	< 10	> 20 $\mu$ M
PF04457845	< 10	> 20 $\mu$ M	< 10	> 20 $\mu$ M	< 10	> 20 $\mu$ M
BIA 10-2639	< 10	> 20 $\mu$ M	< 10	> 20 $\mu$ M	< 10	> 20 $\mu$ M

Inhibitor	TRPV4		TRPA1		TRPM8
	Efficacy	IC <sub>50</sub>	Efficacy	IC <sub>50</sub>	IC <sub>50</sub>
	% Ionomycin 4 $\mu$ M	GSK 10 nM	% AITC 100 $\mu$ M	AITC 100 $\mu$ M	Icilin 0.25 $\mu$ M
BIA 10-2474	< 10	> 20 $\mu$ M	< 10	> 20 $\mu$ M	> 20 $\mu$ M
PF04457845	< 10	> 20 $\mu$ M	< 10	> 20 $\mu$ M	> 20 $\mu$ M
BIA 10-2639	< 10	> 20 $\mu$ M	< 10	> 20 $\mu$ M	> 20 $\mu$ M

**Table S3 | Lipids significantly altered by *in situ* BIA 10-2474 treatment of human cortical neurons.** Lipids identified as significant based on *t*-test (with a post-hoc false discovery rate (FDR) correction applied using Benjamini-Hochberg procedure) and fold changes are divided into their different classes together with their trend. All lipids had an FDR rate less than 25%.

Lipid class	Metabolites identified as significant due to treatment	Effect
Phosphatidylcholines (PC)	C38:2, C38:6, C38:7, C40:6, C40:7, C40:8	Increased
Lysophosphatidylcholines (LPC)	sn1&2: C14:0, C22:6, C16:0, C16:1, C18:0, C18:1, C18:2, C20:4	Increased
	sn1: C18:2, C20:1, C20:2 C20:4, C22:6, C20:3 ( $\omega$ 3 $\omega$ 6)	
	sn2: C14:0, C18:2, C20:4, C22:6, C20:3 ( $\omega$ 3 $\omega$ 6)	
Fatty acids	C20:4 ( $\omega$ 6), C20:5 ( $\omega$ 3), C22:4, C25:5 ( $\omega$ 3 $\omega$ 6)	Decreased
Plasmalogen phosphatidylcholines (pPC)	C36:4, C36:6, C38:4, C38:5, C38:7, C40:6	Decreased
Triglycerides	C46:1, C48:1, C48:2, C48:3, C50:1, C52:1, C54:1	Increased
N-Acylethanolamines	C20:4, C22:6, C18:1, C16:0, C16:1, C18:0	Increased
Mono&di-acylglycerols	sn1:C18:1, C18:2 & sn2: C18:1, C18:2	Increased
Sphingomyelins	C18:1/24:1	Increased



**Figure S1 | Serine hydrolase profiling in human brain proteome by comparative ABPP.** (A-B) Labeling comparison between human cerebellum and cortex, membrane (M) and cytosol (C) fractions of three independent donors. Human proteome was labeled with MB064 (250 nM) (A) or FP-TAMRA (500 nM) (B) (20 min, rt).

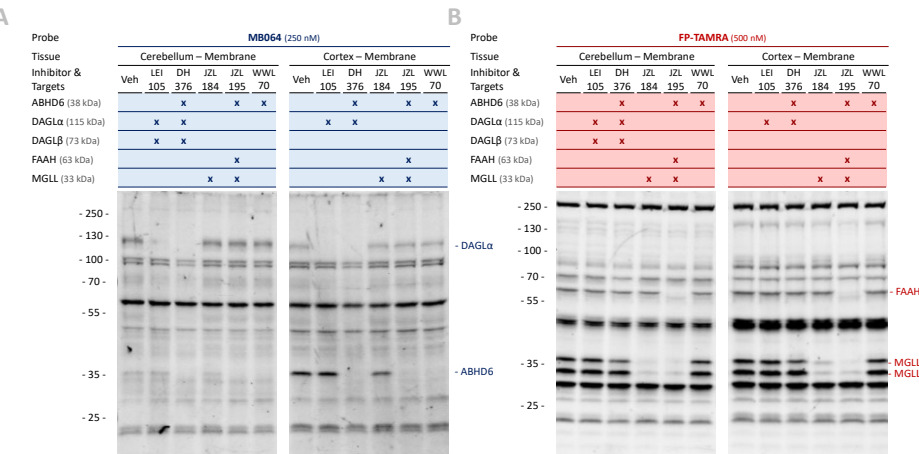


**Figure S2 | Band identification in human brain proteome by competitive ABPP.** (A-B) Human proteome (cerebellum and cortex, membrane fraction) was incubated with vehicle or reference inhibitors LEI105<sup>14</sup>, DH376<sup>25</sup>, JZL184<sup>42</sup>, JZL195<sup>8</sup>, WWL70<sup>43</sup> (10 μM, 30 min, 37 °C) and subsequently labeled with MB064 (250 nM) (A) or FP-TAMRA (500 nM) (B) (20 min, rt). Inhibitor targets and identified bands are indicated in the figure.

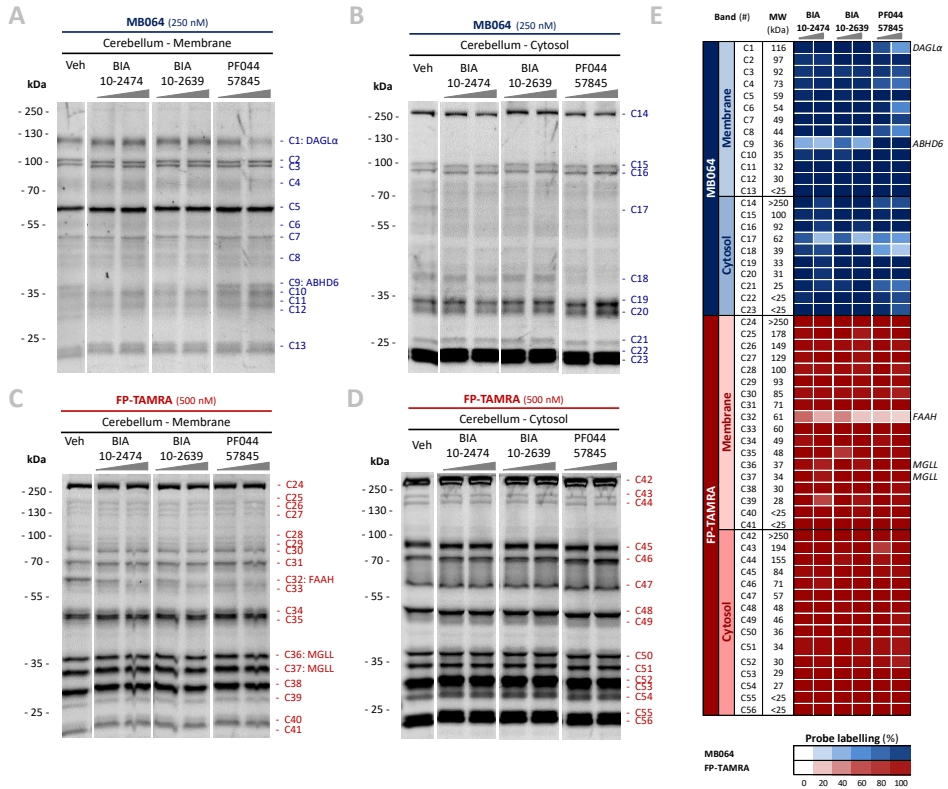


**Figure S3 | Identification of FAAH and ABHD6 as *in vitro* targets of BIA 10-2474 by competitive ABPP on serine hydrolases.** Gel-based ABPP analysis of human cerebellum proteome incubated *in vitro* with vehicle or inhibitor BIA 10-2474, BIA 10-2639 or PF04457845 (10/50  $\mu$ M, 30 min, 37  $^{\circ}$ C) and subsequently labeled with MB064 (250 nM) (**A-B**) or FP-TAMRA (500 nM) (**B, D**) (20 min, rt). (**E**) Heat-map summary of all 56 quantified bands, normalized for protein loading and expressed relative to control (n=3).

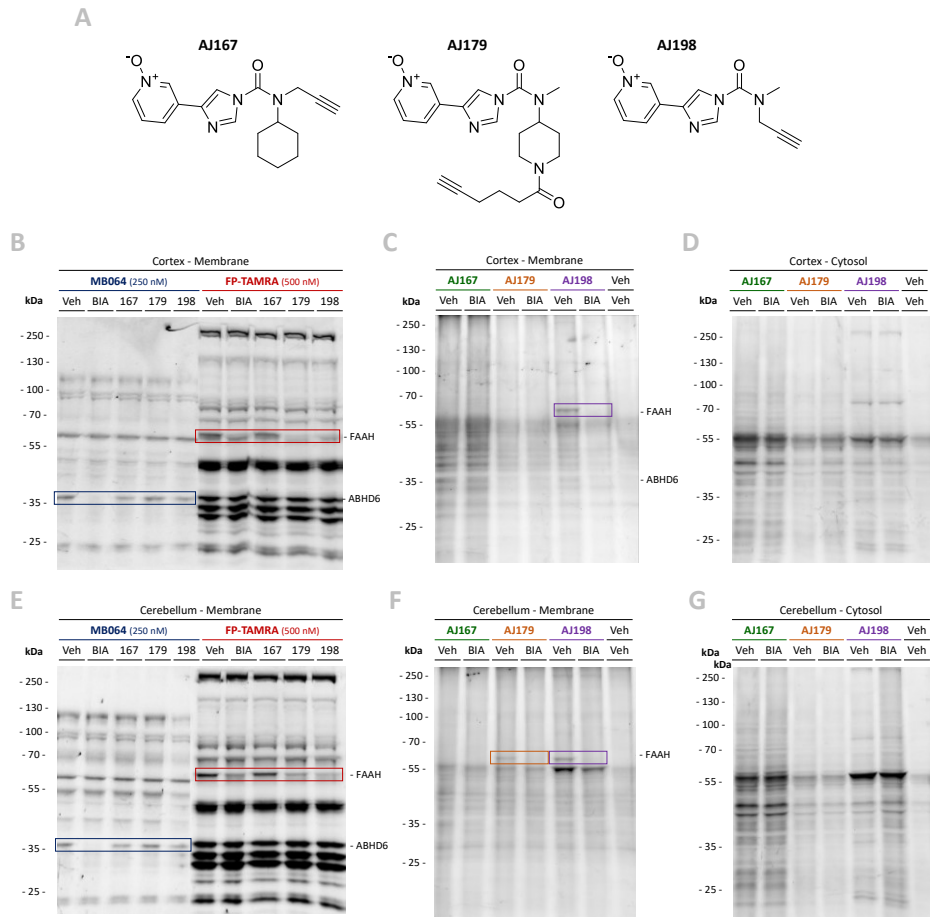


**Figure S4 | BIA 10-2474 interaction profiling by two-step labeling of human cortex and cerebellum with BIA-derived two-step probes.** (A) Chemical structures of BIA 10-2474 derived two-step probes AJ167, AJ179, and AJ198. (B, E) Two-step probe validation by competitive ABPP with BIA 10-2474 and AJ167, AJ179, AJ198. Human cortex (B) or cerebellum (E) membranes were incubated with vehicle, BIA 10-2474, or two-step probe (50  $\mu$ M, 30 min, 37  $^{\circ}$ C) and subsequently labeled with MB064 (250 nM) or FP-TAMRA (500 nM) (20 min, rt). (C-D, F-G) Competitive two-step ABPP with BIA 10-2474 and two-step probes. Human cortex (C-D) or cerebellum (F-G) proteome was incubated *in vitro* with vehicle or BIA 10-2474 (50  $\mu$ M, 30 min, 37  $^{\circ}$ C) and subsequently labeled with two step probe (AJ167, AJ179 or AJ198) (50  $\mu$ M, 30 min, 37  $^{\circ}$ C). Cy5-azide was conjugated to the bound probe by copper-catalyzed click reaction.



## References

1. Eddleston, M., Cohen, A. F. & Webb, D. J. Implications of the BIA-102474-101 study for review of first-into-human clinical trials. *British Journal of Clinical Pharmacology* **81**, 582–586 (2016).
2. Butler, D. & Callaway, E. Scientists in the dark after French clinical trial proves fatal. *Nature* **529**, 263–264 (2016).
3. Kerbrat, A. *et al.* Acute Neurologic Disorder from an Inhibitor of Fatty Acid Amide Hydrolase. *N. Engl. J. Med.* **375**, 1717–1725 (2016).
4. Bégaud, B. *et al.* BIA 10-2474: Minutes of the Temporary Specialist Scientific Committee (TSSC) meeting on ‘FAAH (Fatty Acid Amide Hydrolase) Inhibitors’. *Meet. Minutes* 1–14 (2016).
5. Cravatt, B. F. *et al.* Molecular characterization of an enzyme that degrades neuromodulatory fatty-acid amides. *Nature* **384**, 83–87 (1996).
6. Kathuria, S. *et al.* Modulation of anxiety through blockade of anandamide hydrolysis. *Nat. Med.* **9**, 76–81 (2003).
7. Devane, W. A. *et al.* Isolation and structure of a brain constituent that binds to the cannabinoid receptor. *Science (80-. )*. **258**, 1946–1949 (1992).
8. Long, J. Z. *et al.* Dual blockade of FAAH and MAGL identifies behavioral processes regulated by endocannabinoid crosstalk in vivo. *Proc. Natl. Acad. Sci. U. S. A.* **106**, 20270–5 (2009).
9. Van Der Stelt, M. *et al.* Anandamide acts as an intracellular messenger amplifying Ca<sup>2+</sup> influx via TRPV1 channels. *EMBO J.* **24**, 3026–3037 (2005).
10. Hampson, A. J. *et al.* Dual Effects of Anandamide on NMDA Receptor-Mediated Responses and Neurotransmission. *J. Neurochem.* **70**, 671–676 (2002).
11. Huggins, J. P., Smart, T. S., Langman, S., Taylor, L. & Young, T. An efficient randomised, placebo-controlled clinical trial with the irreversible fatty acid amide hydrolase-1 inhibitor PF-04457845, which modulates endocannabinoids but fails to induce effective analgesia in patients with pain due to osteoarthritis of the. *Pain* **153**, 1837–1846 (2012).
12. Li, G. L. *et al.* Assessment of the pharmacology and tolerability of PF-04457845, an irreversible inhibitor of fatty acid amide hydrolase-1, in healthy subjects. *Br. J. Clin. Pharmacol.* **73**, 706–716 (2012).
13. Niphakis, M. J. & Cravatt, B. F. Enzyme Inhibitor Discovery by Activity-Based Protein Profiling. *Annu. Rev. Biochem.* **83**, 341–377 (2014).
14. Baggelaar, M. P. *et al.* Highly Selective, Reversible Inhibitor Identified by Comparative Chemoproteomics Modulates Diacylglycerol Lipase Activity in Neurons. *J. Am. Chem. Soc.* **137**, 8851–8857 (2015).
15. Liu, Y., Patricelli, M. P. & Cravatt, B. F. Activity-based protein profiling: The serine hydrolases. *Proc. Natl. Acad. Sci.* **96**, 14694–14699 (1999).
16. Ahn, K. *et al.* Mechanistic and Pharmacological Characterization of PF-04457845: A Highly Potent and Selective Fatty Acid Amide Hydrolase Inhibitor That Reduces Inflammatory and Noninflammatory Pain. *J. Pharmacol. Exp. Ther.* **338**, 114–124 (2011).
17. van der Wel, T. *et al.* A natural substrate-based fluorescence assay for inhibitor screening on diacylglycerol lipase  $\alpha$ . *J. Lipid Res.* **56**, 927–935 (2015).
18. Van Esbroeck, A. C. M. *et al.* Activity-based protein profiling reveals off-target proteins of the FAAH inhibitor BIA 10-2474. *Science (80-. )*. **356**, 1084–1087 (2017).
19. Rostovtsev, V. V., Green, L. G., Fokin, V. V. & Sharpless, K. B. A stepwise Huisgen cycloaddition process: Copper(I)-catalyzed regioselective ‘ligation’ of azides and terminal alkynes. *Angew. Chemie - Int. Ed.* **41**, 2596–2599 (2002).
20. Wei, B. Q., Mikkelsen, T. S., McKinney, M. K., Lander, E. S. & Cravatt, B. F. A second fatty acid amide hydrolase with variable distribution among placental mammals. *J. Biol. Chem.* **281**, 36569–36578 (2006).

21. Lanning, B. R. *et al.* A road map to evaluate the proteome-wide selectivity of covalent kinase inhibitors. *Nat. Chem. Biol.* **10**, 760–767 (2014).
22. Thomas, G. *et al.* The Serine Hydrolase ABHD6 Is a Critical Regulator of the Metabolic Syndrome. *Cell Rep.* **5**, 508–520 (2013).
23. Chang, P. A. & Wu, Y. J. Neuropathy target esterase: An essential enzyme for neural development and axonal maintenance. *International Journal of Biochemistry and Cell Biology* **42**, 573–575 (2010).
24. Baggelaar, M. P. *et al.* Development of an activity-based probe and in silico design reveal highly selective inhibitors for diacylglycerol lipase- $\alpha$  in brain. *Angew. Chemie - Int. Ed.* **52**, 12081–12085 (2013).
25. Ogasawara, D. *et al.* Rapid and profound rewiring of brain lipid signaling networks by acute diacylglycerol lipase inhibition. *Proc. Natl. Acad. Sci.* **113**, 26–33 (2016).
26. Li, Y. *et al.* Carboxylesterase 2 prevents liver steatosis by modulating lipolysis, endoplasmic reticulum stress, and lipogenesis and is regulated by hepatocyte nuclear factor 4  $\alpha$  in mice. *Hepatology* **63**, 1860–1874 (2016).
27. Shayman, J. A. & Abe, A. Drug induced phospholipidosis: An acquired lysosomal storage disorder. *Biochim. Biophys. Acta - Mol. Cell Biol. Lipids* **1831**, 602–611 (2013).
28. Blankman, J. L., Simon, G. M. & Cravatt, B. F. A comprehensive profile of brain enzymes that hydrolyze the endocannabinoid 2-arachidonoylglycerol. *Chem. Biol.* **14**, 1347–1356 (2007).
29. Pribasniig, M. A. *et al.*  $\alpha/\beta$  hydrolase domain-containing 6 (ABHD6) degrades the late Endosomal/Lysosomal lipid Bis(Monoacylglycero)phosphate. *J. Biol. Chem.* **290**, 29869–29881 (2015).
30. Wei, M. *et al.*  $\alpha/\beta$ -Hydrolase domain-containing 6 (ABHD6) negatively regulates the surface delivery and synaptic function of AMPA receptors. *Proc. Natl. Acad. Sci.* **113**, E2695–E2704 (2016).
31. Erlenhardt, N. *et al.* Porcupine Controls Hippocampal AMPAR Levels, Composition, and Synaptic Transmission. *Cell Rep.* **14**, 782–794 (2016).
32. Kolter, T. & Wendeler, M. Chemical chaperones - A new concept in drug research. *ChemBioChem* **4**, 260–264 (2003).
33. Richardson, R. J., Hein, N. D., Wijeyesakere, S. J., Fink, J. K. & Makhaeva, G. F. Neuropathy target esterase (NTE): Overview and future. in *Chemico-Biological Interactions* **203**, 238–244 (2013).
34. Read, D. J., Li, Y., Chao, M. V., Cavanagh, J. B. & Glynn, P. Neuropathy Target Esterase Is Required for Adult Vertebrate Axon Maintenance. *J. Neurosci.* **29**, 11594–11600 (2009).
35. Moser, M. *et al.* Cloning and expression of the murine sws/NTE gene. *Mech. Dev.* **90**, 279–282 (2000).
36. Bachovchin, D. A. *et al.* Superfamily-wide portrait of serine hydrolase inhibition achieved by library-versus-library screening. *Proc. Natl. Acad. Sci.* **107**, 20941–20946 (2010).
37. Hu, C. *et al.* RPLC-Ion-trap-FTMS method for lipid profiling of plasma: Method validation And application to p53 mutant mouse model. *J. Proteome Res.* **7**, 4982–4991 (2008).
38. Gattinoni, S. *et al.* Enol carbamates as inhibitors of fatty acid amide hydrolase (FAAH) endowed with high selectivity for FAAH over the other targets of the endocannabinoid system. *ChemMedChem* **5**, 357–360 (2010).
39. Janssen, F. J. *et al.* Discovery of glycine sulfonamides as dual inhibitors of sn-1-diacylglycerol lipase  $\alpha$  and  $\alpha/\beta$ -hydrolase domain 6. *J. Med. Chem.* **57**, 6610–6622 (2014).
40. Peppard, J. V., Mehdi, S., Li, Z. & Duguid, M. S. Assay methods for identifying agents that modify the activity of nape-pld or Abhd4. (2010).
41. Mukhopadhyay, P. *et al.* The novel, orally available and peripherally restricted selective cannabinoid CB2receptor agonist LEI-101 prevents cisplatin-induced nephrotoxicity. *Br. J. Pharmacol.* **173**, 446–458 (2016).

42. Long, J. Z. *et al.* Selective blockade of 2-arachidonoylglycerol hydrolysis produces cannabinoid behavioral effects. *Nat. Chem. Biol.* **5**, 37–44 (2009).
43. Li, W., Blankman, J. L. & Cravatt, B. F. A functional proteomic strategy to discover inhibitors for uncharacterized hydrolases. *J. Am. Chem. Soc.* **129**, 9594–9595 (2007).





A.C.M. van Esbroeck  
X. Di  
V. Kantae  
T. van der Wel  
H. den Dulk  
A.T. Bakker  
B.I. Florea  
H.S. Overkleeft  
T. Hankemeier  
M. van der Stelt

# Identification of ABHD6 as a diacylglycerol lipase

**ABSTRACT** | The endocannabinoid 2-arachidonoylglycerol (2-AG) is an important signaling lipid, which is involved in neuronal differentiation. This study aimed to identify the biosynthetic enzymes responsible for 2-AG production during retinoic acid (RA)-induced neurite outgrowth of Neuro-2a cells, a widely used cellular model for neuronal differentiation. First, it was confirmed that RA stimulation of Neuro-2a cells led to 2-AG production and neurite outgrowth. The diacylglycerol lipase (DAGL) inhibitor DH376 abolished 2-AG levels and delayed neuronal differentiation. Surprisingly, CRISPR/Cas9-mediated knockdown of the 2-AG producing enzymes DAGL $\alpha$  and DAGL $\beta$  in Neuro-2a cells did not reduce cellular 2-AG levels, suggesting there are other enzymes capable of producing 2-AG in this cell line. Chemical proteomics revealed DAGL $\beta$  and  $\alpha,\beta$ -hydrolase domain containing protein (ABHD6) as the only targets of DH376 in Neuro-2a cells. Biochemical, genetic and lipidomic studies demonstrated that ABHD6 possesses diacylglycerol lipase activity in conjunction with its previously reported role as monoacylglycerol lipase. RA treatment of Neuro-2a cells resulted in a three-fold increase in ABHD6 activity, whereas DAGL $\beta$  activity was decreased. Thus, these data extend the role of ABHD6 as a MAG lipase to a DAG lipase and suggest it is involved in neuronal differentiation.

## Introduction

The endocannabinoid 2-arachidonoylglycerol (2-AG) is an important signaling lipid in the central nervous system (CNS). It acts as a retrograde messenger that activates the presynaptic cannabinoid receptor type 1 (CB1R), thereby regulating neurotransmitter release. 2-AG is involved in a variety of physiological processes, including modulation of memory, energy balance and emotional states, such as stress and anxiety<sup>1</sup>. Biochemical, pharmacological and genetic studies have established diacylglycerol lipases  $\alpha$  and  $\beta$  (DAGL $\alpha$ , DAGL $\beta$ ) as the main biosynthetic enzymes that produce 2-AG in the brain by catalyzing the *sn*-1-specific hydrolysis of diacylglycerol (DAG) to generate 2-AG<sup>2</sup> (Figure 1). For example, congenital deletion of DAGL $\alpha$  or DAGL $\beta$  resulted in 80% and 50% reduction, respectively, of brain 2-AG levels in knockout (KO) mice as compared to wildtype (WT) littermates<sup>3</sup>. Pharmacological studies with covalent, irreversible, dual DAGL inhibitors, such as DH376 and DO34, showed that acute blockade of 2-AG biosynthesis in the mouse brain reduced neuroinflammatory responses<sup>4</sup>, reversed LPS-induced anapyrexia<sup>4</sup>, reduced food intake<sup>5</sup> and modulated cocaine-seeking behavior<sup>6</sup> and stress responses<sup>7</sup>.

The life span of 2-AG signaling at the synapse is tightly controlled. Monoacylglycerol lipase (MGLL)<sup>8</sup> and  $\alpha,\beta$ -hydrolase domain containing protein 6 and 12 (ABHD6, ABHD12) have been identified as the key enzymes terminating the physiological role of 2-AG. They hydrolyze the ester bond in 2-AG, thereby generating glycerol and arachidonic acid (AA)<sup>9,10</sup> (Figure 1). MGLL is the predominant lipase in the brain covering over 85% of 2-AG hydrolysis, whereas ABHD6 and ABHD12 account for 4 and 9%, respectively<sup>11</sup>.

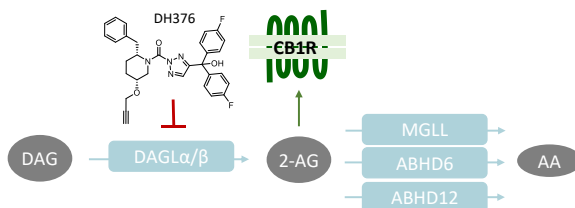


**Figure 1 | Schematic overview of 2-AG signaling and metabolism.** CB1R: Cannabinoid receptor type 1, DAGL: diacylglycerol lipase, MGLL: monoacylglycerol lipase, ABHD:  $\alpha,\beta$ -hydrolase domain containing protein, DAG: diacylglycerol, 2-AG: 2-arachidonoylglycerol, AA: arachidonic acid.

2-AG signaling is not only important in the adult brain, but multiple studies have also provided evidence of a functional role of 2-AG during neural developmental processes<sup>12</sup>, including axonal growth and guidance<sup>2,13–15</sup>, differentiation<sup>16</sup>, and neurogenesis<sup>3,17</sup>. In adult mice, DAGL $\alpha$  is mainly restricted to postsynaptic sites on neurons, whereas DAGL $\beta$  is expressed in microglial cells, but during neuronal development their expression pattern is different. Both DAGL $\alpha$  and DAGL $\beta$  were found in neurons at developing axonal tracts<sup>2,14,17,18</sup>. Jung and colleagues have investigated the role of DAGLs in neuronal differentiation using retinoic acid (RA)-induced neurite outgrowth in murine neuroblastoma cell line Neuro-2a<sup>16</sup>. They found that RA elevated cellular 2-AG levels in Neuro-2a cells during differentiation and recombinant expression of DAGL $\alpha$  or DAGL $\beta$

increased neurite outgrowth, whereas silencing the expression of DAGLs using shRNAs reduced the number of cells with neurites<sup>16</sup>. The contribution of the endogenously expressed DAGL enzymes to 2-AG biosynthesis in these cells is, however, less clear.

Here, we sought to revisit this question and aimed to dissect the role of the two DAGL isoforms in 2-AG biosynthesis in Neuro-2a using pharmacological and genetic methods. Surprisingly, CRISPR/Cas9-mediated knockdown (KD) of DAGL $\alpha$  and/or DAGL $\beta$  did not reduce 2-AG levels in Neuro-2a, suggesting that other enzymes contribute to 2-AG biosynthesis in these cells. Interestingly, treatment of the cells with the DAGL inhibitor DH376 almost completely abolished cellular 2-AG levels. Chemical proteomics of DH376-treated Neuro-2a revealed ABHD6 as the only other target of DH376. Additional biochemical, genetic and lipidomics studies showed that ABHD6 possesses diacylglycerol lipase activity, next to its previously reported role as monoacylglycerol (MAG) lipase. The identification of ABHD6 as a general lipase using both DAGs and MAGs as substrates, may have important implications for its proposed role in the endocannabinoid system.

## Results & Discussion

To investigate the role of DAGL in neuronal differentiation, Neuro-2a cells were incubated with RA, which induced a time-dependent outgrowth of neurites (Figure 2A-B). This was accompanied by increased cellular 2-AG levels as determined by liquid chromatography-mass spectrometry (LC-MS) (Figure 2C). These findings confirm the results of Jung *et al.*<sup>16</sup>. Of note, anandamide (AEA) and arachidonic acid (AA) levels were also significantly increased (Figure 2C). To check whether endogenously expressed DAGLs are responsible for the 2-AG production during differentiation, the cells were incubated with the dual DAGL inhibitor DH376. Cellular 2-AG and AA, but not AEA, levels were strongly reduced by DH376 (Figure 2D). The inhibitor also induced a significant delay in the differentiation of Neuro-2a cells, expressed as the fraction of neurite bearing cells after 24, 48, and 72 h of RA stimulation (Figure 2B). This suggested that DAGL-dependent 2-AG and/or AA production plays a role in the differentiation process, which is in line with the previous observations by Jung *et al.*<sup>16</sup>.

To investigate which DAGL isoform is responsible for 2-AG production in Neuro-2a cells a genetic approach was used, because there are currently no subtype-specific DAGL inhibitors available. Of note, single cell heterogeneity (in 2-AG production and neurite outgrowth) prevented the unequivocal analysis of single cell clone knockouts (Supplementary Figure S1). Therefore, disruption of DAGL $\alpha$  and DAGL $\beta$  genes was performed by three sequential rounds of transfection of Cas9 and single guide RNA's (sgRNA) in Neuro-2a cell populations (Supplementary Figure S2A-C). This yielded three different Neuro-2a knockdown (KD) populations: DAGL $\alpha$  KD, DAGL $\beta$  KD and DAGL $\alpha$ - $\beta$  KD. DAGL $\alpha$  and DAGL $\beta$  activity in these cell populations was measured using activity-based protein profiling (ABPP) to determine the efficiency of the genetic disruption. ABPP is a chemical proteomic method that uses chemical probes (e.g

fluorophosphonates (FP) or  $\beta$ -lactones) to assess the functional state of DAGL $\alpha$  and DAGL $\beta$  (and other serine hydrolases) in native biological systems. When coupled to fluorescent reporter groups, activity-based probes (ABPs) enable visualization of enzymatic activity in complex proteomes by sodium dodecyl sulfate polyacrylamide gel electrophoresis (SDS-PAGE) and in-gel fluorescence scanning. When coupled to a biotin reporter group, ABPs enable affinity enrichment and identification of enzyme activities by mass spectrometry (MS)-based proteomics. Gel-based ABPP with a fluorescent FP-probe (FP-TAMRA) and  $\beta$ -lactone probe MB064 showed a strong reduction (> 70%) of DAGL $\beta$  activity in the DAGL $\beta$  KD and DAGL $\alpha$ - $\beta$  KD populations (Figure 3A-B), whereas other serine hydrolase activities were not affected. LC-MS-based chemical proteomics confirmed these findings (Figure 3C). Of note, no DAGL $\alpha$  activity was observed in either of the populations, including WT Neuro-2a (Figure 3A-B). The residual DAGL $\beta$  activity can be explained by a transfection efficiency below 100% and by insertion or deletion of a full codon upon Cas9-mediated DNA modification, thus preventing the frameshift that generally results in an early STOP-codon.

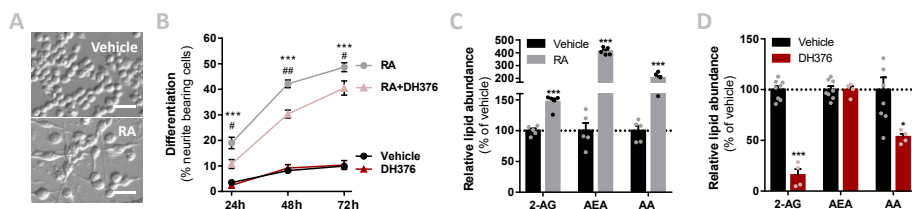


**Figure 2 | RA-induced differentiation increased cellular 2-AG levels and is delayed by DH376 treatment.** (A-C) Neuro-2a cells were differentiated with RA (50  $\mu$ M, 2% serum, 24-72 h) in the presence or absence of inhibitor DH376 (100 nM). (A) Phase contrast microscopy of representative differentiated and non-differentiated Neuro-2a cultures (72 h incubation). Scale bar: 50  $\mu$ m. (B) Neuro-2a differentiation was quantified as the percentage of neurite bearing cells (mean  $\pm$  SEM (n=3), t-test: \*\*\* p < 0.001 vehicle versus RA, # p < 0.05, ## p < 0.01 RA versus RA-DH376). (C) Lipidomics analysis on vehicle and RA-stimulated cells (72 h). Lipid abundance was normalized to the number of cells. Data is expressed as % of vehicle (mean  $\pm$  SEM (n=5), t-test: \*\*\* p < 0.001). (D) Lipidomics analysis on *in situ* DH376-treated Neuro-2a (100 nM, 2 h). Lipid abundance was normalized for the amount of protein. Data is expressed as % of vehicle (mean  $\pm$  SEM (Veh: n=8, DH376: n=4), t-test: \* p < 0.05, \*\*\* p < 0.001).

Next, the cellular 2-AG levels of these genetically modified Neuro-2a populations were determined using LC-MS. Surprisingly, despite having > 70% reduction in DAGL $\beta$  activity and no detectable DAGL $\alpha$  activity, the 2-AG levels in the DAGL $\alpha$  KD, DAGL $\beta$  KD or double DAGL $\alpha$ - $\beta$  KD populations were not significantly different from WT populations (Figure 3C). To test whether the 2-AG production in the KD populations was still sensitive to DH376 treatment, the cells were incubated *in situ* with DH376 (100 nM, 2 h). Lipidomics analysis on these samples revealed that DH376 again abolished cellular 2-AG levels and reduced AA by 50% in all cell types (Figure 3C). Of note, a small but significant increase in AEA levels in the double DAGL $\alpha$ - $\beta$  KD populations was observed (Figure 3C), which might be the result of increased ABHD4 activity (Figure 3D). Taken together, these data suggest that residual DAGL $\beta$  activity may be responsible for the entire pool of 2-AG,



which seems unlikely, or that an alternative, unidentified enzyme, which is sensitive to DH376, contributes to 2-AG biosynthesis in Neuro-2a cells.

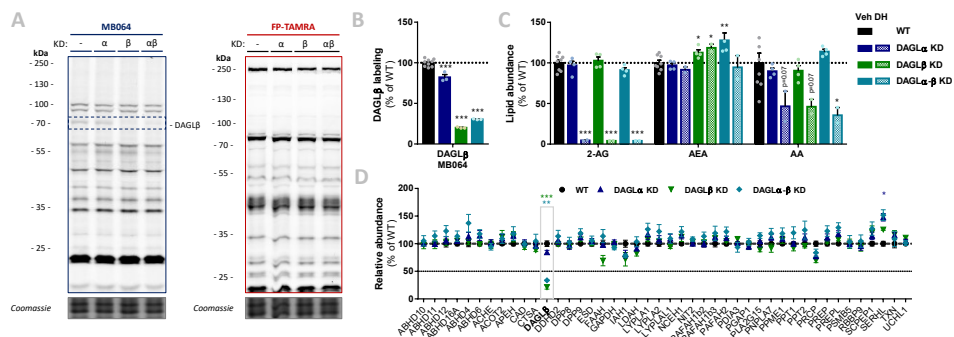


**Figure 3 | DAGL KD did not alter 2-AG levels in Neuro-2a, whereas 2-AG was abolished by DAGL inhibitor DH376.** (A-B) DAGL KD populations were analyzed by gel-based ABPP using probes MB064 (2 μM) and FP-TAMRA (500 nM) (20 min, rt). Coomassie served as protein loading control. (B) Probe labeling of DAGLβ was quantified and normalized for protein loading. Data is expressed as % of vehicle (mean ± SEM (WT: n=9, KD: n=3), *t*-test: \*\*\* *p* < 0.001). (C) Lipidomics analysis on WT and DAGL KD Neuro-2a populations treated *in situ* with vehicle or DH376 (100 nM, serum-free, 2 h). Lipid abundance was normalized for the amount of protein. Data is expressed as % of vehicle (mean ± SEM (WT: n=8, KD: n=4/2), *t*-test: \* *p* < 0.05, \*\* *p* < 0.01, \*\*\* *p* < 0.001). (D) DAGL KD efficiency was assessed by chemical proteomics on WT and KD Neuro-2a cells using probes MB108 and FP-biotin (10 μM each, 30 min, 37 °C). Data is expressed as % of WT-vehicle (mean ± SEM (n=4), *t*-test with Holm-Sidak multiple comparison correction: \* *p* < 0.05, \*\* *p* < 0.01, \*\*\* *p* < 0.001).

To identify all 2-AG producing enzymes targeted by DH376 in Neuro-2a, a chemical proteomics strategy was employed. The alkyne moiety of DH376 served as a ligation handle to introduce a reporter group via a copper(I)-catalyzed azide-alkyne cycloaddition (“click” chemistry)<sup>19</sup>. Neuro-2a cells were incubated with DH376, lysed and the covalently bound inhibitor-targets were conjugated to Cy5-azide, resolved by SDS-PAGE and visualized by in-gel fluorescence scanning (Figure 4A-B). Apart from DAGLβ, one other fluorescent band with a molecular weight of ~ 35 kDa was observed. Competitive ABPP using MB064 and FP-TAMRA suggested that this fluorescent band could be ABHD6, which was previously also reported as an off-target of DH376<sup>4,20</sup>. To confirm the identity of this protein in Neuro-2a cells, chemical proteomics was employed (Figure 4C). DAGLβ and ABHD6 were identified as the only targets of DH376 in Neuro-2a cells (Figure 4D). Thus, combined these data suggested that ABHD6 could be responsible for 2-AG production in conjunction with DAGLβ.

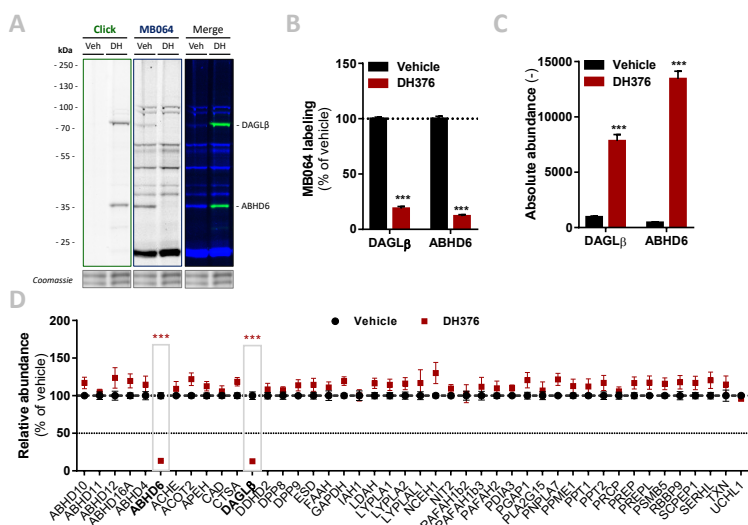


**Figure 4 | DH376 targets DAGLβ and ABHD6 in Neuro-2a.** Neuro-2a cells were treated *in situ* with vehicle or DH376 (100 nM, serum-free, 2 h) to investigate the DH376 interaction profile. **(A, B)** *In situ* DH376 targets were visualized by gel-based ABPP after conjugation of DH376 to Cy5-azide (5 μM, 60 min, rt) or with probe MB064 (2 μM, 20 min, rt). Coomassie served as a protein loading control. **(B)** Probe labeling was quantified and normalized for protein loading. Data is expressed as % of vehicle (mean ± SEM (Veh n=9, DH376 n=3), *t*-test: \*\*\* *p* < 0.001). **(C)** Chemical proteomics enabled DH376 target identification. Lysates of *in situ* DH376-treated Neuro-2a cells were conjugated to biotin-azide (40 μM, 60 min, 37 °C). Vehicle treated samples served as a negative control. Data is expressed as absolute abundance (mean ± SEM (n=4), *t*-test: \*\*\* *p* < 0.001). **(D)** Competitive proteomics validated ABHD6 and DAGLβ as DH376 targets in *in situ* treated Neuro-2a cells, using probes MB108 and FP-biotin (10 μM each, 30 min, 37 °C). Data is expressed as % of WT-Vehicle (mean ± SEM (n=4), *t*-test with Holm-Sidak multiple comparison correction: \*\*\* *p* < 0.001).

ABHD6 has previously been reported as a promiscuous lipase that not only uses 2-AG, but also various lysophosphatidyl species<sup>21</sup> and bis(monoacylglycerol)phosphate<sup>22</sup> as substrates. Therefore, to confirm that ABHD6 can act also as a general lipase using DAG as a substrate, a DAG hydrolysis assay was developed based on fluorescent 1-nitrobenzoxadiazole-decanoyl-2-decanoyl-*sn*-glycerol (NBD-DAG) substrate. Lysates from human embryonic kidney 293-T (HEK293-T) cells overexpressing recombinant human ABHD6 (Figure 5A) or its catalytically inactive mutant (ABHD6<sup>S148A</sup>) as a negative control, were incubated with NBD-DAG and analyzed by high performance thin layer chromatography (HPTLC). Lysates from HEK293-T cells expressing DAGLα or its catalytically inactive mutant (DAGLα<sup>S472A</sup>) served as positive and negative controls respectively (Supplementary Figure S3A). Both DAGLα and ABHD6 exhibited DAG-lipase activity as their overexpression resulted in the hydrolysis of NBD-DAG, whereas their mutants did not (Figure 5B-C, Supplementary Figure S3C-D), thereby showing that ABHD6 is able to hydrolyze the *sn*-1 ester bond of an *sn*-1-acyl-2-decanoyl-glycerol. Of note, the NBD-DAG hydrolysis observed in HEK293-T cells expressing GFP reflects conversion of the substrate by endogenous hydrolases, including ABHD6 and to a lesser extent DAGLβ.

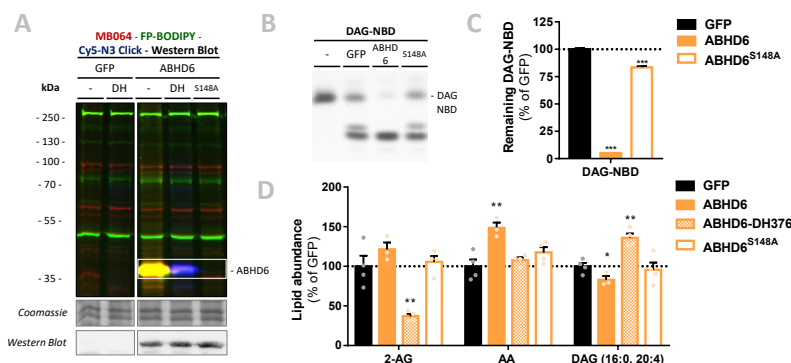


**Figure 5 | Recombinant ABHD6 possesses DAG-lipase activity *in vitro* and *in situ*.** HEK293-T cells were transiently transfected with GFP, ABHD6, or its catalytically inactive serine mutant (S148A) and treated *in situ* with vehicle or DH376 (DH, 1  $\mu$ M, 2 h, serum-free). **(A)** Protein activity and expression was confirmed by gel-based ABPP and western blot. Samples were subsequently incubated with probes MB064 (red; 500 nM, 10 min, rt), FP-BODIPY (green; 500 nM, 10 min, rt), and Cy5-azide click mix (blue; 2.5  $\mu$ M, 30 min, rt). Coomassie served as a protein loading control. Western blot with mouse-anti-FLAG (1:2500, 45 min, rt) verified expression of the catalytically inactive protein. **(B-C)** Whole cell lysates were incubated with DAG-NBD (5  $\mu$ M, 30 min, 37  $^{\circ}$ C), lipids were extracted and analyzed by HPTLC. **(C)** DAG hydrolysis was quantified and expressed as % of GFP (mean  $\pm$  SEM (n=3), *t*-test: \*\*\*  $p < 0.001$ ). **(D)** Lipid abundance of transfected and *in situ* treated cells was measured and normalized to the amount of protein. Data is expressed as % of GFP-Vehicle (mean  $\pm$  SEM (n=4), *t*-test: \*  $p < 0.05$ , \*\*  $p < 0.01$ ).

Next, it was determined whether ABHD6 could utilize endogenous DAGs in a cellular context. To this end, recombinant ABHD6 was overexpressed in HEK293-T cells (DAGL $\alpha$  as positive control and the catalytically inactive mutants as negative controls) and endogenous DAG (16:0, 20:4) levels were determined by targeted lipidomics (Figure 5D, Supplementary Figure S3D). Both ABHD6 and DAGL $\alpha$  overexpression reduced the levels of DAG (16:0, 20:4), whereas overexpression of the catalytically inactive mutants had no effect on the DAG-levels. DH376 treatment of the transfected cells prevented the reduction in DAG levels and even led to an increase in this lipid species, indicating that this DAG species serves also as an endogenous substrate for DAGL $\alpha$ /ABHD6. Overexpression of ABHD6 did not significantly affect 2-AG levels, in line with the dual MAG/DAG-lipase character of ABHD6, whereas its final product AA was increased (Figure 5D). In summary, these data indicate that ABHD6 is able to act as a DAG/MAG-lipase using DAG (16:0, 20:4) as an endogenous substrate.

To check whether endogenous cellular levels of 2-AG and AA are under control of ABHD6, a Neuro-2a ABHD6 KD population and a triple DAGL $\alpha$ - $\beta$ -ABHD6 KD population were generated (Figure 6A, Supplementary Figure S2D-F). ABHD6 KD had no effects on 2-AG or AA levels (Figure 6C), which suggests that DAGL $\beta$  and ABHD6 can compensate for each other. The KD efficiency at the protein level was reduced in the triple DAGL $\alpha$ -DAGL $\beta$ -ABHD6 KD as compared to the single KDs as determined by gel-based ABPP (Figure 6A-B) and chemical proteomics (Figure 6D). It was estimated that approximately 40-50% of ABHD6 activity was remaining, as well as 30-40% DAGL $\beta$  activity. In line with the reduced ABHD6 and DAGL activity in the triple KD, both 2-AG and AA levels were reduced by approximately 30%.

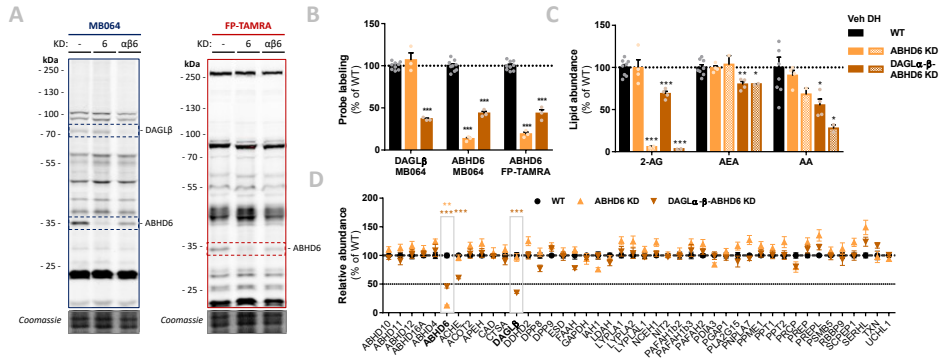


**Figure 6 | Neuro-2a DAGLα-β-ABHD6 triple KD populations have decreased 2-AG levels.** (A-B) ABHD6 and DAGLα-β-ABHD6 KD populations were analyzed by gel-based ABPP using probes MB064 (2 μM) and FP-TAMRA (500 nM) (20 min, rt). Coomassie served as a protein loading control. (B) Probe labeling was normalized for protein loading. Data is expressed as % of vehicle (mean ± SEM (WT: n=9, KD: n=3), *t*-test: \*\*\* *p* < 0.001). (C) Lipidomics analysis on WT and ABHD6 KD Neuro-2a populations treated *in situ* with vehicle or DH376 (100 nM, serum-free, 2 h). Lipid abundance was normalized for the amount of protein. Data is expressed as % of vehicle (mean ± SEM (WT: n=8, KD: n=4/2), *t*-test: \* *p* < 0.05, \*\* *p* < 0.01, \*\*\* *p* < 0.001). (D) DAGL and ABHD6 KD efficiency was assessed by chemical proteomics on WT and KD Neuro-2a populations using probes MB108 and FP-biotin (10 μM each, 30 min, 37 °C). Data is expressed as % of WT-vehicle (mean ± SEM (n=4), *t*-test with Holm-Sidak multiple comparison correction: \*\* *p* < 0.01, \*\*\* *p* < 0.001).

Finally, in light of the finding that ABHD6 can act as a DAG lipase, the DAGLβ and ABHD6 activity in Neuro-2a cells during RA-induced differentiation was mapped by gel-based ABPP (Figure 7A). A threefold increase in ABHD6 activity was observed in differentiated Neuro-2a cells, whereas DAGLβ activity was decreased (Figure 7B). These data indicate that the RA-induced 2-AG and AA production (Figure 1B) in Neuro-2a cells is due to increased ABHD6 activity.

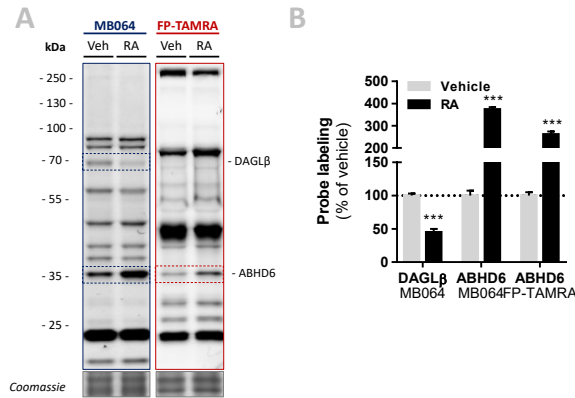


**Figure 7 | DAGLβ activity decreased, while ABHD6 activity increased during RA-induced differentiation of Neuro-2a.** Neuro-2a cells were stimulated by *in situ* treatment with retinoic acid (RA, 50 μM, 2% serum, 72 h). (A) Whole lysates of vehicle or RA stimulated cells were analyzed by gel-based ABPP using activity-based probes MB064 (2 μM) or FP-TAMRA (500 nM) (20 min, rt). Coomassie served as a protein loading control. (B) Probe labeling was normalized to loading control. Data is expressed as % of vehicle (mean ± SEM (n=3), *t*-test, \*\*\* *p* < 0.001).

## Conclusion

DAGL-dependent endocannabinoid signaling is required for axonal growth and guidance in the developing brain. DAGL $\alpha$  and DAGL $\beta$  are reported as the main enzymes that produce the endocannabinoid 2-AG. It has been estimated that 10-20% of the 2-AG pool in mouse brain may result from alternative biosynthetic pathways. Here, ABHD6 is identified as an additional DAG lipase, which is supported by several lines of biochemical, genetic, and pharmacological evidence. First, genetic knockdown of both DAGL $\alpha$  and DAGL $\beta$  in Neuro-2a cells had no effect on cellular 2-AG levels. Second, the dual DAGL/ABHD6 inhibitor DH376 completely abolished cellular 2-AG levels. Third, ABHD6 catalyzed the degradation of a fluorescent DAG substrate. Fourth, overexpression of ABHD6, but not its catalytically inactive mutant, reduced endogenous DAG (16:0, 20:4) levels, which was inhibited by DH376. Fifth, cellular 2-AG levels decreased upon triple KD of DAGL $\alpha$ - $\beta$ -ABHD6 in Neuro-2a. These data thus extend the role of ABHD6 from a MAG lipase to a DAG lipase and suggest a role for ABHD6 in neuronal differentiation.

## Experimental procedures

### Materials, probes, and inhibitors

Fluorophosphonate-rhodamine (FP-TAMRA) was purchased from Thermo Fisher, as well as synthesized in-house as previously described<sup>23</sup>. FP-Biotin was purchased from Santa Cruz Biotechnology. Fluorophosphonate-BODIPY (FP-BODIPY)<sup>23</sup>, MB064<sup>24</sup>, MB108<sup>24</sup>, and DH376<sup>4</sup> were synthesized as previously described. All synthesized compounds were at least 95% pure and were analyzed by LC-MS, NMR, and HRMS. Primers were ordered from Sigma Aldrich or Integrated DNA Technologies. Other chemicals, reagents were purchased from Sigma Aldrich, unless indicated otherwise.

### Cloning general

Full-length human DAGL $\alpha$  and ABHD6 cDNA (Source Bioscience) was cloned into the mammalian expression vector pcDNA3.1, containing ampicillin and neomycin resistance genes. The inserts were cloned in frame with a C-terminal FLAG-tag and site-directed mutagenesis was used to generate the catalytically inactive DAGL $\alpha$ <sup>S472A</sup> and ABHD6<sup>S148A</sup> mutants. pcDNA3.1 containing the gene for eGFP was used as a transfection control. Plasmids were isolated from transformed XL-10 Z-competent cells (Midi/Maxi Prep, Qiagen) and sequenced at the Leiden Genome Technology Center. Sequences were analyzed and verified (CLC Main Workbench).

### Cell culture

#### *General*

Neuro-2a (murine neuroblastoma) and HEK293-T (human embryonic kidney) cells were cultured at 37 °C under 7% CO<sub>2</sub> in DMEM containing phenol red, stable glutamine, newborn bovine serum (10% v/v; Thermo Fisher), and penicillin and streptomycin (200 µg/mL each; Duchefa). Medium was refreshed every 2-3 days and cells were passaged twice a week at ~ 90% confluence by resuspension in fresh medium. Cell lines were purchased from ATCC and were regularly tested for mycoplasma contamination. Cultures were discarded after 2-3 months of use.

#### *Single cell clone generation*

Single cell clones of Neuro-2a cells were generated by seeding cells at a density of 0.5, 1, 2, or 4 cells per well in 96-wells plates. After several days, wells plates were screened for growth of single cell clones by phase-contrast microscopy (EVOS Auto FL2). Single cell clones were selected and expanded to full cultures.

#### *Transient transfections (HEK293-T)*

One day prior to transfection, HEK293-T cells were seeded at  $1 \times 10^6$  cells/well in 6-wells plates or at  $0.3 \times 10^6$  cells/well in 12-wells plates. Prior to transfection, culture medium was aspirated and a minimal amount of complete medium was added. A 3:1 (m/m) mixture of polyethyleneimine (PEI) and plasmid DNA (1.25 µg per 6-well, 0.625 µg per 12-well) was prepared in serum-free culture medium and incubated for 15 min at rt. Transfection was performed by dropwise addition of the PEI/DNA mixture to the cells. Transfection with pcDNA3.1 encoding GFP was used to generate control samples. 24 h Post-transfection culture medium was refreshed. *In situ* treatments were initiated 48 h post-transfection. Transfection efficiency was checked by fluorescence microscopy on eGFP transfected samples (EVOS FL2 Auto, GFP-channel).

### *In situ treatments*

Neuro-2a cells were seeded at appropriate density ( $0.3 \times 10^6$  cells/well in 12-wells plates,  $2.5 \times 10^6$  cells/dish in 6 cm dishes) 48 h prior to treatment. Alternatively, HEK293-T cells from transient transfections were used at 24-48 h post-transfection. Culture medium was aspirated and after a careful PBS wash, treatment medium (serum-free DMEM) containing vehicle (0.1% DMSO) or DH376 (100 nM – 1  $\mu$ M, as indicated in figure legends) was added. After incubation for 2 h at 37 °C and 7% CO<sub>2</sub>, treatment medium was aspirated and cells were carefully washed with PBS. Subsequently cells were harvested by resuspension in PBS and spun down (1000 g, 3 min, rt). Cell pellets were flash frozen in liquid nitrogen and stored at -80 °C until further use.

### *Retinoic acid stimulation*

Neuro-2a cells were seeded at  $1 \times 10^5$  cells/well in 6-well plates or  $1 \times 10^6$  cells/ dish in 10 cm dishes. One day after seeding, medium was aspirated and retinoic acid stimulation was initiated by adding DMEM containing 2% newborn bovine serum and all-*trans*-retinoic acid (50  $\mu$ M) or vehicle (0.1% DMSO). For Figure 2D, co-treatment was done with vehicle (0.1% DMSO) or DH376 (100 nM) throughout the entire differentiation process. After 24, 48 or 72 h of stimulation, neurite outgrowth was investigated using phase contrast microscopy (Olympus or EVOS FL2 Auto, phase contrast, large ring). Neurite outgrowth was quantified by counting the number of cells with a minimum of 2 outgrowth processes longer than the cell body, as a percentage of the total number of cells (3 dishes, 5 images per dish). Cell count and viability were checked by Trypan blue staining and automated cell counting (TC20™ Cell Counter, Bio-Rad).

## CRISPR/Cas9-mediated knockdowns

### *Guide design & constructs*

Two sgRNA's, in early exons, with high efficiency and specificity as predicted by CHOPCHOP v2 online web tool<sup>25</sup> (<http://chopchop.cbu.uib.no>) were selected. Guides were cloned into the BbsI restriction site of plasmid px330-U6-Chimeric\_BB-CBh-hSpCas9 (gift from Feng Zhang, Addgene plasmid #42230) as previously described<sup>26,27</sup>. Constructs and primers are annotated in Table 1.

### *Knockdown population generation*

Neuro-2a cells were transfected sequentially (3 times within the course of 10 days) to yield populations with a high knockdown efficiency. Cells were seeded at day 0, 3, and 6 and transfected at day 1, 4, and 7. Samples for T7E1 assays, and ABPP were harvested at day 2, 5, and 11 and after several weeks of culturing the cells. One day prior to the first transfection, Neuro-2a cells were seeded to a 6-well plate to reach 80% confluence at the time of transfection. Prior to transfection, culture medium was aspirated and 2 mL of fresh medium was added. A 5:1 (m/m) mixture of polyethyleneimine (PEI) (17.5  $\mu$ g per well) and plasmid DNA (total 3.5  $\mu$ g per well) was prepared in serum-free culture medium (250  $\mu$ L each) and incubated (15 min, rt). Transfection was performed by dropwise addition of the PEI/DNA mixture to the cells. 24 h Post-transfection the culture medium was refreshed, a small amount of cells was harvested for analysis by T7E1 assay and ABPP, while the remainder was kept in culture under standard conditions for following transfections. After three transfection rounds, the cells were cultured according to standard protocol. Ampoules of knockdown populations were prepared (complete DMEM, 10% DMSO) and stored at -150 °C. Efficiency of knockdown was checked over time. Cells were discarded after 3 months of culture.

### *T7E1 assay*

Genomic DNA was obtained by mixing 50  $\mu$ L QuickExtract™ (Epicentre) with cell pellet (~ 10% of a well from a 6-well plate). The samples were incubated at 65 °C for 6 min, mixed by vortexing and then incubated at 98 °C for 2 min. Genomic DNA extracts were diluted in sterile water and directly used in PCR reactions. Genomic PCR reactions were performed on 2.5-5  $\mu$ L isolated genomic DNA

extract using Phusion High-Fidelity DNA Polymerase (Thermo Fisher) in Phusion HF buffer Green (Thermo Fisher) in a final volume of 20  $\mu$ L, for primers see Table 1.

For the T7E1 assay, genomic PCR products were denatured and reannealed in a thermocycler using the following program: 5 min at 95 °C, 95 to 85 °C using a ramp rate of -2 °C/s, 85 °C to 25 °C using a ramp rate of -0.2 °C/s. Annealed PCR product (8.5  $\mu$ L) was mixed with NEB2 buffer (1  $\mu$ L) and T7 endonuclease I (5 U, 0.5  $\mu$ L; New England Biolabs), followed by a 30 min incubation at 37 °C. Digested PCR products were analyzed using agarose gel electrophoresis with ethidium bromide staining. A sample without T7 endonuclease I was taken along as control. Agarose gels were analyzed using ImageLab™ Software (Bio-Rad) and DNA modification efficiency was expressed as percentage T7E cleavage (volume integral of digested bands / volume integral all bands \* 100%).

**Table 1 | sgRNA targets, sgRNA oligos (top, bottom) and T7E1 primers (forward, reverse).** Constructs indicated with an asterisk (\*) were used to generate double and triple knockdowns.

sgRNA Target	Construct	Primer Sequences	
<b>Dagla – Exon 2</b>	447*	Top:	CACCGAGGATTACAAACCTGCAGAG
		Bottom:	AAACCTCTGCAGGTTTGTAACTCCTC
		Forward:	GAAGTGGGGTCTTTTGTCTG
		Reverse:	CAAGGAAGAACAGGTAACCAGG
<b>– Exon 3</b>	485	Top:	CACCGCATGGCTGGCAGCTCTGGG
		Bottom:	AAACCCAGAGCTGCCAGCCATGC
		Forward:	GGTAGTAGTTACTGCCGATGCC
		Reverse:	CTCTTCAGGGCTGACTCAGTTT
<b>Daglb – Exon 1</b>	449*	Top:	CACCGTGGGAGGTGCCCATGCCG
		Bottom:	AAACCGGCATGGCGCACCTCCAC
		Forward:	TAAACAGAAATGACCACACCG
		Reverse:	CCTGTTTCTATGAATTGCTCC
<b>– Exon 2</b>	450	Top:	CACCGTGTATCTCACGCACAGAAGG
		Bottom:	AAACCTTCTGTGCGTGAGATACAC
		Forward:	CTCCTACATCTTTGCTTGCCT
		Reverse:	ACACAAATGGTAGCGCAGTATG
<b>Abhd6 – Exon 2</b>	724	Top:	CACCGTTAACATGTTTGTGATTG
		Bottom:	AAACCAATCACAAACATGTTAACC
		Forward:	GATCCATGGTATACCCCTAACCACTGAGTCATCTC
		Reverse:	TGACTCGAGATTGGAATGGCGATATGTTTACACT
<b>– Exon 3</b>	725*	Top:	CACCAAGTTCGCTACGCACACCATG
		Bottom:	AAACCATGGTGTGCGTAGCGAACT
		Forward:	TCCAAGCTTATGCCTGCTTTGCTTTTATTT
		Reverse:	CAACACCGGTATCCTATGTGAGCTCACTCCACCC

### Whole lysate preparation

Cells were harvested in PBS and pelleted by centrifugation (1000 *g*, 3-5 min, rt). Cell pellets were snap-frozen and stored at -80 °C until further use. Cell pellets were thawed on ice, resuspended in cold lysis buffer (20 mM HEPES pH 7.2, 2 mM DTT, 250 mM sucrose, 1 mM MgCl<sub>2</sub>, 2.5 U/mL benzonase) and incubated on ice (15-30 min). Protein concentrations were determined by a Quick Start™ Bradford Protein Assay (Bio-Rad). After dilution to 2 mg/mL in sucrose lysis buffer or storage buffer (20 mM HEPES pH 7.2, 2 mM DTT), samples were used or flash frozen in liquid nitrogen and stored at -80 °C until further use. DTT was left out of all buffers for samples intended for click-chemistry.



## Activity-based protein profiling

### *Gel-based ABPP: Single probe*

Whole lysate (2 mg/mL) was incubated with activity-based probes MB064 (250 nM - 2  $\mu$ M, 20 min, rt) or FP-TAMRA (500 nM, 20 min, rt). The reaction was quenched with Laemmli buffer (30 min, rt) and 20  $\mu$ g protein was resolved by SDS-PAGE (10% acrylamide gel) along with protein marker (PageRuler™ Plus, Thermo Fisher). In-gel fluorescence was detected in the Cy3- and Cy5-channel on a ChemiDoc™ MP imaging system (Bio-Rad) and gels were stained with coomassie after scanning. Fluorescence was quantified and normalized to coomassie staining using ImageLab™ software (Bio-Rad) and data was processed in Excel (Microsoft) and GraphPad Prism 7 (GraphPad).

### *Gel-based ABPP: Probe mixture*

Whole lysates (DTT-free, 2 mg/mL) were incubated with activity-based probe MB064 (2  $\mu$ M, 10 min, rt), followed by incubation with FP-TAMRA (500 nM, 10 min, rt) and a subsequent conjugation to Cy5-azide by incubation with click-mix (2.5/10  $\mu$ M Cy5-N<sub>3</sub>, 67 mM sodium ascorbate, 4 mM CuSO<sub>4</sub>(H<sub>2</sub>O)<sub>5</sub>, 1.3 mM THPTA; 30 min, rt). The reaction was quenched with Laemmli buffer (30 min, rt) and 15  $\mu$ g protein was resolved by SDS-PAGE (10% acrylamide gel) along with protein marker (PageRuler™ Plus, Thermo Fisher). In-gel fluorescence was detected in the Cy3- and Cy5-channel on a ChemiDoc™ MP imaging system (Bio-Rad) and gels were stained with coomassie after scanning. Fluorescence was quantified and normalized to coomassie staining using ImageLab™ software (Bio-Rad) and data was processed in Excel (Microsoft) and GraphPad Prism 7 (GraphPad).

### *Chemical proteomics with label-free quantification*

The chemical proteomics workflow was modified from a previously published protocol<sup>20</sup>. In short, for general profiling of the serine hydrolases the whole lysates (250  $\mu$ g protein, n=4) were incubated with serine hydrolase probe cocktail (10  $\mu$ M MB108, 10  $\mu$ M FP-Biotin, 30 min, 37 °C, 300 rpm). A denatured protein sample (1% SDS, 5 min, 100 °C) was taken along as a negative control. For DH376 target identification, the whole lysates of DH376 treated cells (250  $\mu$ g protein, n=4) were conjugated to biotin-azide by the addition of 10x concentrated click mix (final: 1 mM CuSO<sub>4</sub>(H<sub>2</sub>O)<sub>5</sub>, 0.56 mM sodium ascorbate, 0.2 mM THPTA, 0.04 mM biotin-azide in MilliQ) and subsequent incubation (60 min, 37 °C, 300 rpm). A vehicle treated sample was taken along as a negative control. Precipitation, alkylation, avidin enrichment, on-bead digestion and sample preparation was performed according to protocol<sup>20</sup>. Dried peptides were stored at -20 °C until LC-MS analysis. Prior to measurement, samples were reconstituted in 50  $\mu$ L LC-MS solution and transferred to LC-MS vials. Analysis was performed using Progenesis Q1P (Waters) as published, using the following cut-offs:  $\geq$  2-fold enrichment compared to negative control,  $\geq$  2 peptides,  $\geq$  1 unique peptide, peptide ion correlations  $\geq$  0.7.

## Lipidomics

### *Sample preparation: Neuro-2a retinoic acid stimulation*

Neuro-2a cells were seeded at  $0.75 \times 10^6$  cells/dish in a 10 cm dish. One day after seeding, medium was aspirated and retinoic acid stimulation was initiated by adding DMEM containing 2% serum and retinoic acid (50  $\mu$ M) or vehicle (0.1% DMSO). After 72 h neurite outgrowth was investigated using phase contrast microscopy (Olympus). Cells were carefully washed with PBS and harvested by resuspension in PBS (for retinoic acid stimulated cells, 5 dishes were combined to yield sufficient cells). Cells were pelleted (200 g, 10 min, rt) and resuspended in 1 mL PBS. Cell count and viability were checked by Trypan blue staining and automated cell counting (TC20™ Cell Counter, Bio-Rad) and  $2 \times 10^6$  cells were pelleted (1000 g, 3 min, rt). Pellets were flash frozen in liquid nitrogen and stored at -80 °C until lipid extraction.

*Sample preparation: Neuro-2a single cell clones*

Neuro-2a cells were seeded at  $1.25 \times 10^6$  cells/ dish in a 10 cm dish. One day after seeding, medium was aspirated and cells were cultured in 2% serum and vehicle (0.1% DMSO). After 48 h cells were carefully washed with PBS and harvested by resuspension in. Cells were pelleted (200 g, 5 min, rt) and resuspended in PBS. Cell count and viability were checked by Trypan blue staining and automated cell counting (TC20™ Cell Counter, Bio-Rad) and  $1 \times 10^6$  cells were pelleted (1000 g, 3 min, rt). Pellets were flash frozen in liquid nitrogen and stored at  $-80^\circ\text{C}$  until lipid extraction.

*Sample preparation: Neuro-2a knockdown populations*

Neuro-2a cells were seeded at  $2.5 \times 10^6$  cells/dish in a 6 cm dish 48 h prior to treatment. Alternatively, HEK293-T cells from transient transfections were used at 48 h post-transfection (6-wells format). Culture medium was aspirated and after a careful PBS wash, treatment medium (serum-free DMEM) containing vehicle (0.1% DMSO) or DH376 (100 nM) was added. After incubation for 2 h at  $37^\circ\text{C}$  and 7%  $\text{CO}_2$ , treatment medium was aspirated and cells were carefully washed with PBS. Subsequently cells were harvested by resuspension in 1250  $\mu\text{L}$  PBS. Cell count and viability were checked by Trypan blue staining and automated cell counting (TC20™ Cell Counter, Bio-Rad). Cells from 1000  $\mu\text{L}$  suspension were spun down (1000 g, 3 min, rt) in a low binding Eppendorf tube. Pellets were flash frozen in liquid nitrogen and stored at  $-80^\circ\text{C}$  until lipid extraction. The remaining cell suspension ( $\sim 200 \mu\text{L}$ ) was flash frozen and used to determine the protein concentration of each sample. The suspension was thawed on ice and cells were lysed by sonication using a probe sonicator (Heidolph; 5 s per sample, 10% amplitude). Protein concentrations ( $\sim 1 \text{ mg/mL}$ ) were determined by a Quick Start™ Bradford Protein Assay (Bio-Rad) and were used for normalization of the lipid abundance.

*Lipid extraction*

Lipid extraction was performed as previously described<sup>28</sup> with minor adaptations. In brief, cell pellets were transferred into 1.5 mL Eppendorf tubes, spiked with 10  $\mu\text{L}$  of deuterated internal standard mix (Table 2), followed by addition of 200  $\mu\text{L}$  of ammonium acetate buffer (0.1 M, pH 4) was added. After addition of 1000  $\mu\text{L}$  methyl *tert*-butyl ether (MTBE), the tubes were thoroughly mixed for 5 min using a bullet blender (Next Advance) at medium speed, followed by a centrifugation step (16,000 g, 5 min,  $4^\circ\text{C}$ ). Then 850  $\mu\text{L}$  of the upper MTBE layer was transferred to clean 1.5 mL Eppendorf tubes. Samples were dried in a SpeedVac (Eppendorf) followed by reconstitution in 50  $\mu\text{L}$  of acetonitrile:water (90:10, v/v). The reconstituted samples were centrifuged (16,000 g, 3 min,  $4^\circ\text{C}$ ) before transferring into LC-MS vials. 5  $\mu\text{L}$  of each sample was injected into the LC-MS/MS system.

*General LC-MS/MS Analysis*

LC-MS/MS analysis was performed as previously described<sup>28</sup> with minor adaptations. A targeted analysis of 31 compounds, including endocannabinoids and related *N*-acylethanolamines (NAEs) and free fatty acids (Table 2), was measured using an Acquity UPLC I class Binary solvent manager pump (Waters) in conjugation with AB SCIEX 6500 quadrupole-ion trap (AB Sciex). The separation was performed with an Acquity HSS T3 column ( $2.1 \times 100 \text{ mm}$ ,  $1.8 \mu\text{m}$ ) maintained at  $45^\circ\text{C}$ . The aqueous mobile phase A consisted of 2 mM ammonium formate and 10 mM formic acid, and the organic mobile phase B was acetonitrile. The flow rate was set to 0.55 mL/min; initial gradient conditions were 55% B held for 2 min and linearly ramped to 100% B over 6 min and held for 2 min; after 10 s the system returned to initial conditions and held 2 min before next injection. Electrospray ionization-MS and a selective Multiple Reaction Mode (sMRM) was used for endocannabinoid quantification. Individually optimized MRM transitions using their synthetic standards for target compounds and internal standards are described in Table 2.

### DAG Analysis

LC-MS/MS analysis of DAG (16:0, 20:4) was performed as described in the above section with the following adaptations. The mobile phase A was 10 mM ammonium formate and 10 mM formic acid in 60:40 (v/v%) acetonitrile:water, the mobile phase B was 10 mM ammonium formate and 10 mM formic acid in 10:90 (v/v%) acetonitrile:isopropanol. The flow rate was set to 0.4 mL/min; initial gradient conditions were 50% B for 0.5 min and linearly ramped to 60% B at 2 min, then ramped to 90% B at 6 min; after 6 seconds the system returned to initial conditions and held 1.4 min before next injection.

**Table 2 | LC-MS Standards and internal standards for lipidomics analysis.**

Standards				
Abbreviation	Metabolite	Q1	Q3	Polarity
DAG (16:0, 20:4)	1-Palmitoyl-2-arachidonoyl-sn-glycerol	634	313	+
1&2-AG	2&1-Arachidonoylglycerol (20:4)	379	287	+
AEA	Anandamide (20:4)	348	62	+
DHEA	N-Docosahexaenoylethanolamide (22:6)	372	62	+
LEA	N-Linoleoylethanolamide (18:2)	324	62	+
NADA	N-Arachidonoyl dopamine (28:4)	440	137	+
OEA	N-Oleoylethanolamide (18:1)	326	62	+
PEA	N-Palmitoylethanolamide (16:0)	300	62	+
SEA	N-Stearoylethanolamide (18:0)	328	62	+
2-AGE	2-Arachidonyl glycerol ether (20:4)	365	273	+
DEA	N-Docosatetraenoylethanolamide (22:4)	376	62	+
DGLEA	Dihomo-γ-Linolenoyl Ethanolamide (18:3)	350	62	+
O-AEA	O-Arachidonoyl ethanolamine (20:4)	348	62	+
2-LG	2-Linoleoyl glycerol (18:2)	355	263	+
1-LG	1-Linoleoyl glycerol (18:2)	355	263	+
2-OG	2-Oleoyl glycerol (18:1)	357	265	+
EPEA	Eicosapentaenoyl ethanolamide (20:5)	346	62	+
POEA	N-Palmitoleoylethanolamide (16:1)	298	62	+
ETAEA	Eicosatrienoic acid ethanolamide (20:3)	350	62	+
PDEA	N-Pentadecanoylethanolamide (15:0)	286	62	+
α-LEA	N-α-Linolenylethanolamide (18:2)	322	62	+
OA	Oleic acid (18:1)	281	263	-
LA	Linoleic acid (18:2-ω6)	279	261	-
α-LA	α-Linolenic acid (18:3-ω3)	277	233	-
γ-LA	γ-Linolenic acid (18:3-ω6)	277	233	-
DGLA	Dihomo-γ-linolenic acid (20:3-ω6)	305	261	-
MA	Mead acid (20:3-ω9)	305	261	-
AA	Arachidonic Acid (20:4-ω6)	303	259	-
EPA	Eicosapentaenoic acid (20:5-ω3)	301	257	-
DTA	Docosatetraenoic acid (22:4-ω6)	332	288	-
DHA	Docosahexaenoic acid (22:6-ω3)	327	283	-
Internal standards				
Abbreviation	Metabolite	Q1	Q3	Polarity
DAG (34:0)	1-Margaroyl-2-margaroyl-sn-glycerol	614	327	+
2-AG (20:4)-d8	2-Arachidonoylglycerol-d8	387	294	+
PEA (16:0)-d4	Palmitoyl ethanolamide-d4	304	62	+
SEA (18:0)-d3	Stearoyl ethanolamide-d3	331	62	+
OEA (18:1)-d4	Oleoyl ethanolamide-d4	330	66	+
LEA (18:2)-d4	Linoleoyl ethanolamide-d4	328	66	+
AEA (20:4)-d8	Arachidonoyl ethanolamide-d8	356	62	+
DHEA (22:6)-d4	Docosahexaenoyl ethanolamide-d4	376	66	+
NADA (28:4)-d8	N-Arachidonoyl dopamine-d8	448	137	+

### NBD-HPTLC assay

Whole lysates of HEK293-T transiently expressing eGFP (control), DAGL $\alpha$ , ABHD6 or their catalytically inactive serine mutants were prepared as described above. Lysate (100  $\mu$ g protein) was mixed with 5  $\mu$ M DAG-NBD (Cayman Chemical; 2 mM stock in EtOH) in HEPES buffer (20 mM HEPES pH7.2, 2 mM DTT) and incubated (30 min, 37 °C, 600 rpm, dark). As a control, a sample without protein was taken along. After incubation, lipids were extracted by a Bligh and Dyer extraction. In short, 800  $\mu$ L chloroform:methanol (1:1, v/v) and 110  $\mu$ L MilliQ were added to the sample. Phases were separated by centrifugation (5 min, 13,000 *g*) and the bottom layer was transferred to a dark Eppendorf tube. The upper layer was extracted once more by adding 400  $\mu$ L chloroform. The lipid extract was dried in a speedvac (Eppendorf) (45 min, 45 °C). Lipids were reconstituted in 40  $\mu$ L methanol, and lipids (2  $\mu$ L, *n*=3) were separated by thin layer chromatography on HPTLC Silica gel 60 plates (Merck) using chloroform:methanol (80:20, v/v) as eluent. NBD-labeled lipids were detected using a Typhoon Imaging system (GE Healthcare Bio-Science) (Alexa488 channel, 250V). Fluorescence was quantified using ImageLab™ software (Bio-Rad). Excel (Microsoft) and GraphPad Prism 7 (GraphPad) were used for further analysis. DAG-NBD was expressed as fraction of the total NBD intensity in each lane and normalized to eGFP samples.

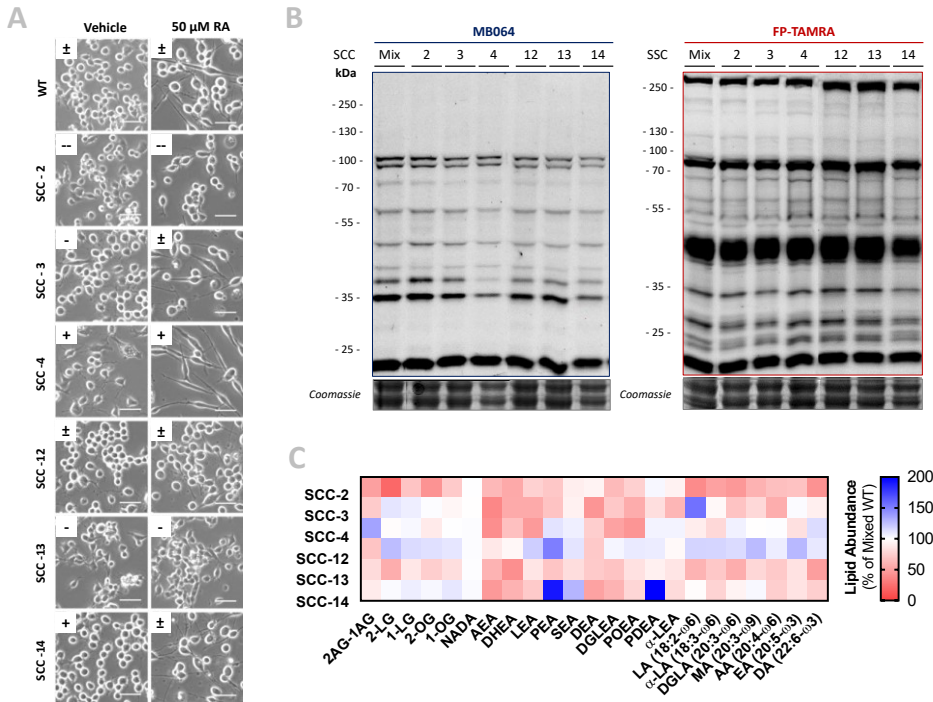
### Western blot

Cell lysates were denatured with Laemmli buffer (30 min, rt) and 20  $\mu$ g lysate was resolved on a 10% acrylamide SDS-PAGE gel along with PageRuler™ Plus Protein Marker (Thermo Scientific). Proteins were transferred to 0.2  $\mu$ m polyvinylidene difluoride membranes by Trans-Blot Turbo™ Transfer system (Bio-Rad). Membranes were washed with TBS (50 mM Tris, 150 mM NaCl) and blocked with 5% milk in TBS-T (50 mM Tris, 150 mM NaCl, 0.05% Tween 20) (1 h, rt). Membranes were then incubated with primary antibody mouse-anti-FLAG (F3156, Sigma Aldrich; 1:2500 in 5% milk in TBS-T, 45 min, rt) washed with TBS-T, incubated with secondary donkey-anti-mouse-Alexa647 (A-31571, Thermo Fisher; 1:10000 in 5% milk TBS-T, 45 min, rt), and washed with TBS-T and TBS. Fluorescence was detected on the ChemiDoc™ MP imaging system (Bio-Rad) in the Alexa647 channel, and Cy3/Cy5 channels for the protein marker. Signal was normalized to coomassie staining using ImageLab™ software (Bio-Rad) and data was processed in Excel (Microsoft) and GraphPad Prism 7 (GraphPad).

### Statistical methods

All statistical measures and methods are included in the respective figure or table captions. In brief: all data are shown as the mean  $\pm$  SEM, unless indicated otherwise. A Student's *t*-test (two-tailed, unpaired) was used to determine statistical significance, with a Holm-Sidak multi-comparison correction for proteomics data using GraphPad Prism 7 (GraphPad). Samples were compared to WT/Vehicle/GFP controls and statistical significance is indicated as \* *p* < 0.05, \*\* *p* < 0.01, \*\*\* *p* < 0.001.

# Supplementary data



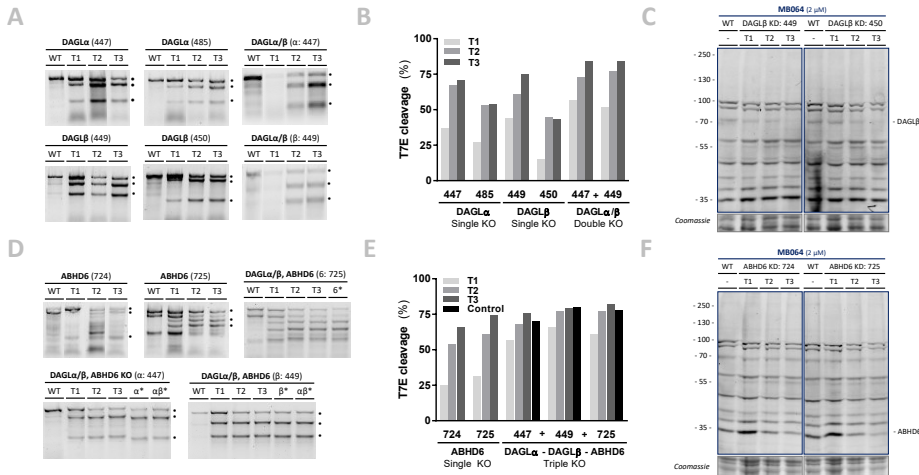


**Figure S2 | Efficiency of CRISPR/Cas9-mediated knockdown in Neuro-2a.** Knockdown populations were generated by three sequential transfections (T1-T3) with Cas9 and two different separate guides for each target. Most efficient guides were used to generate double and triple knockdowns. **(A-B, D-E)** Knockdown efficiency is determined by a T7E1 assay on genomic DNA was analyzed after each round of transfection and quantified for DAGL **(A-B)** and ABHD6 **(D-E)** knockdowns. **(C, F)** ABPP analysis of knockdown efficiency. After each transfection, whole lysates were incubated with MB064 (2  $\mu$ M, 20 min, rt) and analyzed by SDS-PAGE.

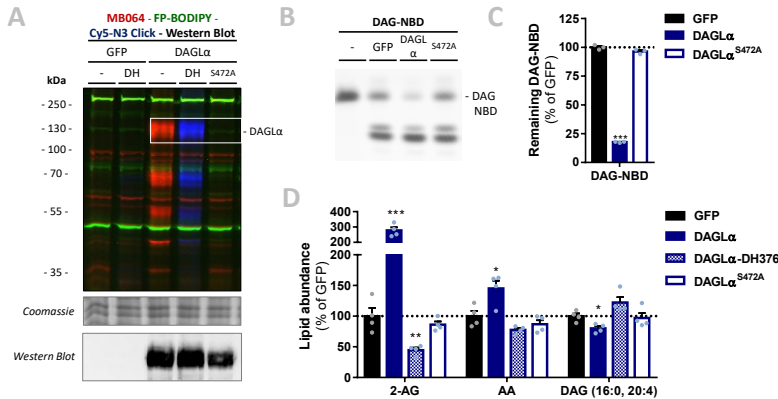


**Figure S3 | Recombinant DAGLα possesses DAG-lipase activity *in vitro* and *in situ*.** HEK293-T cells were transiently transfected with GFP, DAGLα or its catalytically inactive serine mutants (S472A) and treated *in situ* with vehicle or DH376 (DH, 1  $\mu$ M, 2 h, serum-free). **(A)** Protein activity and expression were confirmed by gel-based ABPP and western blot. Samples were subsequently incubated with probes MB064 (500 nM, 10 min, rt), FP-BODIPY (500 nM, 10 min, rt), and Cy5-azide click mix (2.5  $\mu$ M, 30 min, rt). Coomassie served as a protein loading control. Western blot with mouse-anti-FLAG (1:2500, 45 min, rt) verified expression of the catalytically inactive protein. **(B-C)** Whole lysates were incubated with DAG-NBD (5  $\mu$ M, 30 min, 37  $^{\circ}$ C, 600 rpm). Lipids were extracted and analyzed by HPTLC (n=3). DAG hydrolysis was quantified and expressed as % of GFP (mean  $\pm$  SEM (n=3), *t*-test: \*\*\* *p* < 0.001). **(D)** Lipid abundance of transfected and *in situ* treated cells was measured and normalized to the amount of protein (n=4). Data is expressed as % of GFP-Vehicle (mean  $\pm$  SEM (n=4), *t*-test: \* *p* < 0.05, \*\* *p* < 0.01, \*\*\* *p* < 0.001).

## References

1. Di Marzo, V. Endocannabinoid signaling in the brain: biosynthetic mechanisms in the limelight. *Nat. Neurosci.* **14**, 9–15 (2011).
2. Bisogno, T. *et al.* Cloning of the first sn1-DAG lipases points to the spatial and temporal regulation of endocannabinoid signaling in the brain. *J. Cell Biol.* **163**, 463–468 (2003).
3. Gao, Y. *et al.* Loss of Retrograde Endocannabinoid Signaling and Reduced Adult Neurogenesis in Diacylglycerol Lipase Knock-out Mice. *J. Neurosci.* **30**, 2017–2024 (2010).
4. Ogasawara, D. *et al.* Rapid and profound rewiring of brain lipid signaling networks by acute diacylglycerol lipase inhibition. *Proc. Natl. Acad. Sci.* **113**, 26–33 (2016).
5. Deng, H. *et al.* Triazole Ureas Act as Diacylglycerol Lipase Inhibitors and Prevent Fasting-Induced Refeeding. *J. Med. Chem.* **60**, 428–440 (2017).
6. McReynolds, J. R. *et al.* Stress Promotes Drug Seeking Through Glucocorticoid-Dependent Endocannabinoid Mobilization in the Prelimbic Cortex. *Biol. Psychiatry* **84**, 85–94 (2018).
7. Bluett, R. J. *et al.* Endocannabinoid signalling modulates susceptibility to traumatic stress exposure. *Nat. Commun.* **8**, 14782 (2017).
8. Dinh, T. P., Freund, T. F. & Piomelli, D. A role for monoglyceride lipase in 2-arachidonoylglycerol inactivation. in *Chemistry and Physics of Lipids* **121**, 149–158 (2002).
9. Marrs, W. R. *et al.* The serine hydrolase ABHD6 controls the accumulation and efficacy of 2-AG at cannabinoid receptors. *Nat. Neurosci.* **13**, 951–7 (2010).
10. Blankman, J. L., Simon, G. M. & Cravatt, B. F. A comprehensive profile of brain enzymes that hydrolyze the endocannabinoid 2-arachidonoylglycerol. *Chem. Biol.* **14**, 1347–1356 (2007).
11. Savinainen, J. R., Saario, S. M. & Laitinen, J. T. The serine hydrolases MAGL, ABHD6 and ABHD12 as guardians of 2-arachidonoylglycerol signalling through cannabinoid receptors. *Acta Physiologica* **204**, 267–276 (2012).
12. Oudin, M. J., Hobbs, C. & Doherty, P. DAGL-dependent endocannabinoid signalling: Roles in axonal pathfinding, synaptic plasticity and adult neurogenesis. *European Journal of Neuroscience* **34**, 1634–1646 (2011).
13. Harkany, T. *et al.* The emerging functions of endocannabinoid signaling during CNS development. *Trends in Pharmacological Sciences* **28**, 83–92 (2007).
14. Watson, S., Chambers, D., Hobbs, C., Doherty, P. & Graham, A. The endocannabinoid receptor, CB1, is required for normal axonal growth and fasciculation. *Mol. Cell. Neurosci.* **38**, 89–97 (2008).
15. Wu, C. S. *et al.* Requirement of cannabinoid CB1receptors in cortical pyramidal neurons for appropriate development of corticothalamic and thalamocortical projections. *Eur. J. Neurosci.* **32**, 693–706 (2010).
16. Jung, K.-M., Astarita, G., Thongkham, D. & Piomelli, D. Diacylglycerol lipase- $\alpha$  and - $\beta$  control neurite outgrowth in neuro-2a cells through distinct molecular mechanisms. *Mol. Pharmacol.* **80**, 60–7 (2011).
17. Oudin, M. J. *et al.* Endocannabinoids Regulate the Migration of Subventricular Zone-Derived Neuroblasts in the Postnatal Brain. *J. Neurosci.* **31**, 4000–4011 (2011).
18. Berghuis, P. *et al.* Hardwiring the brain: Endocannabinoids shape neuronal connectivity. *Science* **316**, 1212–1216 (2007).
19. Rostovtsev, V. V., Green, L. G., Fokin, V. V. & Sharpless, K. B. A stepwise Huisgen cycloaddition process: Copper(I)-catalyzed regioselective ‘ligation’ of azides and terminal alkynes. *Angew. Chemie - Int. Ed.* **41**, 2596–2599 (2002).
20. van Rooden, E. J. *et al.* Mapping in vivo target interaction profiles of covalent inhibitors using chemical proteomics with label-free quantification. *Nat. Protoc.* **13**, 752–767 (2018).
21. Thomas, G. *et al.* The Serine Hydrolase ABHD6 Is a Critical Regulator of the Metabolic Syndrome. *Cell Rep.* **5**, 508–520 (2013).

22. Pribasnig, M. A. *et al.*  $\alpha/\beta$  hydrolase domain-containing 6 (ABHD6) degrades the late Endosomal/Lysosomal lipid Bis(Monoacylglycero)phosphate. *J. Biol. Chem.* **290**, 29869–29881 (2015).
23. Janssen, A. P. A. *et al.* Development of a Multiplexed Activity-Based Protein Profiling Assay to Evaluate Activity of Endocannabinoid Hydrolase Inhibitors. *ACS Chem. Biol.* **13**, 2406–2413 (2018).
24. Baggelaar, M. P. *et al.* Development of an activity-based probe and in silico design reveal highly selective inhibitors for diacylglycerol lipase- $\alpha$  in brain. *Angew. Chemie - Int. Ed.* **52**, 12081–12085 (2013).
25. Labun, K., Montague, T. G., Gagnon, J. A., Thyme, S. B. & Valen, E. CHOPCHOP v2: a web tool for the next generation of CRISPR genome engineering. *Nucleic Acids Res.* **44**, W272–W276 (2016).
26. Ran, F. A. *et al.* Genome engineering using the CRISPR-Cas9 system. *Nat Protoc* **8**, 2281–2308 (2013).
27. Cong, L. *et al.* Multiplex genome engineering using CRISPR/Cas systems. *Science* **339**, 819–823 (2013).
28. Van Esbroeck, A. C. M. *et al.* Activity-based protein profiling reveals off-target proteins of the FAAH inhibitor BIA 10-2474. *Science* **356**, 1084–1087 (2017).





## Summary & future prospects

*The aim of this thesis was to explore activity-based protein profiling (ABPP) as a tool in drug discovery and cell biology.*

**Chapter 1** discussed the different phases of the drug discovery process, such as target discovery and hit identification. ABPP is introduced as a versatile chemical tool, which may aid in addressing these challenges. ABPP employs active site-directed probes to assess the functional state of an entire enzyme class (e.g. serine hydrolases and kinases) in complex protein samples. Fluorescently labeled activity-based probes (ABPs) allow rapid analysis of the functional state of the enzymes by in-gel fluorescence scanning, whereas probes with affinity tags enable target enrichment and identification by mass spectrometry (MS)<sup>1,2</sup>. The ABPP methodology can be used in a comparative setup to map the activity landscape of different biological samples (e.g. healthy versus diseased) (Figure 1A). Alternatively, a competitive setup with inhibitors can be used for target engagement studies or selectivity profiling (Figure 1B).

The serine hydrolases play a central role in the research performed in this thesis. They represent a large protein family (~ 1% of the mammalian proteome) and are involved in a broad spectrum of physiological processes, including signaling and metabolism<sup>2</sup>. In the described work, a special focus was set on the serine hydrolases of the endocannabinoid system (ECS), which were also introduced in **Chapter 1**.

The ECS regulates a broad spectrum of physiological and pathological processes, including memory, pain, anxiety, appetite, metabolism and inflammation. The versatile role of the ECS in physiology makes the ECS interesting for therapeutic exploitation<sup>3,4</sup>. The ECS is comprised of the cannabinoid receptor type 1 and 2 (CB1R, CB2R), their endogenous ligands, the endocannabinoids 2-arachidonoylglycerol (2-AG) and anandamide (AEA), and their metabolic enzymes<sup>5</sup>. Diacylglycerol lipase  $\alpha$  and  $\beta$  (DAGL $\alpha$ , DAGL $\beta$ ) are the two main 2-AG biosynthetic enzymes<sup>6</sup>. Monoacylglycerol lipase (MGLL) and  $\alpha,\beta$ -hydrolase domain containing protein 6 and 12 (ABHD6, ABHD12) can terminate 2-AG signaling by its hydrolysis to arachidonic acid (AA) and glycerol<sup>7–10</sup>. There are multiple AEA biosynthetic pathways, but hydrolysis of *N*-acylphosphatidylethanolamines (NAPEs) to *N*-acylethanolamines (NAEs, including AEA), by NAPE phospholipase D (NAPE-PLD) is considered to be the canonical pathway<sup>11</sup>. Fatty acid amide hydrolase (FAAH) hydrolyzes the NAEs to ethanolamines and free fatty acids<sup>12,13</sup>. With the exception of NAPE-PLD, all endocannabinoid metabolic enzymes are part of the serine hydrolase family.

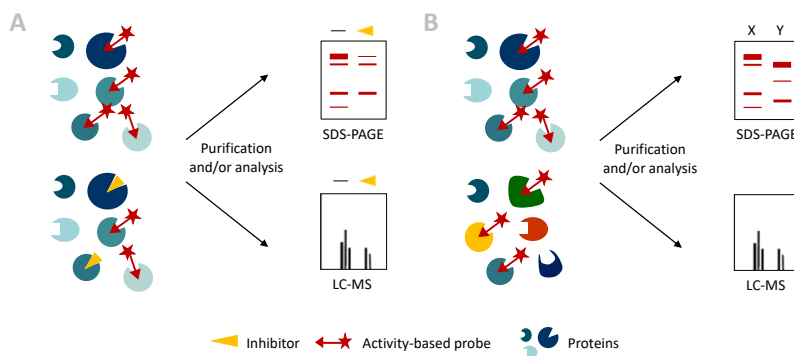


Figure 1 | Schematic representation of competitive (A) and comparative (B) ABPP.

**Chapter 2** demonstrated comparative ABPP as a tool for rapid mapping of the serine hydrolase activity profile in ischemic cardiac tissue. The endocannabinoids and their receptors have emerged as important modulators of the cardiovascular system, especially under diseased conditions<sup>14–16</sup>. The role of endocannabinoid metabolizing enzymes, however, has been investigated less extensively. Cardiac tissues from patients with terminal-stage heart failure (due to previous ischemic pathology) and non-failing control hearts were used to determine the endocannabinoid levels and the activity of the endocannabinoid hydrolases. mRNA expression of *DAGL $\beta$* , *MGLL*, *ABHD6* and *NAPEPLD* was decreased in the ischemic tissues. Two subgroups were identified within the ischemic group by lipidomics and ABPP analysis; the first similar to control hearts and the second with reduced levels of the endocannabinoid 2-AG and drastically increased levels of AEA, NAEs and free fatty acids. The aberrations in the lipid profile were accompanied by decreased activity of 13 hydrolases, including the 2-AG hydrolytic enzyme MGLL. The distinct profiles of the two ischemic subgroups indicate the existence

of differential biological states and may be related to more severe cardiac damage in the second subgroup, based on the significant reduction in cardiac output and the increase in systemic vascular resistance within this patient group.

In a similar setup as described in **Chapter 2**, comparative ABPP has contributed to the discovery of novel therapeutic targets or biomarkers for a variety of clinical indications. For example, in cancer research, the strength of the technique was demonstrated by the identification of enhanced MGLL activity in aggressive human cancer cells and primary tumors. Overexpression of MGLL in non-aggressive cancer cells increased their pathogenicity and the effects could be reversed with a MGLL inhibitor<sup>17</sup>. Similarly, elevated levels of KIAA1363 activity were detected in aggressive cancer cells. Inhibition of this hydrolase disrupted lipid metabolism in cancerous cells, thereby impairing cell migration and tumor growth *in vivo*<sup>18</sup>. Upon further investigation, MGLL and KIAA1363 may serve as biomarkers for tumor malignancy and as therapeutic targets for the treatment of certain aggressive tumors.

In **Chapter 3**, the ABPP methodology was extended to an *in vivo* model system. Recently, the zebrafish (*Danio rerio*) has emerged as a model system for embryonic development.<sup>19,20</sup> Furthermore, zebrafish larvae are increasingly used as a pre-clinical vertebrate model in drug discovery<sup>21,22</sup> and toxicological screening<sup>23–25</sup>. Thus far, most biochemical studies were limited to protein<sup>26,27</sup> and gene expression<sup>28,29</sup> profiles, whereas the protein activity component was often not taken into account. This limitation was addressed in **Chapter 3**, which described the development of an ABPP method for broad-spectrum profiling of serine hydrolase and kinase activity in zebrafish larvae. ABPP coupled to MS-analysis enabled the identification and mapping of 45 hydrolases (including ECS-related MGLL, ABHD6a, ABHD12 and FAAH2a) and 51 kinases throughout early zebrafish development (0–5 days post fertilization). The number of detected hydrolases and kinases increased during development and could be correlated to specific developmental processes. **Chapter 3** also showcased how zebrafish larvae can be used as pre-clinical animal model for *in vivo* target engagement and selectivity screening. FAAH inhibitor PF04457845 was used in a competitive ABPP setup and was found to be a highly selective compound. Inhibitor uptake and downstream effects on the lipid profile were confirmed using MS-based methods.

Phenotypic screening in intact animals, rather than in a single cell type, takes the complexity of the complete organism into account. For example, dorsomorphin, an inhibitor of the bone morphogenetic protein (BMP) (ALK8 in zebrafish, ALK2 in humans), was discovered in a phenotypic screen, because it triggered dorsalization in early zebrafish embryogenesis. Its target was identified based on phenotypic similarity to larvae carrying a genetic *Alk8* mutation<sup>21,30</sup>. The large collection of zebrafish phenotypes associated with specific genetic mutations has been an effective tool for target identification in the past<sup>21</sup>. Nevertheless, without a phenotypic match target identification remains challenging, especially when the phenotype is the result of

simultaneous modulation of multiple targets. In such cases, competitive ABPP can serve as a valuable tool for target identification and selectivity profiling, complementary to existing methods. In addition, *in vivo* treatment of the larvae can provide a rapid readout for basic toxicological studies during hit/lead identification and optimization, while monitoring inhibitor selectivity by competitive ABPP. Likewise, comparative ABPP may aid in target discovery by identifying altered enzyme activities in zebrafish disease models.

In **Chapter 4**, competitive ABPP was used to investigate the interaction landscape of FAAH inhibitor BIA 10-2474. A recent phase I clinical trial with this inhibitor resulted in the death of one volunteer and hospitalization of four others with mild-to-severe neurological symptoms<sup>31–34</sup>. Considering the clinical safety profile of other FAAH inhibitors, it was postulated that off-target activities of BIA 10-2474 may have played a role. In a competitive ABPP assay with human brain lysates, BIA 10-2474 was a poorly potent, but apparently selective FAAH inhibitor with ABHD6 as the only off-target. However, BIA 10-2474's inhibitory potency towards recombinant FAAH, FAAH2 (a human FAAH orthologue) and ABHD6 improved drastically in a cellular system. In this light, the *in situ* interaction landscape of BIA 10-2474 was investigated in human cortical neurons and three additional off-targets were identified; patatin-like phospholipase domain containing protein 6 (PNPLA6), carboxyl esterase 2 (CES2) and phospholipase 2 group XV (PLA2G15). Importantly these lipases, except for FAAH and FAAH2, were not targeted by PF04457845, a highly selective and clinically safe FAAH inhibitor<sup>35,36</sup>. Prolonged BIA 10-2474, but not PF04457845, exposure produced substantial alterations in the lipid network of primary neurons, in accordance with the role of the BIA 10-2474 targets in cellular lipid metabolism. BIA 10-2474 thus acts a promiscuous lipase inhibitor, with the potential to cause metabolic dysregulation in the nervous system, which in turn may have contributed to the observed clinical neurotoxicity. The relative causality of the identified BIA 10-2474 off-targets, however, could not be established in this study, because clinical samples of the patients were not available. Integration of chemical proteomics in the drug discovery workflow as a tool to assess on-target engagement and off-target activity may guide therapeutic development and will hopefully contribute to the safety of clinical trials.

Remarkably, prolonged *in situ* BIA 10-2474 treatment (48 h) of HEK293-T cells recombinantly expressing ABHD6 or FAAH resulted in accumulation of inhibited ABHD6 protein, but not of inhibited FAAH protein (Figure 2A). This effect was mimicked using ABHD6 inhibitor KT195<sup>37</sup> (Figure 2A) and similar increases in ABHD6 levels were obtained in a second human cell line (U2-OS) as well as in the murine cell line Neuro-2a (Figure 2B). No other BIA 10-2474 targets accumulated upon inhibition (Figure 2C). These data suggest that the increase in ABHD6 protein levels is not due to general interference with protein metabolism or biosynthesis, but rather suggests that ABHD6 proteostasis is modulated specifically upon its inhibition. Some enzyme inhibitors are known to act as chemical chaperones increasing cellular protein levels by reducing

proteolysis or by enhancing protein biosynthesis and folding<sup>38</sup>, and BIA 10-2474 and KT195 may function as such. Of note, no suitable antibodies were available to study the effect of ABHD6 inhibition on endogenous protein levels. Alternatively, BIA 10-2474 analogs AJ167, AJ179, and AJ198 (described in Chapter 4) containing a bio-orthogonal ligation handle, were used to enable target visualization using two-step ABPP. However, these analogs did not inhibit ABHD6 substantially (Figure 2D).

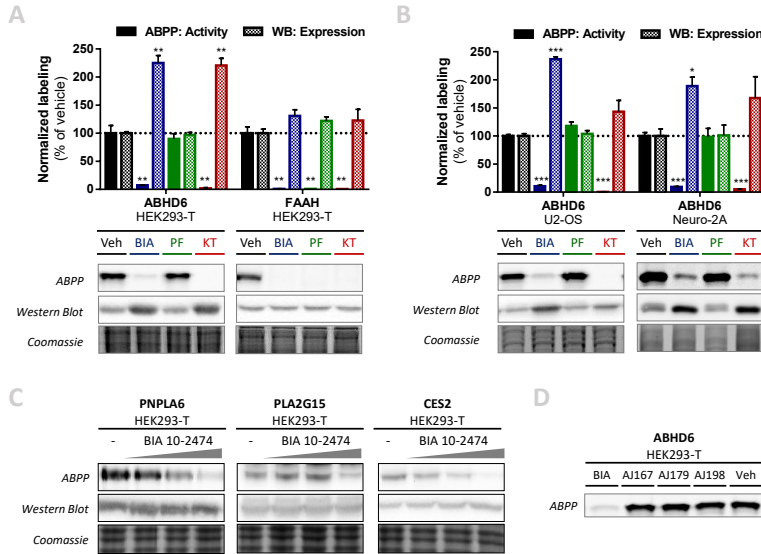


**Figure 2 | ABHD6, but no other BIA 10-2474 targets, accumulates upon BIA 10-2474 inhibition.** (A–B) HEK293-T (A), U2-OS, and Neuro-2a (B) cells were transiently transfected with FLAG-tagged ABHD6 (A, B) or FAAH (A). Cells were treated *in situ* with vehicle, BIA 10-2474 (10  $\mu$ M), PFO4457845 (1  $\mu$ M), or KT 195 (10  $\mu$ M) for 48 h. Protein activity and expression was analyzed by gel-based ABPP with FP-TAMRA (500 nM) (A) or MB064 (250 nM) (20 min, rt) (B) and western blot against the FLAG-tag. Coomassie staining served as a protein loading control. Labeling was quantified and normalized for protein loading and is expressed as % of vehicle (mean  $\pm$  SEM (n=3), *t*-test with Holm-Sidak multiple comparison correction: \*  $p < 0.05$ , \*\*  $p < 0.01$ , \*\*\*  $p < 0.001$ ). (C) HEK293-T cells were transiently transfected with FLAG-tagged PNPLA6, PLA2G15 or CES2 and were treated *in situ* with vehicle or BIA 10-2474 (1, 10, 100  $\mu$ M) for 48 h. Protein activity and expression was analyzed by gel-based ABPP with FP-TAMRA (500 nM, 20 min, rt) and western blot against the FLAG-tag. Coomassie staining served as a protein loading control. (D) HEK293-T cells were transiently transfected with ABHD6 and treated *in situ* with vehicle, BIA 10-2474, AJ167, AJ179, or AJ198 (10  $\mu$ M, 48 h). ABHD6 activity is visualized by gel-based ABPP with probe MB064 (250 nM, 20 min, rt) (n=2).

The accumulation of inhibited ABHD6 is especially relevant considering the scaffolding function of ABHD6, which is independent of its catalytic function. ABHD6 acts as a potent negative regulator of cell surface trafficking of GluR1-subunit of the  $\alpha$ -amino-3-hydroxy-5-methyl-4-isoxazolepropionic acid receptors (AMPA receptors), one of the major postsynaptic ionotropic glutamate receptors mediating excitatory synaptic neurotransmission in the central nervous system. Provided that endogenous ABHD6 also accumulates upon inhibition, BIA 10-2474 may cause aberrations in AMPAR-mediated glutamatergic signaling as a result of ABHD6 accumulation, which in turn may contribute to BIA 10-2474's clinical neurotoxicity. Electrophysiological studies will be valuable in

assessing the effects of BIA 10-2474 and ABHD6 inhibition on glutamatergic signaling and thus on excitotoxicity.

In **Chapter 5** ABPP is employed to identify the enzymes involved in neuronal differentiation. Retinoic acid (RA)-stimulation of Neuro-2a cells was previously shown to induce neurite outgrowth and to increase cellular 2-AG levels<sup>39</sup>. The contribution of endogenously expressed DAGL $\alpha$  and DAGL $\beta$  was investigated using pharmacological, genetic, and chemical proteomic methods. DAGL inhibitor DH376 completely abolished cellular 2-AG levels and delayed RA-induced neuronal differentiation. Surprisingly, CRISPR/Cas9-mediated knockdown (KD) of the 2-AG biosynthetic DAGL $\alpha$  and DAGL $\beta$  in Neuro-2a cells did not affect cellular 2-AG levels, suggesting the presence of other enzymes capable of 2-AG biosynthesis. A bio-orthogonal ligation handle in DH376 enabled target identification by chemical proteomics. DAGL $\beta$  and ABHD6 were identified as the only DH376-targets in Neuro-2a cells. ABHD6 has been reported as a promiscuous lipase that uses 2-AG, as well as various lysophosphatidyl species<sup>40</sup> and bis(monoacylglycero)phosphate<sup>41</sup> as substrates. Biochemical, genetic and lipidomic studies revealed that ABHD6 possesses diacylglycerol (DAG) lipase activity in conjunction with its previously reported role as a monoacylglycerol (MAG) lipase. During RA-induced differentiation an elevation of ABHD6 activity was observed along with a reduction in DAGL $\beta$  activity, suggesting a physiological role of ABHD6 in 2-AG signaling.

The exact physiological role of ABHD6 in 2-AG metabolism, however, is difficult to assess due to its dual MAG and DAG lipase activities. It is likely that the reactions are driven by the relative substrate and product concentrations. This could be further studied using radiolabeled substrates. Triple DAGL and ABHD6 KO mice may also provide information on the physiological role of ABHD6 in 2-AG signaling. In a dual DAGL $\alpha$  and DAGL $\beta$  knockout mouse model, brain 2-AG levels were not completely abolished<sup>42</sup> and it is tempting to speculate that ABHD6 may account for the remainder of the 2-AG content.

In the study by Jung and colleagues, RA-induced differentiation was mediated by CB1R<sup>39</sup>. Notably, in **Chapter 5** both 2-AG and AEA levels increased during RA-induced differentiation, suggesting that either endocannabinoid may be responsible for the CB1R-mediated effects in differentiating Neuro-2a cells. Remarkably, also other NAE levels increased during differentiation, ranging from a 2- to a 15-fold increase (Figure 3). These pronounced alterations propose a role of the NAEs in neuronal differentiation. The NAE *N*-docosahexaenoylethanolamine (DHEA, synaptamide) has already been described as a potent neurogenic metabolite. A biotinylated DHEA analog enabled affinity purification of the DHEA interaction partners and resulted in the identification of G-protein coupled receptor 110 (GPR110) as the synaptamide receptor mediating the neurogenic effects of DHEA<sup>43</sup>. Similar approaches could enable identification of the interaction partners of other NAEs and may thereby contribute to understanding their role in neuronal differentiation.

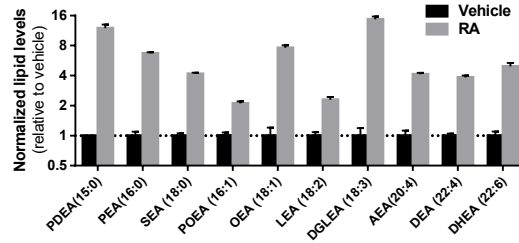


**Figure 3 | NAE levels increase during RA-induced differentiation of Neuro-2a.** Neuro-2a cells were stimulated by *in situ* treatment with retinoic acid (RA, 50  $\mu$ M, 2 % serum, 72 h). Lipids were extracted and analyzed by LC-MS/MS. Lipid abundance was normalized to the number of cells. Data is expressed as a fraction of vehicle (mean  $\pm$  SEM (n=5)). Vehicle and RA-treatment are statistically significant with  $p < 0.001$  for all NAE's (t-test with Holm-Sidak multiple comparison correction).

To investigate the role of AEA and the NAE's in differentiation, NAPE-PLD and FAAH KD populations were generated (Figure 4). Over 90% KD efficiency was reached based on western blot analysis (Figure 4A, C). Upon NAPE-PLD KD, most NAEs were strongly reduced, including AEA (Figure 4B). KD of FAAH resulted in elevated levels of a few NAE species, but not of AEA (Figure 4D), suggesting the existence of other AEA metabolic pathways in these cells. Automation of the neurite outgrowth analysis, e.g. with applications like NeuriteTracer<sup>44</sup>, is required to properly assess the differentiation process over time. Fluorescence imaging instead of phase contrast imaging, which was used in **Chapter 5**, would significantly aid these types of studies. Comparison of Neuro-2a WT and KD populations during differentiation, as well as the effects of spiking endocannabinoids and NAEs to the differentiation medium may help establish the role of these lipids in RA-induced differentiation in Neuro-2a.

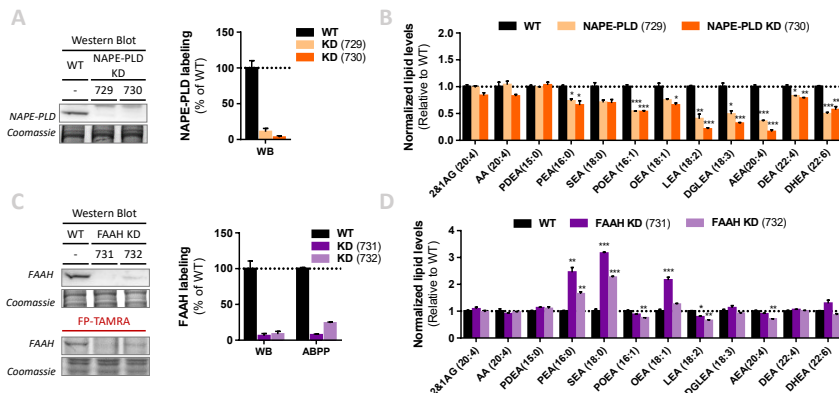


**Figure 4 | NAE levels are altered in Neuro-2a NAPE-PLD and FAAH KD populations.** (A-D) Neuro-2a KD populations of NAPE-PLD (A-B) and FAAH (C-D) were generated by three sequential transfections with Cas9 and two separate guides for each target (NAPE-PLD: 729, 730; FAAH: 731, 732). (A, C) Western blot showed a high KD efficiency of NAPE-PLD and FAAH using antibodies against each target. FAAH activity was strongly decreased in FAAH KD populations, based on gel-based ABPP using FP-TAMRA (500 nM, 20 min, rt). Labeling was quantified and is expressed as % of vehicle (mean  $\pm$  SEM, n=3). (B, D) Lipids were extracted from WT and KD cells and analyzed by LC-MS/MS. Lipid abundance was normalized for the amount of protein. Data is expressed as a fraction of vehicle (mean  $\pm$  SEM (n=4), t-test with Holm-Sidak multiple comparison correction: \*  $p < 0.05$ , \*\*  $p < 0.01$ , \*\*\*  $p < 0.001$ ).

## Opportunities and challenges in ABPP

The continuous development of the ABPP methodology contributes to its maturation and further extend on its already versatile character. Novel broad-spectrum probes targeting other protein classes will increase the biological reach of the technique, whereas highly specific probes enable alternative experimental approaches, e.g. imaging enzyme activity in living cells, assessing subcellular localization of active protein using correlative light and electron microscopy (CLEM)<sup>45</sup>, or visualizing activity *in vivo* using ABPs containing a positron emission tomography (PET) radiotracer<sup>46</sup>. The development of new analytical platforms and analysis methods can improve the experimental throughput and provide new experimental approaches to biological questions. For example, the recently developed label-free quantification method for chemical proteomics<sup>47</sup> enables comparison of multiple sample types within one experiment. This analysis method circumvents the previously required sample pairing, which could lead to distortions due to divergence between biological replicates. Technical advances in MS-analysis will contribute to further exploitation of ABPP as a tool in cellular biology, for example by facilitating the characterization of post-translational modifications (PTMs)<sup>48</sup> in intact proteins (top-down proteomics)<sup>49</sup>.

Further integration of competitive ABPP in the drug discovery process is a promising perspective for this method. In target-based drug discovery, activity assays with purified enzyme often serve as the primary screening method<sup>50</sup>. By taking the proteins out of their biological context, external factors such as protein-protein interactions cannot be accounted for. This may result in limited *in vitro* to *in situ/in vivo* translatability. For now, high-throughput screening (HTS)-compatible ABPP assays, such as fluorescence polarization<sup>51</sup> and EnPlex<sup>52</sup> still require the use of purified protein. However, these techniques do have major advantages as they do not require prior knowledge on the enzyme's substrate and (with limited modifications) the same assay can be used for other targets of the same ABP. After hit identification, gel- and MS-based ABPP can guide the lead optimization and preclinical phases, by enabling rapid assessment of potency and selectivity within the native proteome and in biologically relevant systems. Patient-derived inducible pluripotent stem cells (iPSCs) may provide particularly promising disease models and may prove valuable in competitive ABPP approaches for phenotype- and target-based drug discovery.

Even though the competitive ABPP method provides a lot of information on the inhibitor interaction profile, it is still limited to the enzymes that react with the probe. In the case of covalent inhibitors, a ligation handle can aid identification of covalent targets (e.g. DH376 in Chapter 5). However, incorporation of a ligation handle may change the inhibitor reactivity and selectivity, as was observed for the BIA 10-2474 alkyne derivatives in Figure 2. Non-covalent targets may be identified using a photoactivatable group, which interacts covalently with the associated proteins after UV-irradiation. In a similar fashion, non-enzymatic proteins, e.g. receptors, can be targeted using these so called photoaffinity probes<sup>53</sup>.



## Conclusion

Taken together, this thesis described several ABPP strategies and applications in drug discovery and cell biology (Figure 5). In a comparative setup, ABPP enabled rapid assessment of clinical samples to identify molecular role players in disease, which may lead to the discovery of novel therapeutic targets or biomarkers. Competitive ABPP, on the other hand, provides information on the drug interaction landscape. It enabled target engagement studies and inhibitor selectivity profiling, as demonstrated with BIA 10-2474, an inhibitor that caused severe neurological symptoms in a phase I clinical trial. Integration of competitive ABPP in preclinical testing will provide better insight in drug selectivity and drug safety. In zebrafish larvae the comparative ABPP methodology served as a tool to map the kinase and serine hydrolase landscape throughout embryonic development, thereby providing new activity-based insights in embryonic development. In addition, competitive ABPP in these larvae enabled *in vivo* target engagement and selectivity profiling. Lastly, a combined approach of ABPP, CRISPR/Cas9-mediated genetic modification, biochemistry and lipidomics resulted in the identification of ABHD6 as a 2-AG biosynthetic diacylglycerol lipase in retinoic acid-induced differentiation of Neuro-2a.

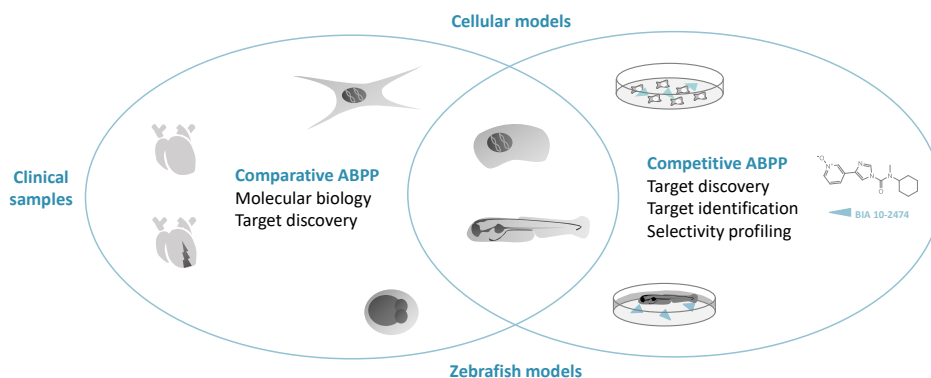


Figure 5 | Visual summary of ABPP strategies and their applications described in this thesis.

*To conclude, activity-based protein profiling is a versatile and powerful chemical tool and its integration in cell biology and drug discovery research is anticipated to bring forward new insights in both research fields.*

## Experimental procedures

### Materials, probes, and inhibitors

Fluorophosphonate-TAMRA (FP-TAMRA) was purchased from Thermo Fisher. MB064, BIA 10-2474, AJ167, AJ179, AJ198 were synthesized as previously described<sup>54,55</sup>. All synthesized compounds were at least 95% pure and were analyzed by LC/MS, NMR, and HRMS. Primers were ordered from Sigma Aldrich or Integrated DNA Technologies. Other chemicals and reagents were purchased from Sigma Aldrich, unless indicated otherwise.

### Cloning

Full-length human cDNA of ABHD6, FAAH, PNPLA6, PLA2G15, CES2 (Source Bioscience) was cloned into mammalian expression vector pcDNA3.1, containing genes for ampicillin and neomycin resistance. The inserts were cloned in frame with a C-terminal FLAG-tag and site-directed mutagenesis was used to remove restriction sites by silent point mutations. pcDNA3.1 containing the gene for eGFP was used as a transfection control. Plasmids were isolated from transformed XL-10 Z-competent cells (Maxi Prep kit: Qiagen) and sequenced at the Leiden Genome Technology Center. Sequences were analyzed and verified (CLC Main Workbench).

### Cell Culture

#### *General*

HEK293-T (human embryonic kidney), U2-OS (human osteosarcoma) and Neuro-2a (murine neuroblastoma) cells were cultured at 37 °C under 7% CO<sub>2</sub> in DMEM containing phenol red, stable glutamine, newborn bovine serum (10%, v/v; Thermo Fisher), and penicillin and streptomycin (200 µg/mL each; Duchefa). Medium was refreshed every 2-3 days and cells were passaged twice a week at ~ 90% confluence by resuspension in fresh medium (HEK293-T, Neuro-2a) or trypsinization (U2-OS). Cell lines were purchased from ATCC and were regularly tested for mycoplasma contamination. Cultures were discarded after 2-3 months of use.

#### *Transient transfections*

One day prior to transfection, cells were seeded at  $0.3 \times 10^6$  cells/well in a 12-wells plate. Prior to transfection, culture medium was aspirated and a minimal amount of complete medium was added. A mixture (HEK293-T, U2-OS: 3:1 (m/m); Neuro-2a: 5:1 (m/m)) of polyethylenimine (PEI) and plasmid DNA (0.625 µg/well) was prepared in serum-free culture medium and incubated (15 min, rt). Transfection was performed by dropwise addition of the PEI/DNA mixture to the cells. Transfection with pcDNA3.1 encoding GFP or empty pcDNA3.1 vector was used to generate control samples. 24 h Post-transfection culture medium was refreshed. Transfection efficiency was checked by fluorescence microscopy on eGFP-transfected samples (EVOS FL2 Auto, GFP-channel).

#### *In situ treatments*

Cells from transient transfections were used at 24h post-transfection. Culture medium was aspirated and after a careful PBS wash treatment medium containing vehicle (0.1% DMSO) or inhibitor (1-100 µM as indicated in figure legends) was added. After incubation for 48 h at 37 °C and 7% CO<sub>2</sub>, treatment medium was aspirated and cells were carefully washed with PBS. Subsequently cells were harvested by resuspension or scraping in PBS and were spun down (1000 g, 3-5 min, rt). Cell pellets were flash frozen in liquid nitrogen and stored at -80 °C until further use.

## CRISPR/Cas9 knockdowns

### Guide design & constructs

Two sgRNA's, in early exons, with high efficiency and specificity as predicted by CHOPCHOP v2 online web tool<sup>56</sup> (<http://chopchop.cbu.uib.no>) were selected. Guides were cloned into the BbsI restriction site of plasmid px330-U6-Chimeric\_BB-CBh-hSpCas9 (gift from Feng Zhang, Addgene plasmid #42230) as previously described<sup>57,58</sup>. Constructs and primers are annotated in Table 1.

### Knockdown population generation

Neuro-2a cells were transfected sequentially to yield populations with a high knockdown efficiency. The full experimental procedure is provided in **Chapter 5**. After three transfection rounds, the cells were cultured according to standard protocol. Knockdown efficiency was determined by T7E assay, gel-based ABPP and western blot. Ampoules of knockdown populations were prepared (complete DMEM, 10% DMSO) and stored at -150 °C. Cells were discarded after 3 months of culture.

**Table 1 | sgRNA targets, sgRNA oligos (top, bottom) and T7E1 primers (forward, reverse).**

sgRNA Target	Construct	Primer Sequences	
<b><i>Nape-pld</i> – Exon 2</b>	729	Top:	CACCGATAGCTTGGCGCTGGAGAC
		Bottom:	AAACGTCTCCAGCGCCAAGCTATC
<b>– Exon 3</b>	730	Top:	CACCAAGTTCGCTTATTGTACACGG
		Bottom:	AAACCCGTGTACAATAAGCGAACT
<b><i>Faah</i> – Exon 1</b>	731	Top:	CACCGCGCTGCACCGCCTTGTCCA
		Bottom:	AAACTGGACAAGGCGGTGCAGCGC
<b>– Exon 2</b>	732	Top:	CACCGAATCCAGGTCAGGATTCTG
		Bottom:	AAACCAGAATCCTGACCTGGATTC

## Whole lysate preparation

Cell pellets were thawed on ice, resuspended in cold lysis buffer (20 mM HEPES pH 7.2, 2 mM DTT, 250 mM sucrose, 1 mM MgCl<sub>2</sub>, 2.5 U/mL benzonase) and incubated on ice (15 min). Protein concentrations were determined by a Quick Start™ Bradford Protein Assay (Bio-Rad). After dilution to 2 mg/mL in sucrose lysis buffer or storage buffer (20 mM HEPES pH 7.2, 2 mM DTT), samples were used or flash frozen in liquid nitrogen and stored at -80 °C until further use. DTT was left out of all buffers for samples intended for click-chemistry.

## Activity-based protein profiling

Whole lysate (2 mg/mL) was incubated with activity-based probes MB064 (250 nM, 20 min, rt) or FP-TAMRA (500 nM, 20 min, rt). The reaction was quenched with Laemmli buffer (30 min, rt) and 20 µg protein was resolved by SDS-PAGE (10% acrylamide gel) along with protein marker PageRuler™ Plus (Thermo Fisher). In-gel fluorescence was detected in the Cy3- and Cy5-channel on a ChemiDoc™ MP imaging system (Bio-Rad) and gels were stained with coomassie after scanning. Fluorescence was quantified and normalized to coomassie staining using ImageLab™ software (Bio-Rad) and data was processed in Excel (Microsoft) and GraphPad Prism 7 (GraphPad).

## Western blot

Cell lysates were denatured with Laemmli buffer (30 min, rt) and 20 µg lysate was resolved on a 10% acrylamide SDS-PAGE gel along with PageRuler™ Plus Protein Marker (Thermo Scientific). Proteins were transferred to 0.2 µm polyvinylidene difluoride membranes by Trans-Blot Turbo™ Transfer system (Bio-Rad). Membranes were washed with TBS (50 mM Tris, 150 mM NaCl) and blocked with 5% milk in TBS-T (50 mM Tris, 150 mM NaCl, 0.05% Tween 20) (1 h, rt). Membranes

were subsequently incubated with primary antibody mouse-anti-FLAG (F3156, Sigma Aldrich; 1:5000 in 5% milk in TBS-T, 45 min at rt or O/N at 4 °C), rabbit-anti-NAPE-PLD (ab95397, Abcam; 1:200 in TBS-T, O/N, 4 °C), or mouse-anti-FAAH (CST2942, Cell Signaling Technologies; 1:1000 in 5% milk in TBS-T, O/N, 4 °C). After incubation membranes were washed with TBS-T and incubated with secondary goat-anti-mouse-HRP or goat-anti-rabbit-HRP (sc-2005, sc-2004, Santa Cruz Biotechnologies; 1:5000 in 5% milk TBS-T, 45 min, rt) and washed with TBS-T and TBS. Chemiluminescence (developed with ECL) was detected on the ChemiDoc™ MP (Bio-Rad) in the chemiluminescence channel, and colorimetric channel for the protein marker. Signal was normalized to coomassie staining using ImageLab™ software (Bio-Rad) and data was processed in Excel (Microsoft) and GraphPad Prism 7 (GraphPad).

## Lipidomics

### *Sample preparation: Neuro-2a retinoic acid stimulation*

Neuro-2a cells were seeded at  $0.75 \times 10^6$  cells/dish in a 10 cm dish. One day after seeding, medium was aspirated and retinoic acid stimulation was initiated by adding DMEM containing 2% serum and retinoic acid (50  $\mu$ M) or vehicle (0.1% DMSO). After 72 h neurite outgrowth was investigated using phase contrast microscopy (Olympus). Cells were carefully washed with PBS and harvested by resuspension in PBS (for retinoic acid stimulated cells, 5 dishes were combined to yield sufficient cells). Cells were pelleted (200 g, 10 min, rt) and resuspended in 1 mL PBS. Cell count and viability were checked by Trypan blue staining and automated cell counting (TC20™ Cell Counter, Bio-Rad) and  $2 \times 10^6$  cells were pelleted (1000 g, 3 min, rt). Pellets were flash frozen in liquid nitrogen and stored at -80 °C until lipid extraction.

### *Sample preparation: Neuro-2a knockdown populations*

Neuro-2a cells (WT or KD) were seeded at  $2 \times 10^6$  cells/dish in a 10 cm dish. Cells were harvested when confluence was reached. Culture medium was aspirated and cells were resuspended in DMEM. Cell count and viability were checked by Trypan blue staining and automated cell counting (TC20™ Cell Counter, Bio-Rad) and  $2 \times 10^6$  cells were pelleted (1000 g, 3 min, rt) (n=3 pellets). Pellets were washed twice with PBS (5 min, 1000 g), flash frozen in liquid nitrogen and stored at -80 °C until lipid extraction.

### *Lipid extraction & LC-MS/MS Analysis*

Lipid extraction was performed as previously described<sup>55</sup> with minor adaptations. The full experimental procedure is provided in **Chapter 5**.

## Statistical methods

Experiments were performed in an appropriate number of replicates, as indicated in figure legends. A t-test was used to determine statistical significance, with Holm-Sidak multi-comparison correction using GraphPad Prism 7 (GraphPad). Samples were compared to vehicle or wildtype controls and statistical significance is indicated as \*  $p < 0.05$ , \*\*  $p < 0.01$ , \*\*\*  $p < 0.001$ .

## References

1. Niphakis, M. J. & Cravatt, B. F. Enzyme Inhibitor Discovery by Activity-Based Protein Profiling. *Annu. Rev. Biochem.* **83**, 341–377 (2014).
2. Liu, Y., Patricelli, M. P. & Cravatt, B. F. Activity-based protein profiling: The serine hydrolases. *Proc. Natl. Acad. Sci.* **96**, 14694–14699 (1999).
3. Mechoulam, R. & Parker, L. A. The Endocannabinoid System and the Brain. *Annu. Rev. Psychol.* **64**, 21–47 (2012).
4. Di Marzo, V., Bifulco, M. & De Petrocellis, L. The endocannabinoid system and its therapeutic exploitation. *Nature Reviews Drug Discovery* **3**, 771–784 (2004).
5. Di Marzo, V. Endocannabinoid signaling in the brain: biosynthetic mechanisms in the limelight. *Nat. Neurosci.* **14**, 9–15 (2011).
6. Bisogno, T. *et al.* Cloning of the first sn1-DAG lipases points to the spatial and temporal regulation of endocannabinoid signaling in the brain. *J. Cell Biol.* **163**, 463–468 (2003).
7. Dinh, T. P., Freund, T. F. & Piomelli, D. A role for monoglyceride lipase in 2-arachidonoylglycerol inactivation. in *Chemistry and Physics of Lipids* **121**, 149–158 (2002).
8. Marrs, W. R. *et al.* The serine hydrolase ABHD6 controls the accumulation and efficacy of 2-AG at cannabinoid receptors. *Nat. Neurosci.* **13**, 951–7 (2010).
9. Blankman, J. L., Simon, G. M. & Cravatt, B. F. A comprehensive profile of brain enzymes that hydrolyze the endocannabinoid 2-arachidonoylglycerol. *Chem. Biol.* **14**, 1347–1356 (2007).
10. Savinainen, J. R., Saario, S. M. & Laitinen, J. T. The serine hydrolases MAGL, ABHD6 and ABHD12 as guardians of 2-arachidonoylglycerol signalling through cannabinoid receptors. *Acta Physiologica* **204**, 267–276 (2012).
11. Ueda, N., Tsuboi, K. & Uyama, T. Metabolism of endocannabinoids and related N-acylethanolamines: Canonical and alternative pathways. *FEBS J.* **280**, 1874–1894 (2013).
12. Cravatt, B. F. *et al.* Molecular characterization of an enzyme that degrades neuromodulatory fatty-acid amides. *Nature* **384**, 83–87 (1996).
13. McKinney, M. K. & Cravatt, B. F. Structure and function of Fatty Acid Amide Hydrolase. *Annu. Rev. Biochem.* **74**, 411–432 (2005).
14. O'Sullivan, S. E. in *Endocannabinoids* 393–422 (Springer, Cham, 2015). ISBN 9783319208251
15. Pacher, P., Steffens, S., Haskó, G., Schindler, T. H. & Kunos, G. *Cardiovascular effects of marijuana and synthetic cannabinoids: The good, the bad, and the ugly.* *Nature Reviews Cardiology* **15**, 151–166 (Nature Publishing Group, 2018).
16. Pacher, P. *et al.* Modulation of the endocannabinoid system in cardiovascular disease: therapeutic potential and limitations. *Hypertens. (Dallas, Tex. 1979)* **52**, 601–7 (2008).
17. Nomura, D. K. *et al.* Monoacylglycerol Lipase Regulates a Fatty Acid Network that Promotes Cancer Pathogenesis. *Cell* **140**, 49–61 (2010).
18. Chiang, K. P., Niessen, S., Saghatelian, A. & Cravatt, B. F. An Enzyme that Regulates Ether Lipid Signaling Pathways in Cancer Annotated by Multidimensional Profiling. *Chem. Biol.* **13**, 1041–1050 (2006).
19. Kimmel, C. B., Ballard, W. W., Kimmel, S. R., Ullmann, B. & Schilling, T. F. Stages of embryonic development of the zebrafish. *Dev. Dyn.* **203**, 253–310 (1995).
20. Link, B. A. & Megason, S. G. in *Source Book of Models for Biomedical Research* 103–112 (Humana Press, 2008). ISBN: 9781588299338
21. MacRae, C. A. & Peterson, R. T. Zebrafish as tools for drug discovery. *Nat. Rev. Drug Discov.* **14**, 721–731 (2015).
22. Rennekamp, A. J. & Peterson, R. T. 15 Years of Zebrafish Chemical Screening. *Curr. Opin. Chem. Biol.* **24**, 58–70 (2015).
23. Lieschke, G. J. & Currie, P. D. Animal models of human disease: Zebrafish swim into view. *Nature Reviews Genetics* **8**, 353–367 (2007).

24. Bowman, T. V. & Zon, L. I. Swimming into the future of drug discovery: In vivo chemical screens in zebrafish. *ACS Chem. Biol.* **5**, 159–161 (2010).
25. Zon, L. I. & Peterson, R. T. In vivo drug discovery in the zebrafish. *Nature Reviews Drug Discovery* **4**, 35–44 (2005).
26. Tay, T. L. *et al.* Proteomic analysis of protein profiles during early development of the zebrafish, *Danio rerio*. *Proteomics* **6**, 3176–3188 (2006).
27. Alli Shaik, A. *et al.* Functional mapping of the zebrafish early embryo proteome and transcriptome. *J. Proteome Res.* **13**, 5536–5550 (2014).
28. Kudoh, T. *et al.* A gene expression screen in zebrafish embryogenesis. *Genome Res.* **11**, 1979–1987 (2001).
29. White, R. J. *et al.* A high-resolution mRNA expression time course of embryonic development in zebrafish. *Elife* **6**, (2017).
30. Yu, P. B. *et al.* Dorsomorphin inhibits BMP signals required for embryogenesis and iron metabolism. *Nat. Chem. Biol.* **4**, 33–41 (2008).
31. Eddleston, M., Cohen, A. F. & Webb, D. J. Implications of the BIA-102474-101 study for review of first-into-human clinical trials. *British Journal of Clinical Pharmacology* **81**, 582–586 (2016).
32. Butler, D. & Callaway, E. Scientists in the dark after French clinical trial proves fatal. *Nature* **529**, 263–264 (2016).
33. Kerbrat, A. *et al.* Acute Neurologic Disorder from an Inhibitor of Fatty Acid Amide Hydrolase. *N. Engl. J. Med.* **375**, 1717–1725 (2016).
34. Bégaud, B. *et al.* BIA 10-2474: Minutes of the Temporary Specialist Scientific Committee (TSSC) meeting on ‘FAAH (Fatty Acid Amide Hydrolase) Inhibitors’. *Meet. Minutes* 1–14 (2016).
35. Huggins, J. P., Smart, T. S., Langman, S., Taylor, L. & Young, T. An efficient randomised, placebo-controlled clinical trial with the irreversible fatty acid amide hydrolase-1 inhibitor PF-04457845, which modulates endocannabinoids but fails to induce effective analgesia in patients with pain due to osteoarthritis of the. *Pain* **153**, 1837–1846 (2012).
36. Li, G. L. *et al.* Assessment of the pharmacology and tolerability of PF-04457845, an irreversible inhibitor of fatty acid amide hydrolase-1, in healthy subjects. *Br. J. Clin. Pharmacol.* **73**, 706–716 (2012).
37. Hsu, K. L. *et al.* DAGL $\beta$  inhibition perturbs a lipid network involved in macrophage inflammatory responses. *Nat. Chem. Biol.* **8**, 999–1007 (2012).
38. Kolter, T. & Wendeler, M. Chemical chaperones - A new concept in drug research. *ChemBioChem* **4**, 260–264 (2003).
39. Jung, K.-M., Astarita, G., Thongkham, D. & Piomelli, D. Diacylglycerol lipase- $\alpha$  and - $\beta$  control neurite outgrowth in neuro-2a cells through distinct molecular mechanisms. *Mol. Pharmacol.* **80**, 60–7 (2011).
40. Thomas, G. *et al.* The Serine Hydrolase ABHD6 Is a Critical Regulator of the Metabolic Syndrome. *Cell Rep.* **5**, 508–520 (2013).
41. Pribasniig, M. A. *et al.*  $\alpha/\beta$  hydrolase domain-containing 6 (ABHD6) degrades the late Endosomal/Lysosomal lipid Bis(Monoacylglycero)phosphate. *J. Biol. Chem.* **290**, 29869–29881 (2015).
42. Yoshino, H. *et al.* Postsynaptic diacylglycerol lipase  $\alpha$  mediates retrograde endocannabinoid suppression of inhibition in mouse prefrontal cortex. *J. Physiol.* **589**, 4857–4884 (2011).
43. Lee, J. W. *et al.* Orphan GPR110 (ADGRF1) targeted by N-docosahexaenylethanolamine in development of neurons and cognitive function. *Nat. Commun.* **7**, 13123 (2016).
44. Pool, M., Thiemann, J., Bar-Or, A. & Fournier, A. E. NeuriteTracer: A novel ImageJ plugin for automated quantification of neurite outgrowth. *J. Neurosci. Methods* **168**, 134–139 (2008).
45. Giepmans, B. N. G., Adams, S. R., Ellisman, M. H. & Tsien, R. Y. The fluorescent toolbox for assessing protein location and function. *Science* **312**, 217–224 (2006).

46. Phelps, M. E. Positron emission tomography provides molecular imaging of biological processes. *Proc. Natl. Acad. Sci.* **97**, 9226–9233 (2000).
47. van Rooden, E. J. *et al.* Mapping in vivo target interaction profiles of covalent inhibitors using chemical proteomics with label-free quantification. *Nat. Protoc.* **13**, 752–767 (2018).
48. Mann, M. & Jensen, O. N. Proteomic analysis of post-translational modifications. *Nature Biotechnology* **21**, 255–261 (2003).
49. Catherman, A. D., Skinner, O. S. & Kelleher, N. L. Top Down proteomics: Facts and perspectives. *Biochemical and Biophysical Research Communications* **445**, 683–693 (2014).
50. Khanna, I. Drug discovery in pharmaceutical industry: Productivity challenges and trends. *Drug Discovery Today* **17**, 1088–1102 (2012).
51. Bachovchin, D. A., Brown, S. J., Rosen, H. & Cravatt, B. F. Identification of selective inhibitors of uncharacterized enzymes by high-throughput screening with fluorescent activity-based probes. *Nat. Biotechnol.* **27**, 387–394 (2009).
52. Bachovchin, D. A. *et al.* A high-throughput, multiplexed assay for superfamily-wide profiling of enzyme activity. *Nat. Chem. Biol.* **10**, 656–663 (2014).
53. Geurink, P. P., Prely, L. M., Van Der Marel, G. A., Bischoff, R. & Overkleeft, H. S. Photoaffinity labeling in activity-based protein profiling. *Topics in Current Chemistry* **324**, 85–113 (2012).
54. Baggelaar, M. P. *et al.* Development of an activity-based probe and in silico design reveal highly selective inhibitors for diacylglycerol lipase- $\alpha$  in brain. *Angew. Chemie - Int. Ed.* **52**, 12081–12085 (2013).
55. Van Esbroeck, A. C. M. *et al.* Activity-based protein profiling reveals off-target proteins of the FAAH inhibitor BIA 10-2474. *Science* **356**, 1084–1087 (2017).
56. Labun, K., Montague, T. G., Gagnon, J. A., Thyme, S. B. & Valen, E. CHOPCHOP v2: a web tool for the next generation of CRISPR genome engineering. *Nucleic Acids Res.* **44**, W272–W276 (2016).
57. Ran, F. A. *et al.* Genome engineering using the CRISPR-Cas9 system. *Nat Protoc* **8**, 2281–2308 (2013).
58. Cong, L. *et al.* Multiplex genome engineering using CRISPR/Cas systems. *Science* **339**, 819–823 (2013).







# Nederlandse samenvatting

*Het doel van het onderzoek beschreven in dit proefschrift is het verkennen van de toepasbaarheid van activiteit gebaseerde eiwitprofilering in medicijnontwikkeling.*

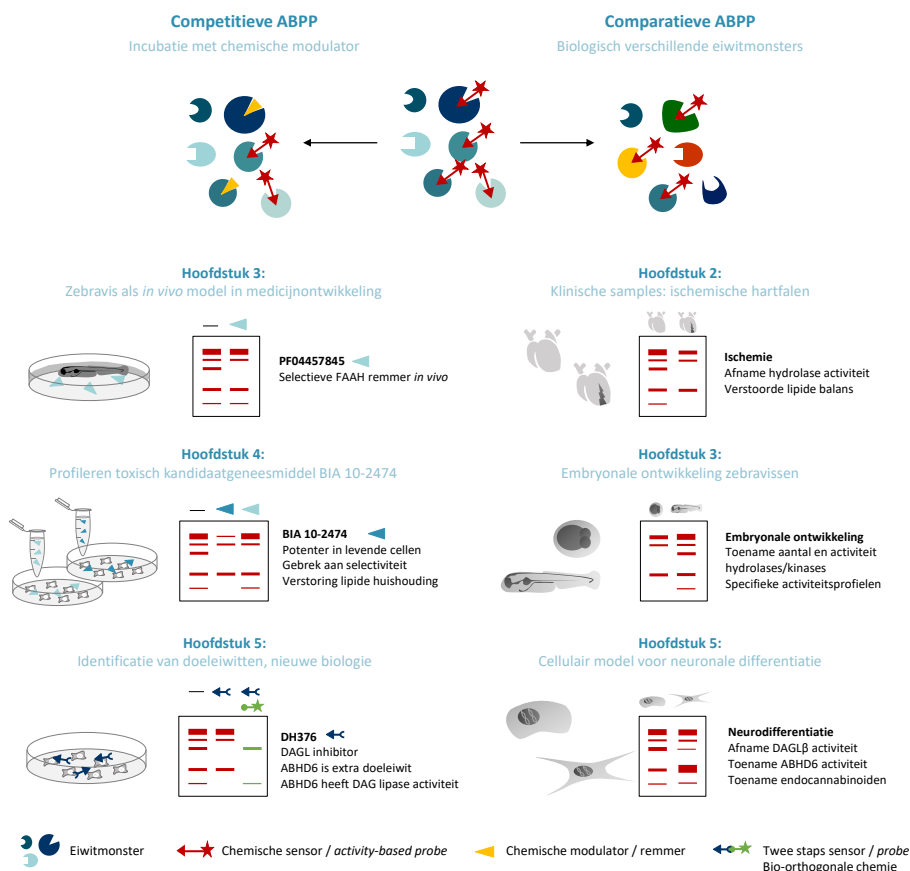
De zoektocht naar behandelmethoden voor ziekten en voor symptoomverlichting gaat enkele duizenden jaren terug. Ondanks grote ontwikkelingen in de medische wetenschap is medicijnontwikkeling nog steeds een ingewikkeld en uitdagend proces. **Hoofdstuk 1** beschrijft de gang van zaken in de moderne medicijnontwikkeling. Deze baseert zich met name op het concept dat een verstoring van de biologische balans een bepaald ziektebeeld met zich meebrengt. Door eiwitten die deze onbalans veroorzaken te moduleren met behulp van chemische stoffen, kan een ziektebeeld (deels) verholpen worden. De identificatie en validatie van een eiwit als therapeutisch aangrijpingspunt vormt vaak het begin van het medicijnontwikkelingsproces. In de daaropvolgende fases worden chemische modulators van het doeleiwit geïdentificeerd, geoptimaliseerd en uitvoerig getest in preklinische modellen, waarna het kandidaat geneesmiddel uiteindelijk ook in de kliniek wordt getest. De gemiddelde doorlooptijd van de ontwikkeling van één nieuw medicijn is 12 tot 14 jaar en de kosten lopen op tot ruim 2,5 miljard dollar. Belangrijke redenen voor de lange duur en hoge kosten van de ontwikkeling zijn onverwachte toxiciteit en onvoldoende werkzaamheid van het kandidaat geneesmiddel in late testfases.

Om het medicijnontwikkelingsproces te verbeteren, worden voortdurend nieuwe technieken en strategieën ontwikkeld. In de laatste jaren is activiteit gebaseerde eiwitprofilering (*activity-based protein profiling*, ABPP) een krachtige techniek gebleken in de ontwikkeling van nieuwe geneesmiddelen (Figuur 1). ABPP maakt het mogelijk om het enzymatisch actieve deel van bepaalde eiwitklassen te bestuderen in complexe eiwitmonsters. De methode maakt gebruik van chemische sensoren (*activity-based probes*) die covalent met actieve enzymen reageren. Een label aan de sensor maakt het mogelijk de doeleiwitten in kaart te brengen, bijvoorbeeld door fluorescente labels voor directe visualisatie met behulp van gel-analyse (*SDS-PAGE*) of een affiniteitslabel voor zuivering en identificatie met behulp van massaspectrometrie (MS). ABPP maakt het mogelijk om het activiteitsprofiel van verschillende biologische toestanden te vergelijken (comparatieve ABPP), zoals ziek en gezond weefsel, wat kan leiden tot de ontdekking van nieuwe therapeutische aangrijpingspunten. Tevens kan de techniek gebruikt worden om de potentie en de selectiviteit van chemische modulators of experimentele geneesmiddelen te testen, door bijvoorbeeld levende cellen met het medicijn te behandelen en vervolgens het activiteitsprofiel van behandelde en onbehandelde cellen te vergelijken (competitieve ABPP).

In **Hoofdstuk 1** wordt tevens het endocannabinoïde systeem (ECS) geïntroduceerd. Het ECS medieert de psychoactieve effecten van THC, de actieve stof in *Cannabis sativa* waaraan het systeem haar naam dankt. De cannabinoïde receptoren werden oorspronkelijk ontdekt als de doeleiwitten van THC, maar kunnen eveneens geactiveerd worden door lichaamseigen liganden, de endocannabinoïden 2-arachidonoylglycerol (2-AG) en anandamide. Samen met de enzymen verantwoordelijk voor hun aanmaak en afbraak en de receptoren vormen zij het ECS. De brede rol van het ECS in verschillende fysiologische en pathologische processen maakt dit systeem een bijzonder interessante bron van potentiële therapeutische aangrijpingspunten.

Het ECS is onder meer betrokken bij diverse cardiovasculaire processen en speelt een belangrijke rol in verschillende hart- en vaatziekten. In **Hoofdstuk 2** werden de endocannabinoïden en de bijbehorende metabole enzymen onderzocht in hartmonsters van patiënten met eindstadium ischemisch hartfalen met behulp van ABPP en lipidomics (een methode voor de analyse van lipiden met behulp van massaspectrometrie). Lipide-analyse bracht twee categorieën aan het licht binnen de ischemische hartmonsters; de een overeenkomstig met de controleharten, de ander met verlaagde niveaus van 2-AG en een sterke toename van anandamide, andere *N*-acylethanolamines en vrije vetzuren. Het afwijkende lipide profiel ging gepaard met een afname in activiteit van 13 van de 31 gedetecteerde hydrolases, inclusief monoacylglycerol lipase, dat betrokken is bij de afbraak van 2-AG. Deze bevindingen suggereren een biologisch verschil tussen de ischemische hartmonsters, ondanks het ontbreken van klinisch kenmerken die de patiënten duidelijk van elkaar onderscheiden.

De ABPP-methodologie werd in **Hoofdstuk 3** toegepast in een *in vivo* modelsysteem. Recentelijk heeft de zebravis (*Danio rerio*) aan populariteit gewonnen als modelsysteem voor vroege embryonale ontwikkeling. Bovendien worden de larven steeds vaker gebruikt als een preklinisch modelorganisme in medicijnontwikkeling en voor toxicologische testen. Met behulp van comparatieve ABPP werd het activiteitsprofiel van twee eiwitklassen, de serine hydrolases en de kinases, in kaart gebracht gedurende de eerste vijf dagen van de embryonale ontwikkeling. In totaal werden met behulp van massaspectrometrie 45 hydrolases en 51 kinases geïdentificeerd. Het aantal gedetecteerde hydrolases en kinases nam toe gedurende de ontwikkeling en correleerde met specifieke ontwikkelingsprocessen. Daarnaast werd de competitieve ABPP-methode toegepast om eenvoudig *in vivo* selectiviteit van chemische modulators te kunnen bepalen. PF04457845, een remmer van de serine hydrolase *fatty acid amide hydrolase* (FAAH), werd gebruikt als modelmolecuul en liet een zeer schoon interactieprofiel zien. Het effect van FAAH-inhibitie werd bevestigd met behulp van lipidomics.



**Figuur 1: Visuele samenvatting.** Schematische weergave van de toepassingen van ABPP in medicijnontwikkeling en celbiologie zoals beschreven in dit proefschrift.

In **Hoofdstuk 4** werd de competitieve ABPP-methode toegepast om het interactieprofiel van het kandidaat geneesmiddel BIA 10-2474, een *fatty acid amide hydrolase* (FAAH) remmer, te onderzoeken. In een recente klinische studie overleed één proefpersoon aan de gevolgen van hersenschade na toediening van BIA 10-2474 en werden vier anderen opgenomen met milde tot ernstige neurologische klachten. Aangezien eerder geteste FAAH-remmers (zoals PF04457845) klinisch veilig waren bevonden, werd er verondersteld dat onbedoelde interacties van BIA 10-2474 met andere eiwitten een bijdrage leverden aan de neurotoxiciteit van het molecuul. *In vitro* bleek BIA 10-2474 een matig potente, maar vrij selectieve FAAH-remmer met  $\alpha$ , $\beta$ -hydrolase domain containing protein 6 (ABHD6) en FAAH2 als enige onbedoeld geremde eiwitten (*off-targets*) in humaan hersenlysaat. In een cellulair systeem bleek BIA 10-2474 echter veel potenter en bovendien beduidend minder selectief. In behandelde celculturen van humane corticale neuronen werden drie extra *off-targets* van BIA 10-2474 geïdentificeerd, te weten patatin-like phospholipase domain containing protein 6, carboxyl esterase 2 en phospholipase 2 group XV. De klinisch veilige PF04457845, daarentegen, was selectief en remde enkel FAAH en FAAH2. Alle geïdentificeerde interactiepartners van BIA 10-2474 zijn betrokken bij lipidestofwisseling. Lipidomics wees uit dat BIA 10-2474 zodoende de lipidehuishouding in zenuwcellen verstoort, wat mogelijk heeft bijgedragen aan de klinische neurotoxiciteit van dit experimentele geneesmiddel. De relatieve causaliteit van de geïdentificeerde BIA 10-2474 *off-targets* kon echter niet worden vastgesteld, mede doordat klinische monsters van de behandelde vrijwilligers niet beschikbaar waren.

**Hoofdstuk 5** demonstreerde dat ABPP, behalve voor medicijnontwikkelingsstudies, ook een zeer waardevolle methode is voor het beantwoorden van celbiologische vraagstukken. De endocannabinoïde 2-AG is een belangrijk signaalmolecuul in het centraal zenuwstelsel, waar het samen met de cannabinoïde receptor (CB1R) een rol speelt in neuronale differentiatie. Biochemische, farmacologische en genetische studies hebben aangetoond dat diacylglycerol lipase  $\alpha$  en  $\beta$  (DAGL $\alpha$ , DAGL $\beta$ ) de voornaamste enzymen zijn die 2-AG produceren in de hersenen, door het katalyseren van de hydrolyse van diacylglycerol (DAG) naar 2-AG. Tijdens retinolzuur-geïnduceerde differentiatie van Neuro-2a, een veelgebruikt cellulair model voor neuronale differentiatie, namen cellulaire 2-AG-niveaus toe. De relatieve bijdrage van de 2-AG-producerende enzymen werd in **Hoofdstuk 5** onderzocht met behulp van ABPP, farmacologische en genetische methoden. Inhibitie van DAGL $\alpha$  en  $\beta$  met DAGL-inhibitor DH376 bracht het cellulaire 2-AG-niveau vrijwel volledig omlaag en vertraagde de differentiatie. Genetische inactivatie van DAGL $\alpha$  en/of DAGL $\beta$  door middel van CRISPR/Cas9-gemedieerde *knockdown* had echter geen effect op cellulaire 2-AG-niveaus. Deze data suggereren de aanwezigheid van alternatieve 2-AG producerende enzymen, die geïnhibeerd worden door DH376. DAGL $\beta$  en ABHD6 werden geïdentificeerd als de enige doelenzymen van DH376 in Neuro-2a met behulp van competitieve ABPP en bio-orthogonale chemie. In een biochemische assay

hydrolyseerde recombinant ABHD6 een fluorescent DAG-substraat, in een cellulair systeem zorgde overexpressie van ABHD6 voor een afname van endogeen DAG en een driedubbele *knockdown* van DAGL $\alpha$ , DAG $\beta$  en ABHD6 verlaagde 2-AG-niveaus in Neuro-2a. Deze data wijzen erop dat ABHD6 diacylglycerol lipase activiteit bezit, naast de eerder gerapporteerde monoacylglycerol lipase activiteit. Ten slotte werd met comparatieve ABPP aangetoond dat DAGL $\beta$  activiteit verminderde tijdens Neuro-2a differentiatie, terwijl ABHD6 activiteit sterk verhoogde, wat een rol voor ABHD6 in neuronale differentiatie impliceert.

In **Hoofdstuk 6** werd het uitgevoerde onderzoek samengevat en werden tevens enkele startpunten voor vervolgonderzoek aangereikt. In navolging op **Hoofdstuk 4**, werd aangetoond dat inhibitie van ABHD6 door BIA 10-2474 resulteerde in ophoping van het inactieve eiwit. Dit is in het bijzonder relevant omdat ABHD6, onafhankelijk van de katalytische activiteit, een rol speelt in het transport van receptoren. Mogelijk kan inhibitie van ABHD6, met ophoping van het inactieve eiwit als gevolg, op deze manier de neuronale signaaltransductie verstoren. Naar aanleiding van **Hoofdstuk 5**, werden ook de niveaus van andere lipiden tijdens de neuronale differentiatie onderzocht. Naast 2-AG was ook de endocannabinoïde anandamide verhoogd, evenals verschillende andere *N*-acylethanolamines. De rol van deze lipiden in differentiatie van Neuro-2a kan in de toekomst verder onderzocht worden met behulp van de CRISPR/Cas9-gemedieerde *knockdowns* van de enzymen verantwoordelijk voor de aanmaak en afbraak van deze lipiden (respectievelijk *N*-acylphosphatidyl ethanolamine phospholipase D (NAPE-PLD) en FAAH) die in **Hoofdstuk 6** omschreven staan. Tot slot werden in **Hoofdstuk 6** de uitdagingen in de ABPP-methodologie besproken en werd het toekomstperspectief van ABPP in medicijnontwikkeling geschetst.

*Tezamen laat het onderzoek dat dit proefschrift beschrijft, zien dat activity-based protein profiling een veelzijdige en waardevolle techniek is in medicijnontwikkeling en celbiologie. Comparatieve ABPP kan bijdragen aan de ontdekking van nieuwe therapeutische aangrijpingspunten door de vergelijking van activiteitsprofielen in klinische monsters te faciliteren (Hoofdstuk 2). Competitieve ABPP daarentegen biedt een uitkomst voor de identificatie van doelenzymen van chemische modulators in fenotypische screens, bijvoorbeeld in zebrafish embryo's (Hoofdstuk 3). Bovendien kan competitieve ABPP tot nieuwe inzichten leiden door het profileren van nieuwe experimentele geneesmiddelen, zowel retrospectief zoals beschreven voor BIA 10-2474 (Hoofdstuk 4), als prospectief door de ontwikkeling van nieuwe geneesmiddelen te sturen. Daarnaast is ABPP een waardevolle toevoeging aan de celbiologische gereedschapskist, waar ze bijdraagt aan nieuwe inzichten in biologische processen zoals embryonale ontwikkeling (Hoofdstuk 3) en neuronale differentiatie (Hoofdstuk 5). Naar verwachting zullen de continue ontwikkelingen in de ABPP-methodologie en verdere integratie van de techniek in onderzoek binnen én buiten de academie, belangrijke inzichten voortbrengen en een waardevolle bijdrage leveren aan medicijnontwikkeling in de (nabije) toekomst.*



## List of publications

### **Chemical proteomics maps brain region specific activity of endocannabinoid hydrolases**

M.P. Baggelaar\*, A.C.M. van Esbroeck\*, E.J. van Rooden, B.I. Florea, H.S. Overkleeft, G. Marsicano, F. Chaouloff, and M. van der Stelt, **2017**, *ACS Chem. Biol.*, 12(3), p. 852-861.

### **Activity-based protein profiling reveals off-target proteins of the FAAH inhibitor BIA 10-2474**

A. C. M. van Esbroeck\*, A. P. A. Janssen\*, A. B. Cognetta, D. Ogasawara\*, G. Shpak, M. van der Kroeg, V. Kantae, M. P. Baggelaar, F. M. S. de Vrij, H. Deng, M. Allarà, F. Fezza, Z. Lin, T. van der Wel, M. Soethoudt, E. D. Mock, H. den Dulk, I. L. Baak, B. I. Florea, G. Hendriks, L. De Petrocellis, H. S. Overkleeft, T. Hankemeier, C. I. De Zeeuw, V. Di Marzo, M. Maccarrone, B. F. Cravatt, S. A. Kushner, and M. van der Stelt, **2017**, *Science*, 356 (6342), p. 1084-1087.

### **Activity-based protein profiling of the human failing ischemic heart**

A. C. M. van Esbroeck\*, Z.V. Varga\*, X. Di, E.J. van Rooden, V.E. Toth, Z. Onódi, P. Leszek, M. Kuśmierczyk, P. Ferandinandy, T. Hankemeier, M. van der Stelt, and P. Pacher, *working title - manuscript in preparation*

### **Applications of activity-based protein profiling in developing zebrafish**

A.C.M. van Esbroeck, A.F. Stevens, V. Kantae, L.T. Lelieveld, E.J. van Rooden, B.I. Florea, R.C. van Wijk, A.C. Harms, P.H. van der Graaf, J.M.F.G. Aerts, T. Hankemeier, H.S. Overkleeft, and M. van der Stelt, *working title - manuscript in preparation*

### **Identification of ABHD6 as diacylglycerol lipase**

A.C.M. van Esbroeck, X. Di, V. Kantae, T. van der Wel, H. den Dulk, A.T. Bakker, B.I. Florea, H.S. Overkleeft, T. Hankemeier, and M. van der Stelt, *working title - manuscript in preparation*

\* authors contributed equally

**Development of an activity-based probe and in silico design reveal highly selective inhibitors for diacylglycerol lipase- $\alpha$  in brain**

M. P. Baggelaar, F. J. Janssen, A. C. M. van Esbroeck, H. den Dulk, M. Allarà, S. Hoogendoorn, R. McGuire, B. I. Florea, N. Meeuwenoord, H. van den Elst, G. A. van der Marel, J. Brouwer, V. Dimarzo, H. S. Overkleeft, and M. van der Stelt, **2013**, *Angew. Chemie - Int. Ed.*, 52(46), p. 12081-12085.

**Discovery of glycine sulfonamides as dual inhibitors of sn-1-diacylglycerol lipase  $\alpha$  and  $\alpha/\beta$ -hydrolase domain 6**

F. J. Janssen, H. Deng, M. P. Baggelaar, M. Allarà, T. van der Wel, H. den Dulk, A. Ligresti, A. C. M. van Esbroeck, R. McGuire, V. Di Marzo, H. S. Overkleeft, and M. van der Stelt, **2014**, *J. Med Chem*, 57(15), p. 6610-6622.

**Mapping *in vivo* target interaction profiles of covalent inhibitors using chemical proteomics with label-free quantification**

E. J. van Rooden, B. I. Florea, H. Deng, M. P. Baggelaar, A. C. M. van Esbroeck, J. Zhou, H. S. Overkleeft, and M. van der Stelt, **2018**, *Nat. Protoc.*, 13(4), p. 752–767.

**Chemical proteomic analysis of serine hydrolase activity in Niemann-Pick type C mouse brain**

E. J. van Rooden, A. C. M. van Esbroeck, M. P. Baggelaar, H. Deng, B. I. Florea, A. R. A. Marques, R. Ottenhoff, R. G. Boot, H. S. Overkleeft, J. M. F. G. Aert, and M. van der Stelt, **2018**, *Front. Neurosci.*, 12, p. 440.

**Design and synthesis of quenched activity-based probes for diacylglycerol lipase and  $\alpha/\beta$ -hydrolase domain containing protein 6**

E. J. van Rooden, M. Kohsiek, R. Kreekel, A. C. M. van Esbroeck, A. M. C. H. van den Nieuwendijk, A. P. A. Janssen, R. J. B. H. N. van den Berg, H. S. Overkleeft, and M. van der Stelt, **2018**, *Chem. - An Asian J.*, 13(22), p. 3491-3500

**Two-step activity-based protein profiling of diacylglycerol lipase**

E. J. van Rooden, R. Kreekel, T. Hansen, A. P. A. Janssen, A. C. M. van Esbroeck, H. den Dulk, R. J. B. H. N. van den Berg, J. D. C. Codée, and M. van der Stelt, **2018**, *Org. Biomol. Chem.*, 16(29), p. 5250-5253.

**Discovery of an *in vivo* active NAPE-PLD inhibitor that reduces brain anandamide levels and pain behavior**

E. D. Mock, M. Mustafa, R. Cinar, V. Kantae, X. Di, Z. V. Varga, J. Paloczi, G. Donvito, A. C. M. van Esbroeck, A. M. F. van der Gracht, I. Kotsogianni, J. K. Park, A. Martella, T. van der Wel, M. Soethoudt, M. Jiang, T. J. Wendel, A. P. A. Janssen, A. T. Bakker, B. I. Florea, J. Wat, H. van der Hurk, M. Wittwer, U. Grether, M. W. Buczynski, C. A. A. van Boeckel, T. Hankemeier, P. Pacher, A. H. Lichtman and M. van der Stelt, *manuscript under review*

**A selective activity-based probe reveals mitochondrial localization of monoacylglycerol lipase**

H. Deng, M. Jiang, A. C. M. van Esbroeck, A. C. P. Zottola, T. van der Wel, D. M. van Elsland, N. Klaassen, S. Eshuis, H. den Dulk, Z. V. Varga, R. J. B. H. N. van der Berg, G. Marsicano, P. Pacher, S. I. van Kasteren, S. E. Le Dévédec, and M. van der Stelt, *working title - manuscript in preparation*

**Discovery of *in vivo* selective sn-1-diacylglycerol lipase  $\alpha$  inhibitors**

A.P.A. Janssen\*, F.J. Janssen\*, M.P. Baggelaar, A.C.M. van Esbroeck, H. den Dulk, H. Deng, E. van Doornmalen, N. Smits, A. Morrison, E. Russel, J. Schultz, L. Brown, J. Hewitt, F. Macleod, J. Robinson, P.P. Geurink, H. Ovaa, B.I. Florea, H.S. Overkleeft, S.P.I. McElroy, C.A.A. van Boeckel, H. Rutjes, P.S. Jones, M. van der Stelt, *working title – manuscript in preparation*



# Curriculum vitae

- 2003 ● **VWO** | Alfrink College Zoetermeer, NL  
**LAPP-TOP** | Pre-university program  
Leiden University, NL
- 2009 ● **BSc** | Life Science & Technology  
Leiden University, Delft University of Technology, NL  
**Internship** | Molecular genetics  
Prof. dr. M. Noteborn, Leiden University, NL
- 2012 ● **MSc** | Life Science & Technology 🏆  
Research track, Leiden University, NL  
**Internship** | Bio-organic synthesis  
Prof. dr. M. van der Stelt, Leiden University, NL  
**Internship** | Endocannabinoids & neuroadaptation  
Dr. G. Marsicano, Neurocentre Magendie, FR
- 2014 ● **PhD** | Molecular physiology  
Prof. Dr. M. van der Stelt, Leiden University, NL  
  
**Posters** | 2016: CHAINS, Veldhoven, NL  
2016: Reedijk, Leiden, NL  
2018: ICRS, Leiden, NL  
  
**Presentations** | 2017: ABPP-BOC, Leiden, NL  
2017: ICRS, Montreal, CA 🇨🇦  
2017: BPS, London, UK 🇬🇧
- 2019 ●



Annelot Clementine Mathilda van Esbroeck was born on November 2, 1990 in Zoetermeer, the Netherlands. During her elementary education she developed a strong interest in genetics and biology, which was further nurtured during her high school period by extracurricular activities at Leiden University. In 2009 she obtained her high school diploma (VWO) at the Alfrink College in Zoetermeer. The same year she started the Bachelor program of Life Science & Technology at Leiden University and Delft University of Technology. After a minor in *disease, signaling and drug targets* in Leiden, she performed a research internship on *Live cell imaging of FAM96A and FAM96B during mitosis* under supervision of prof. dr. Mathieu Noteborn and dr. Claude Backendorf in the Molecular Genetics research group at Leiden University.

After obtaining her Bachelor degree in 2012, Annelot proceeded her academic education with a research master in Life Science & Technology at Leiden University. In the department of Bio-organic synthesis, she did a research internship on *Assay development for identification and characterization of novel DAG-Lipase inhibitors* under supervision of prof. dr. Mario van der Stelt. Supported with an Erasmus grant, she joined the Endocannabinoid & neuroadaptation research group at the Neurocentre Magendie in Bordeaux, France for a second research internship. Supervised by dr. Giovanni Marsicano and dr. Giovanni Bénard, Annelot investigated *The role of the cannabinoid receptor type 1 on mitochondrial turnover*. She obtained her Master of Science degree with honours (*cum laude*) in 2014.

After graduating, Annelot started her PhD under prof. dr. Mario van der Stelt in the Bio-organic synthesis group at Leiden university, which later continued as Molecular physiology. She conducted research on various aspects of the endocannabinoid system and explored activity-based protein profiling as a versatile tool in drug discovery and cell biology. She presented parts of her research at various national and international conferences, including poster presentations at CHAINS (2016, Veldhoven, The Netherlands), the Reedijk symposium (2016, Leiden, Netherlands), the yearly meeting of the International Cannabinoid Research Society (2018, Leiden, The Netherlands) and oral presentations during the annual Activity-Based Protein Profiling and Bio-Orthogonal Chemistry meeting (2017, Leiden, The Netherlands). Her oral presentation at the yearly meeting of the International Cannabinoid Research Society (2017, Montreal, Canada) was awarded best pre-doctoral presentation and her presentation at the European Cannabinoid Workshop (2017, London, United Kingdom) was awarded best oral presentation by the British Pharmaceutical Society.

Her belief that in complex systems new questions arise from each answer, has been a motivation throughout her research. With this curious mindset she will continue her work in science in the research group of prof. dr. Steven Kushner at the Erasmus Medical Centre in Rotterdam.

*Elk antwoord is het begin  
Elk antwoord is het begin van een nieuwe vraag.  
van een nieuwe vraag.*